UNIVERSIDAD DE CHILE
FACULTAD DE CIENCIAS FÍSICAS Y MATEMÁTICAS
DEPARTAMENTO DE FÍSICA

# SPIN DYNAMICS MEDIATED BY NON EQUILIBRIUM ELECTRONS

TESIS PARA OPTAR AL GRADO DE MAGÍSTER EN CIENCIAS, MENCIÓN FÍSICA

**SERGIO TOMÁS LEIVA MONTECINOS**

PROFESOR GUÍA:
ÁLVARO SEBASTIÁN NÚÑEZ VÁSQUEZ

MIEMBROS DE LA COMISIÓN:
RODRIGO ENRIQUE ARIAS FEDERICI
LUIS ENRIQUE FRANCISCO FOÀ TORRES
ALEJANDRO RENÉ ROLDÁN MOLINA

Este trabajo ha sido parcialmente financiado por:
CEDENNA, Fondecyt Regular 1190324.

SANTIAGO DE CHILE
2021

RESUMEN DE LA MEMORIA PARA OPTAR
AL TÍTULO DE MAGÍSTER EN CIENCIAS
DE LA INGENIERÍA
POR: **SERGIO TOMÁS LEIVA MONTECINOS**
FECHA: 2021
PROF. GUÍA: ÁLVARO S. NÚÑEZ

# SPIN DYNAMICS MEDIATED BY NON EQUILIBRIUM ELECTRONS

## English

This thesis focuses on studying the spin dynamics of an electronic device composed of two high-spin molecules subject to a bias voltage through two electrodes. We found that the non-equilibrium configuration induced by the bias voltage generates an effective interaction between the spins. Moreover, we discover that the bias voltage can control the strength and even the sign of those interactions. Furthermore, the system presents a stochastic nature that we study by the Langevin equation and the Fokker-Planck equation.

In the first chapter, we introduce the essential concepts to study and understand this particular system. Here we explain the difference between the well-known Spin Transfer Torque and Spin-Orbit Torque, along with a brief introduction to the Keldysh formalism for non-equilibrium systems.

The second chapter presents the microscopic derivation of the effective interactions, damping, and correlations that describe the system's spin dynamics with a stochastic equation. Here we include a spin-dependent hoping to model the spin-orbit coupling in the device that introduces anisotropic damping along with a Gilbert damping. Moreover, we find three effective interactions that bound the dynamics between the previously free spins.

In the third chapter, we study the average value of the spin's direction for the specific case in which the direction of one spin is kept fixed. By increasing the voltage, we find that the system can switch from a parallel to an antiparallel configuration. We also find that a strong enough spin-orbit coupling can switch the preferred direction due to the Dzyaloshinskii-Moriya interaction.

**Español**

Esta tesis se centra en el estudio de la dinámica de espín de un dispositivo electrónico compuesto por dos moléculas de alto espín sometidas a un voltaje de polarización a través de dos electrodos. Encontramos que la configuración de no equilibrio inducida por el voltaje de polarización genera una interacción efectiva entre los espines. Además, descubrimos que la intensidad e incluso el signo de esas interacciones pueden controlarse mediante el voltaje de polarización. Además, el sistema presenta una naturaleza estocástica que estudiamos mediante la ecuación de Langevin y la ecuación de Fokker-Planck.

En el primer capítulo, presentamos los conceptos esenciales para estudiar y comprender este sistema en particular. Aquí explicamos la diferencia entre los conocidos Torque de transferencia de espín y Torque de espín-órbita, junto con una breve introducción al formalismo Keldysh para sistemas fuera del equilibrio.

El segundo capítulo presenta la derivación microscópica de las interacciones, disipaciones y correlaciones efectivas que describen la dinámica de espín del sistema con una ecuación estocástica. Aquí incluimos una interacción dependiente de espín para modelar el acomplamiento de espín-órbita en el dispositivo, que introduce disipación anisotrópica junto con la disipación de Gilbert. Además, encontramos tres interacciones efectivas que unen la dinámica entre los espines anteriormente libres.

En el tercer capítulo, estudiamos el valor promedio de la dirección del espín para el caso específico en el que la dirección de un espín se mantiene fija. Encontramos que, al aumentar el voltaje, el sistema puede cambiar de una configuración ferromagnética a una antiferromagnética. También encontramos que un acoplamiento de espín-órbita lo suficientemente fuerte puede cambiar la dirección preferida debido a la interacción Dzyaloshinskii-Moriya.

*To my parents, siblings and friends,*
*This is where the fun begins*

# Acknowledgements

Primero quiero agradecer a quienes estuvieron ahí incluso antes de que decidiera seguir el camino de las ciencias, mis profesores de colegio, y dentro de ellos, guardo especial cariño a los profesores "Tuco" Valdebenito, Pablo y Jaime Parada, Sergio Neira, miss Carolina y Benita. Nunca los olvidaré.

Este trabajo nunca hubiera llegado a puerto si no fuera por el apoyo incondicional de mi familia, mis padres Hector y Luz Maria, mis hermanos Vicente, Paulina y Esperanza. No solo supieron qué decir o hacer para subirme el animo y que no me rindiera en los tiempos oscuros, sino que también supieron darme el espacio que necesité para trabajar a mi ritmo. Les estaré eternamente agradecido, espero cumplir sus expectativas y que juntos lleguemos muy lejos.

Mención especial a mi hermano Vicente y al Pablo, el 1001 por siempre en el corazón. Siempre recordaré las cenas descomunales de los días jueves, las sándwiches de la terraza post carretes. Nunca descubrimos quién era la señora que cantaba mal o si existía la azotea, pero hay cosas que valen por su misterio. Por varias que fueron las discusiones, siempre fueron más los momentos agradables y guardaré con cariño los recuerdos de esos 5 años que pasamos juntos. Les deseo lo mejor en sus carreras y en la vida. Que nadie te diga que cuanto queso rallado puedes ponerle a los tallarines y salud por el manjar!.

Mi paso por la universidad no hubiera sido el mismo sin los Cabros de las bancas, esos compañeros de sección que perduraron en el tiempo, nunca los olvidaré y espero que nos veamos pronto. Todavía nos faltan muchos J.V. y muchas estupideces que hacer. A Fabian, PL, Ale, Pino, Franco, Max, Jorge, Feña, Santiago, Hans, Vicho, Carlos, Christian, Claudio, Zamo, Diablo, Milla y el sospecho. Esas chelas y partidos de futbol después de los controles del primer año fueron una motivación que me mantuvo cuerdo ese año solo en Santiago. Brindo por el bar de Sazie para ver la Champions y llegar alegres a los ejercicios de química. Los quiero y extraño.

Una vez que ya entre a la licenciatura conocí gente maravillosa, muchos de los cuales sé que tendremos contacto en los años que siguen. A los que por diversas razones nos tuvimos que alejar F.A. y F.C., aun que no hablemos yo siempre les tendré un lugar especial en mi corazón y nunca los olvidaré. A la Tere, con quien pasamos grande momentos chistosos y no tanto, quiero que sepas que te considero una gran amiga y nada ni nadie cambiará eso. Al Manu, Cris y Jose, muchísimas gracias por todo su apoyo desde la licenciatura cuando estudiábamos ... Numéricos, hasta hoy, por estar en los tiempos más oscuros con palabras de aliento y una conversación amena que me sacara de ahí. Por mucho que nos veamos una vez al año nunca siento que sea hace tanto. Muchas gracias por todo. Son lo más grande que

me pudo pasar.

Durante mi pasar por el Magister conocí gente maravillosa, alegre y por sobre todo muy inteligentes que cada día me demostraron que se puede balancear una vida productiva con ciertos relajos y celebraciones. A la Vero, Rafa, Tebo, Rho, Javi, Bruno, Basti, Brayan y Walter, que supieron sacarme del escritorio para vivir grandes momentos que darían la alegría con la que recuerdo el periodo de ramos y trabajo más intenso. Les deseo el mejor tanto académicamente como en todos los ámbitos de la vida, sé que son personas geniales y llegaran muy lejos en lo que se propongan.

Especial cariño a Rodrigo y Esteban, esos cafés en el tercero, chelas durante las practicas de verano o simplemente sentarnos a conversar tan fácilmente de la vida como de física. Hicieron que un camino casi tortuoso fuera un agrado y algo entretenido. Por las tardes de juegos con la Eli, a quien también le debo parte de este logro, que se hicieron la alegría de las semanas en cuarentena. Espero que por mucho que nos alejemos en la vida, nunca nos alejemos como amigos. Los quiero mucho y les debo mucho más de lo que algún día terminaré de pagar.

Siento que los primeros años, que debieron ser los más difíciles al estar solo en Santiago, fueron realmente buenos. No solo por los amigos que hice en la U, también por los qué conserve desde el colegio. A Renato, quien siempre supo sacarme de los libros, junto con Tomás que en paz descanse pololeando. Amigos, jamás hubiera logrado llegar tan lejos sin ustedes, las palabras no alcanzaran jamás a describir lo agradecido que estoy con ustedes.

Si bien estar fuera de casa fue difícil, siempre se podía volver a Chillan a descansar con gente que realmente quiere bonito. A la Paloma, siempre supiste decirme las cosas como son, con honestidad pero con cariño, nunca olvidaré los días de compras en cal y canto con los pies a reventar. Amigas como tú, son mucho mas difíciles de encontrar que cualquier cosa en este mundo. A Fernanda fuiste una gran amiga que me apaño a lo largo de muchos momentos difíciles, espero que nunca nos alejemos lo suficiente como para dejar de ser amigos, y si pasa siempre guardaré el mas bonito de los recuerdos. A la Sofi, con quien poco nos pudimos ver por la distancia pero mucho nos reímos con los memes y videos, espero que esta cadena siga siendo interminable y nunca falten las risas.

Por sobre todo, me gustaría agradecer a mi profesor guía, Alvaro Nuñez. Siento que durante los años que trabajamos juntos, fuiste tanto un profesor espectacular como un guía y amigo cuando las cosas no salian. Siempre disfruté las reuniones que terminaban en conversaciones amenas sobre cualquier cosa. Me diste el tiempo, la compresión y ayuda que necesite en cada momento. Espero que podamos seguir trabajando y colaborando en tus ideas locas y entretenidas. También me gustaría agradecer a los Profesores Luis y Rodrigo, a quienes fui conociendo en diversos ramos e instancias, quienes siempre estuvieron dispuestos a responder las miles de dudas que tuve ya sea en la sala de clases como en sus oficinas. Para mí, los tres, fueron los profesores más influyentes en mi pasar por la Universidad.

Con estas palabras quedo corto, y por mucho, en cuanto le agradezco a cada uno, como a quienes agradezco por todo.

¡¡ GRACIAS A TODOS Y TODAS !!

# Table of Contents

# Index of illustrations

# Chapter 1

# Introduction

## 1.1. Spintronics

Condensed matter physics is a broad category of research that, in principle, studies substance in their solid-state, from crystalline solids in which we find a regular structure where the position of the atoms of the crystal are very much fixed, to amorphous materials in which the lack of a regular structure provide a variety of interesting phenomena that are, in general, very difficult to model. Nowadays this category can be thought as the study of systems that contains many particles and, in general, exhibit more and different properties than just a collection of the ones that its constituents present, as beautifully explained by Anderson in [3]. This thesis is, in fact, fundamentally motivated by that aspect of the many-body systems.

For a long time, the primary way to pass, store, and read information in electronic devices was using the fundamental property of electrons, their charge. Therefore, in most conventional electronics, the spin of the electrons is completely ignored [51]. This assumption is well justified since the balance between the spin-up and spin-down (where up and down relate to some quantization axis) conducting electrons in those electronic devices allows them to neglect the spin's effect. However, when we look at electronic transport through materials such as ferromagnets [32], we find that the electron's spin separates them into two distinct groups of charge carriers. Therefore, a whole new degree of freedom ready to be exploited. Nowadays, in search of better and more efficient ways to deal with information inside an electronic device, commonly seeking an applicable quantum process to reach quantum computing, it has been useful to take advantage of another fundamental property of particles, the spin. This new physics area is called *Spintronics* (electronics with spin-based transport), and studies the advantage of spin current over electronic current, since it has lesser energy lost through conductance and resistance, therefore an efficient transmission.

The most exceptional success in the field was the discovery of the giant magnetoresistance (GMR) [8, 5]. This led to an increase in hard drives' storage space by a factor of over a hundred times in the following ten years after its discovery. It consists of two ferromagnetic layers, where a third nonmagnetic metallic layer is put in between, forming a three-layer system. This simple configuration has an impressive change in its resistance depending on the relative magnetization orientation, from a relatively small resistance when both ferromagnetic magnetizations are parallel to a significant (hence giant) resistance for an anti-parallel configuration [36]. From this extraordinary discovery, one could say that the current efforts

in the implementation of Spintronics devices so that they can be included in the design of future electronic devices can be separated into two, as explained in [42]. One of them would be, keep perfecting the GMR technology with new materials that can make the giant magnetoresistance even bigger. The other focuses on developing new and better ways to use, control, and generate spin-polarized currents. In this thesis, we focus on an approach more similar to the last one. As can be seen, the Spintronics area is vast, and it has a lot of exciting applications to technology. Many of them have been thoroughly reviewed in [52, 24, 38, 21].

## 1.2. Spin interactions

Throughout this thesis, we get to deal with Spins in a semi-classical way and encounter various interactions and energies. Therefore, here we set a simple review of the most common ones that are of our interest. A complete study and deduction of these ideas can be found in [1, 19].

i) **Exchange interaction:**
This interaction comes from the electron-electron interaction through Coulomb interaction between two sites and their respective statistics. This means that it is the interaction between neighbors' atoms. The mathematical expression is:

$$H_{ex} = -\sum_{i,j} J_{ij} \boldsymbol{S}_i \cdot \boldsymbol{S}_j. \tag{1.1}$$

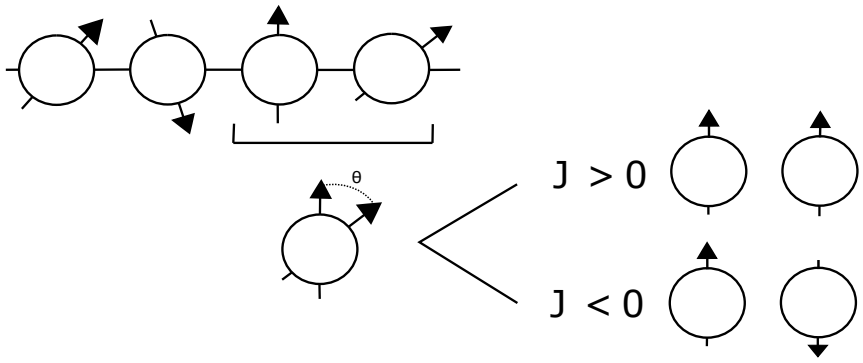


Figure 1.1: Sketch of the exchange interaction. Here we can see that depending on the sign of the exchange constant, the system's minimum energy configuration, i.e., the equilibrium configuration, is ferromagnetic ($J > 0$) or antiferromagnetic ($J < 0$).

Here the exchange matrix can be simplified as an identity with an exchange constant J, i.e. $J_{ij} = J\mathbb{I}_{ij}$. We can see that the minimum energy configuration is where the spins are aligned in a common direction, $\boldsymbol{S}_i \cdot \boldsymbol{S}_j = S^2$, i.e., the angle $\theta$ in figure 1.1 is zero.. However, that assumption is only correct for a positive exchange constant. So,

we can obtain either a Ferromagnetic configuration ($J > 0$) or an Antiferromagnetic configuration ($J < 0$) depending only on J's sign, as depicted in figure 1.1.

ii) **Zeeman interaction:**
The interaction between each site's spin $\boldsymbol{S}$ and an external magnetic field is

$$H_Z = -\sum_i \boldsymbol{S}_i \cdot \boldsymbol{h} \tag{1.2}$$

where $\boldsymbol{h} = \mu_B g \boldsymbol{B}$, $\mu_B$ is the Bohr magneton, $g$ is the Landé g-factor and $\boldsymbol{B}$ is the applied external magnetic field. As we can see, this interaction has the its lower value when every spin $\boldsymbol{S}_i$ is aligned with $\boldsymbol{B}$, as depicted in figure 1.2. A detailed deduction of this interaction can be found in [23].

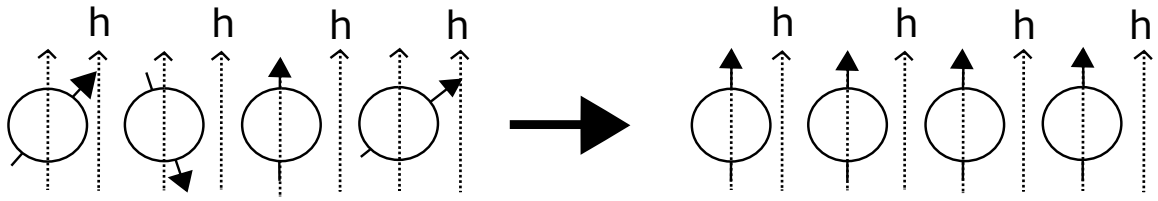


Figure 1.2: Sketch of the Zeeman interaction. Here an external magnetic field $\boldsymbol{h}$ interacts with the spin of each site. With this interaction, the system tends to align with the magnetic field.

iii) **Anisotropic interaction:**
This interaction can be confused into two types, the anisotropic energy that comes from the very nature of the molecule and its approximated shape, and an interaction between two sites depends on a specific direction. The latter can be understood as a modification of the symmetric exchange interaction towards a preferred direction.

The Anisotropic energy has many types of manifestations; the most relevant to us is the uniaxial anisotropy that defines the easy axis or easy plane that tells whether it prefers to align its spins either parallel or perpendicular to a given axis. Throughout this thesis, this energy will be modeled phenomenologically as

$$E_{Ani} = D(S_z)^2 - E[(S_x)^2 - (S_y)^2]. \tag{1.3}$$

This is inspired by ref. [11, 12, 29]. Following the exchange interaction definition, we will consider that an anisotropic interaction has the structure of

$$H_{AI} = -\sum_{ij} \boldsymbol{S}_i \mathbb{A}_{ij} \boldsymbol{S}_j, \tag{1.4}$$

where $\mathbb{A}_{ij}$ can not be described as $A_{ij}\mathbb{I}$, meaning that it is not isotropic like the exchange interaction (1.1).

iv) **Dzyaloshinskii - Moriya interaction:**
The Dzyaloshinskii - Moriya interaction (DMI) or Antisymmetric interaction comes from two main ingredients, the broken symmetry in the lattice and the spin-orbit coupling. We characterize this effect between two spins, $\boldsymbol{S}_1$ and $\boldsymbol{S}_2$, as

$$H_{DMI} = \boldsymbol{D}_{12} \cdot (\boldsymbol{S}_1 \times \boldsymbol{S}_2), \tag{1.5}$$

where $\boldsymbol{D}_{12}$ contains the information of the preferred direction in the system and the interaction's strength. In most cases, this interaction is very weak compared with others in the crystal, so it is not easy to measure it directly. Nevertheless, it minimizes when the spins are perpendicular with each other, and the resultant antisymmetric product is anti-parallel with the vector $\boldsymbol{D}$. This interaction is very well studied in micromagnetism because it produces non-collinear particle-like magnetic textures like skyrmions, that can be used to store information due to their stability [15, 50]. It can also produce a weak magnetism in an antiferromagnet.

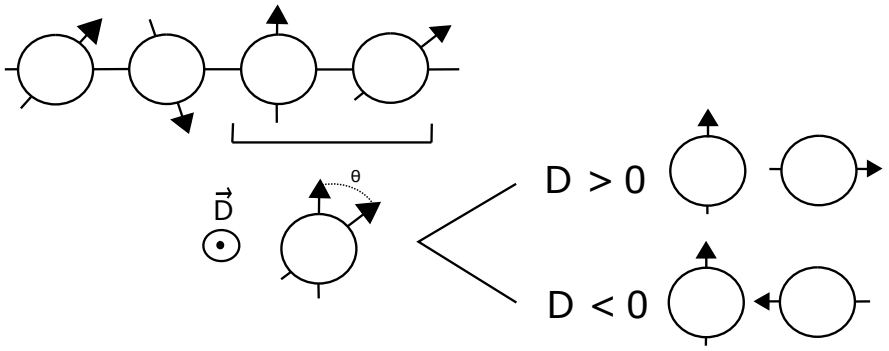


Figure 1.3: Sketch of the DMI interaction. Here, each site interacts with its neighbors, so they tend to be orthogonal to each other, forming a plane with the interaction's vector as the plane's, $\boldsymbol{D}$,normal vector.

## 1.3. Electronic Transport

In this section, we introduce the underlying formalism that we need in order to study our problem. We will start by giving a brief review of what we have to know about Open Quantum Systems and electronic Green's functions. To end up with the Non-equilibrium scheme or Keldysh-Schwinger formalism for non-equilibrium systems. These subjects are very well studied in [9, 10, 39], and here we will only summarize the most relevant parts that we will need in order to make this thesis self-contained.

When we study electronic transport, we have three main ingredients, the source and drain electrodes or leads, which for a general configuration can be as many as we want, and the system or electronic device. In general there are two approaches to study this kind of systems.

The first one is the Landauer-Büttiker formalism [9], where the problem is transformed into a scattering problem assuming ballistic conduction. Here the current is studied from the probability that an electron can transmit through the device. Although this is an intuitive idea, it deserves the time to be explained since there are very important issues like the Voltage across the device or the degeneracy at low temperatures. It was formulated as a correction of Ohm's Law at small dimensions.Two main problems arrived: the conductance does not decrease linearly with the width of the conductor, and that independently of the length of the sample, there is an interface resistance. Aiming to solve those problems, Landauer proposed that the conductance is directly proportional to the transmission probability and the number of propagating modes. Later, Büttiker extended those results to a multi-terminal configuration. We remark that this is not nearly enough to understand the full capacity and depth of the approach, and for a detailed and thorough study, the reader is referred to [9, 10].

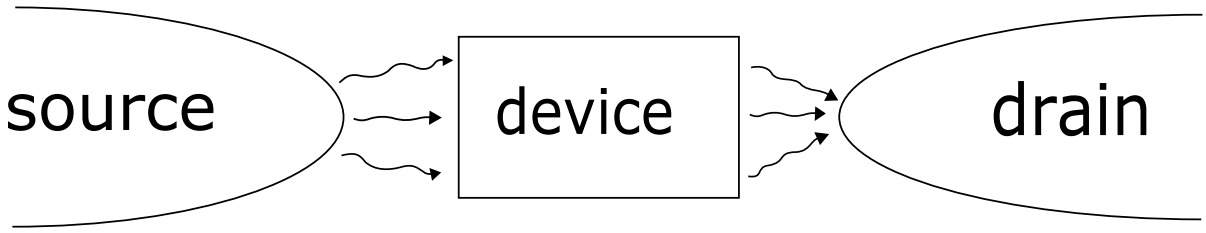


Figure 1.4: Sketch of a generic configuration where we have two electrodes, the source and drain, and an electronic device.

The second approach to deal with the system in figure 1.4 is the so-called Non-Equilibrium Green's Functions (NEGF). Here we consider each part separately as open quantum systems at equilibrium, i.e., first we solve (or attempt to solve) them as isolated system and then "turn on" the connection. Generally, the leads are treated as bath, so they are characterized by their respective temperature and chemical potential. Although these approaches do not seem very distinct since the both use Green's functions formalism, which allow us to calculate (in principle) everything, and we could use them to calculate the scattering matrix as shown in [9]. It is essential to note that they have different limitations; therefore, they are more suitable for some systems or goals. This formalism's real power comes when we deal with non-neglectable interactions inside the device, like electron-electron and photon-electron interactions, because for non-interacting transport, both approaches are equivalent.

**Schwinger-Keldysh Formalism**

This latter approach is a generalization of the usual Quantum Field Theory because, as is usually constructed, it can only deal with asymptotically free systems, for both the far past and future. This means that we need an extended theory to deal with non-equilibrium systems effects since they do not necessarily disappear in the far future.

We can illustrate this new formalism and its benefits by following the deduction presented in [39] for a general system described by a time-dependent Hamiltonian $\mathcal{H}(t)$. We will restrict this system to somehow be at equilibrium and characterize by the temperature T, and described by the Hamiltonian H. This restriction will hold from the far past until a critical time $t_0$. Beyond that time, a time-dependent perturbation $H'(t)$, is applied to the system. So the system Hamiltonian is:

$$\mathcal{H}(t) = H + H'(t), \tag{1.6}$$

where we can see that we are dealing with the perturbation problem. However, since this perturbation is time-dependent, a transformation to the Heisenberg picture is actually more illustrative. To do so, we need a relation between two Heisenberg pictures, ruled by $\mathcal{H}(t)$ and $H$, of an generic operator $\mathcal{O}$. One way to relate them is through the Dyson series that allows us to find a time evolution operator in the interaction picture. A simpler way is by writing the usual picture operator transformation of both pictures by contrasting each one with the Schrodinger picture. So, let us start by defining those picture transformations for a generic operator as

$$A_H(t) \equiv U_H^\dagger(t, t_0) A U_H(t, t_0). \tag{1.7}$$

Therefore, if we want to compare both Heisenberg pictures, we do it by means of the common original operator $A$. Hence, the unitary transformation of the operator $\mathcal{O}$ is:

$$\mathcal{O}_{\mathcal{H}}(t) = \left(U_{\mathcal{H}}^\dagger(t, t_0) U_H(t, t_0)\right) \mathcal{O}_H(t) \left(U_H^\dagger(t, t_0) U_{\mathcal{H}}(t, t_0)\right), \tag{1.8}$$

where the time evolution operators are defined as:

$$U_H(t, t_0) = e^{-iH(t-t_0)} \qquad , \qquad U_{\mathcal{H}}(t, t_0) = \mathcal{T} e^{-i\int_{t_0}^{t} dt' \mathcal{H}(t')}, \tag{1.9}$$

with $\hbar = 1$ for convenience. If we make use of the relation $U^\dagger(t, t') = U(t', t)$, we can read from equation (1.8) that the transformation is defined over a closed time path. In the end, from $U_H(t_0, t) U_{\mathcal{H}}(t, t_0)$, we define that path goes from $t_0$ to $t$, the time at which we want to evaluate the operator, and then goes back to $t_0$, where the time-dependent perturbation is turned on. This contour is called $\mathcal{C}_t$, and is illustrated in figure 1.5.

When we deal with equilibrium situations, that contour analysis can be dismissed. This because the perturbation can be turned on and off adiabatically. Therefore, this process ensures that in the far future, the only effect to the unperturbed ground state is a phase, as we can see from the Gell-Mann-Low theorem [20], and we would not need the above picture transformation to study the time evolution of an operator. That line of thought does not hold for an out-of-equilibrium system since, again, the perturbation does not vanish in time.

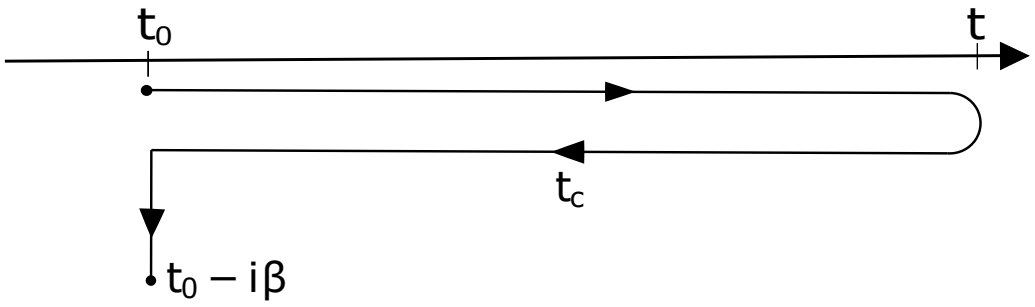


Figure 1.5: Contour path. This path is defined by $t_0$ and $t$, when the non-equilibrium perturbation is turned on and off,respectively. The appendix path $t_0 - i\beta$ is added to calculate the two-point correlation function.

Back to the contour-time, it can be shown that equation (1.8), with yet another transformation to the interacting picture so we can work with a free Hamiltonian $H_0$ as the usual requirement for a well-defined perturbation theory [33, 35], can be written as:

$$\mathcal{O}_{\mathcal{H}}(t) = \mathcal{T}_{\mathcal{C}_t}\left(e^{-i\int_{\mathcal{C}_t} dt_c (H^{(i)}_{H_0}(t_c) + H'_{H_0}(t_c))}\mathcal{O}_{H_0}(t)\right). \tag{1.10}$$

We have defined the contour ordering symbol $\mathcal{T}_{\mathcal{C}_t}$ to order products of operators according to the position of their time argument, $t_c$, over the contour time $\mathcal{C}_t$. The above expression is not so simple to prove, and the reader is referred to [39] for a detailed deduction. If we apply the above expression to a more common operator, we can see that it is much more similar to the regular equilibrium formalism than we could expect. For example, in the two-point correlation function we add the appendix contour from $t_0$ to $t_0 - i\beta$, with $\beta$ the inverse temperature, to the already presented contour time $\mathcal{C}_t$, as shown in figure 1.5. However, since we are not interested in transient phenomena, we can let $t_0$ to approach minus infinity, $t_0 \to \infty$, and the imaginary part of the contour vanish.

$$\langle \mathcal{T}\psi_{\mathcal{H}}(x,t)\psi^{\dagger}_{\mathcal{H}}(x',t')\rangle = Tr\left(\rho_0 \mathcal{T}_{\mathcal{C}_t}\left(e^{-i\int_{\mathcal{C}_t} dt_c (H^{(i)}_{H_0}(t_c) + H'_{H_0}(t_c))}\psi_{\mathcal{H}}(x,t)\psi^{\dagger}_{\mathcal{H}}(x',t')\right)\right), \tag{1.11}$$

with $\rho_0 = \frac{e^{-\beta H_0}}{Tr(e^{-\beta H_0})}$. From the above expression, we can obtain the path integral formalism analogously as the usual treatment. Once again, we stressed that this is a mere presentation of the idea and to clarify the notation. Nevertheless, a neat and simple explanation can be found in [13] and a thorough deduction in [39].

### Green's Functions decomposition

A useful tool that will come in handy throughout this thesis is a Green's function decomposition along the Keldysh contour. A general Green's function $F(t,t')$ can be separated as:

$$F(t,t') = \Theta(t-t')F^{>}(t,t') + \Theta(t'-t)F^{<}(t,t'), \tag{1.12}$$

where we can relay the behavior of the original function $F(t,t')$ into their *Greater* $F^{>}$ and *Lesser* $F^{<}$ components. If $F(t,t')$ is defined over the Keldysh contour, we have to keep in mind that the Heaviside step function $\Theta(t-t')$ is also defined over the Keldysh contour variable $t_c$. These new functions allow us to connect the *real* function $F$ with yet another useful decomposition:

$$F^{(\pm)} = \pm\Theta\left(\pm(t-t')\right)\left[F^{>}(t,t') - F^{<}(t,t')\right], \tag{1.13}$$
$$F^{(K)} = F^{>}(t,t') + F^{<}(t,t'). \tag{1.14}$$

We introduce the *advanced* $F^{-}$ and *retarded* $F^{+}$ Green's functions along with the *Keldysh* $F^{K}$ component. This new set of 5 functions is very well known, and it will be very useful when to give a physical interpretation of our results.

## 1.4. STT vs. SOT

When dealing with non-equilibrium effects in a spin system, we deal with the interaction between itinerant electron's spin, $\boldsymbol{m}_i$, and the system's spins, $\boldsymbol{M}_i$. Over the years this interaction has been studied in several ways. The more common interpretation of this interaction comes from the conservation of angular and linear momentum in the scattering between these two spins. However, for there to be an exchange in angular momentum, the non-equilibrium spin density of the electrons from the electronic current cannot be collinear to the direction of the magnetization. This misalignment depending on its origin can provide different effects on the magnetization.

This interaction gives rise to internal torques, so the global angular momentum is conserved. These torques are called *Spin Transfer Torque* (STT) and *Spin-Orbit Torque* (SOT) [47, 6]. Those effects can be combined, and they are not so easy to separate. Both torques depend on the strength of the non-equilibrium spin density compared to the arriving material's magnetization. As for classical scattering, for strong enough torques, they can influence the magnetization direction (weak magnetization or thin layer), or they can tend to align with the magnetization (large magnetization or thick layer). The fundamental difference between those torques is the spin density origin, i.e., the preferred direction of the electron's spin. However, in both cases, the equation of motion of the magnetization is given by:

$$\frac{\partial \boldsymbol{M}}{\partial t} = -\gamma \boldsymbol{M} \times \boldsymbol{H}_{eff} + \frac{\alpha}{M_s}\boldsymbol{M} \times \frac{\partial \boldsymbol{M}}{\partial t} + M_s \mathbf{T}_{st}(\boldsymbol{M}), \tag{1.15}$$

where the spin torque, $\mathbf{T}_{st}(\boldsymbol{M})$, takes a specific form for each case and the magnetic system we are studying, and $M_s$ is the saturation magnetization.

The STT [7, 45, 37] postulates that when the spin density that appears from the spin transport throughout a collinear magnetization enters a material with another non-collinear magnetization, the spin density exerts a torque on the new magnetization. This torque can

cause a change in the magnetization's direction, switching, and precession. Therefore, the electrons will transfer their polarization into the arriving material; only if the incident electron's polarization is different from the magnetization direction due to the torque between them. When we consider an $s-d$ model with $\Delta$ as the exchange interaction between the localized and itinerant electrons, we can obtain that the above equation takes the form:

$$\frac{\partial \boldsymbol{M}}{\partial t} = -\gamma \boldsymbol{M} \times \boldsymbol{H}_{eff} + \frac{\alpha}{M_s} \boldsymbol{M} \times \frac{\partial \boldsymbol{M}}{\partial t} - \frac{2\Delta}{\hbar} \boldsymbol{M} \times \boldsymbol{m}. \tag{1.16}$$

Another way to understand this process is through the net balance between an in-going spin current and the out-going spin current, indicating the total angular momentum change in the non-collinear magnetization. In the absence of spin-orbit interaction and if we neglect spin-flip scattering, both interpretations are equal.

$$\boldsymbol{T}_{st} = -\frac{2\Delta}{\hbar} \boldsymbol{M} \times \boldsymbol{m} = -\boldsymbol{\nabla} \cdot \mathcal{J}_s \tag{1.17}$$

Therefore, the spin torque can be viewed as the spin transfer due to the spin current, hence spin-transfer torque. Usually, these effects are observed with spin filters, and it has been proposed as a mechanism for quantum computer reading and writing devices.

The SOT [17, 30, 31, 38] arises from a more fundamental property of the molecule or material, the spin-orbit coupling with the itinerant electrons. This interaction is very well known for being a small contribution compared with other interactions, but powerful since it can lead to remarkable results. Like the former interaction, here, the electrons interchange angular momentum with the intrinsic angular momentum of the components of the material. The microscopic origin of this Torque is still on the debate, but at the current state, the Rashba effect [40] and the spin Hall effect [14] are the most accepted proposal. Here we can model the spin-orbit interaction by the Hamiltonian:

$$H_{SO} = \frac{\hbar}{2mc^2} \left( \nabla V \times \hat{p} \right) \cdot \boldsymbol{\sigma}. \tag{1.18}$$

When we assume uniformly magnetized electrodes, a steady-state condition, and a neglected spin-flip effect, we can see that the spin torque is:

$$\boldsymbol{T}_{st} = -\frac{2\Delta}{\hbar} \boldsymbol{M} \times \boldsymbol{m} = -\frac{1}{2m^2c^2} \langle (\nabla V \times \hat{p}) \times \hat{s} \rangle, \tag{1.19}$$

where $\boldsymbol{m} = -\langle \hat{s} \rangle$. In this case, the spin-orbit coupling acts as the source of the spin torque. In contrast to STT, the SOT does not require a spin-polarizer, which is a significant advantage for technological implementation. In both cases, the spin torque can be separated as:

$$\boldsymbol{T}_{st} = \frac{t_f}{M_s} \boldsymbol{M} \times \boldsymbol{t} + \frac{t_d}{M_s^2} \boldsymbol{M} \times (\boldsymbol{t} \times \boldsymbol{M}), \tag{1.20}$$

where $\boldsymbol{t}$ is conveniently chosen for each system. The first term is called the *field-like term*, and the second term is called the *damping-like term*. The factors $t_f$ and $t_d$ are specific for the origin of the spin torque. For example, the Rashba SOC presents both torques [48], but the spin Hall effect's torque mainly presents the damping-like torque.

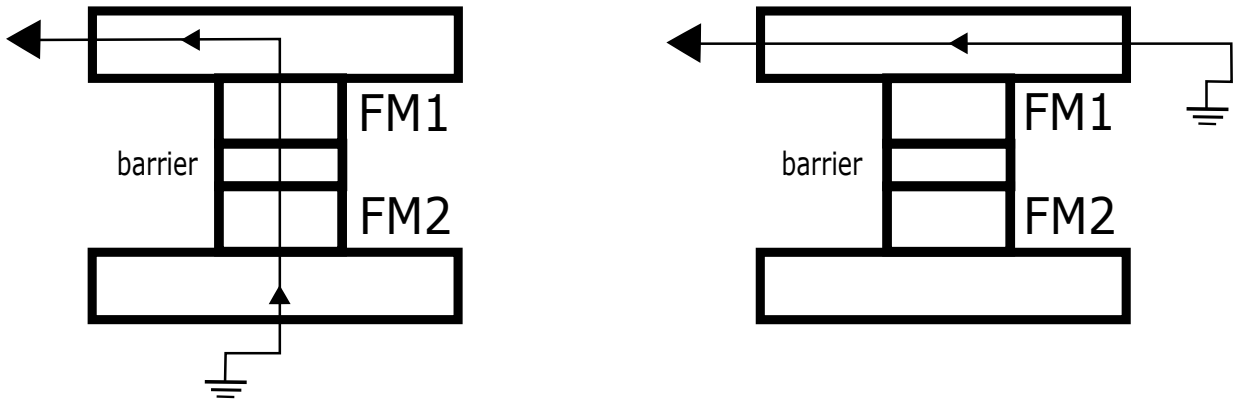


Figure 1.6: Sketch of the standard circuits that include STT and SOT to read and write information. Both configurations are very similar but differ in the path for the itinerant electrons. For the STT, the itinerant electrons pass through both ferromagnetic layers from where they gain a polarization, i.e., an spin density emerges. For the SOT, the itinerant electrons move in-plane, making this circuit more stable, and they acquire the spin density from the barrier's high spin-orbit interaction [47].

The best applications of both torques are the spin manipulation of the receiving material, the spin injection, and transport. All of the above allows them to be exciting tools to read and write in magnetic memories. These new tools are expected to accelerate the electronic devices' reading and writing capabilities, make them smaller, and increase their endurance, and are depicted in figure 1.6. The first writing technique was the field-induced switching of the magnetization of one Ferromagnetic-layer. However, that method of writing information over spin orientation switching was not scalable. Here it presents the more significant advantage and the main reason to develop a functional STT or SOT switching mechanism, since those methods are scalable, as explained in [16].

# Chapter 2

# Effective dynamics for localized spins

## 2.1. Introduction

In this chapter, we develop the main framework of this thesis and its numerical results. We aim to study a toy model that contemplates two leads and an electronic device like figure (2.1). This configuration has been studied in [43, 25, 34, 12], each one with its exciting ingredients. Here we are interested in the non-equilibrium effects, i.e., the effects of an electrical current passing through the device like in [34, 12]. However, now we focus on the effects of a spin-dependent hopping between the sites in the device. We will construct a general formalism to study a 1-D chain of N sites in a non-equilibrium configuration and present all the mathematical tools that we will need to obtain the equation of motion for the spin's direction at each site.

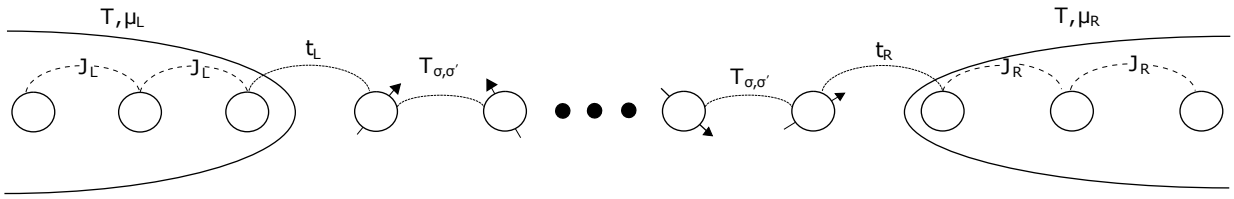


Figure 2.1: Sketch of a one-dimensional chain toy model that includes two semi-infinite leads and an N-sites device.

Once we have computed all the ingredients for the general N sites device, we restrict our analysis to two critical cases. The first one contemplates a one-particle-device [34], from now on, the *monomer case*. This simple configuration will allow us to present the Keldysh formalism introduced in the first chapter and the mathematical approach to deal with the interaction between the spin and electronic degree of freedom to obtain the localized quantum spin's effective dynamics.

A second application adds another particle to the first one, making a two-particles-device [12], the *dimer case*. It comes as a natural extension of the monomer case, with more complications and exciting results. Here we can see how the first case is the building block of our

study, thus the need to study the monomer case, but it turns to be much more than the sum of its independent ingredients, as beautifully explained by Anderson in [3].

## 2.2. The Array of localized spin: Model

This section introduces the model and mathematical approach to study a system that covers both monomer and dimer cases. They share almost all the ingredients. The simplest way to study the effects of electrical current on an electronic device, up to the microscopic level, is by a one-dimensional Tight Binding Model [26, 44] . The first ingredients to analyze are the left and right leads, modeled as

$$H_L = -J_L \sum_{\langle i,j\rangle,\sigma} c^\dagger_{L;i,\sigma} c_{L;j,\sigma}, \tag{2.1}$$

$$H_R = -J_R \sum_{\langle i,j\rangle,\sigma} c^\dagger_{R;i,\sigma} c_{R;j,\sigma}. \tag{2.2}$$

Where $J_L$ and $J_R$ are the spin-independent hopping parameter that, in principle, can be as different as we want, but for simplicity, we will consider them as equal, i.e., $J_L = J_R = J$. Using the second quantization formalism, the operators $c^\dagger_{L(R);i,\sigma}$ and $c_{L(R);i,\sigma}$ represent the fermionic creation and annihilation operator in the left (right) lead, respectively. They create and annihilate an electron at site i with spin $\sigma$ in the left (right) lead. The summation runs over $\langle i, j\rangle$, meaning that only the nearest neighbors interact. The next ingredient is the connection Hamiltonian that models the system-lead interaction by an electronic hopping between the last (first) site in the left (right) lead with the first (last) site of the electronic device,

$$H_{Lc} = -t_L \sum_\sigma \left( c^\dagger_{Ln,\sigma} c_{D1,\sigma} + c^\dagger_{D1,\sigma} c_{Ln,\sigma} \right), \tag{2.3}$$

$$H_{Rc} = -t_R \sum_\sigma \left( c^\dagger_{R1,\sigma} c_{DN,\sigma} + c^\dagger_{DN,\sigma} c_{R1,\sigma} \right). \tag{2.4}$$

Here $t_L$ and $t_R$ are the spin-independent hopping parameters quantifying the coupling between each lead and the system. In this case, $c^\dagger_{Di,\sigma}$ and $c_{Di,\sigma}$ represent the fermionic creation and annihilation operators in the device at site $i$, as shown in figure 2.1. The system is modeled as an array of $N$ sites, each with a spin S molecule. The interactions between them and their environment can be separated into a purely electronic contribution and a mixed one that combines the electronic and spin degrees of freedom, $H_{array} = H_e + H_d$. The mixed Hamiltonian includes the Zeeman interaction, i.e., a fixed external field, and an interaction between the spin of the itinerant electrons and the localized spin of each site by a ferromagnetic exchange coupling $\Delta$. This interaction is called the s-d interaction or Kondo model [27]. So the electronic and mixed Hamiltonian are:

$$H_e = \sum_{a;\sigma} \epsilon_a c^\dagger_{a,\sigma} c_{a,\sigma} - \sum_{\langle a,b\rangle;\sigma,\sigma'} c^\dagger_{a,\sigma} \mathbb{T}_{\sigma,\sigma'} c_{b,\sigma'}, \tag{2.5}$$

$$H_d = \mathcal{E}[\hat{S}^i_a] - \Delta \sum_{i,a;\sigma} \hat{s}^i_a \hat{S}^i_a - \sum_a \boldsymbol{h} \cdot \boldsymbol{S}_a. \tag{2.6}$$

Where $\hat{s}_a^i = \frac{1}{2}\sum_{\sigma,\sigma'} c_{a,\sigma}^\dagger \tau_{\sigma\sigma'}^i c_{a,\sigma'}$ represents the electron's spin at the site $a$, $\tau_{\sigma,\sigma'}^i$ is the i-th component of the vector containing the Pauli matrices like $\vec{\tau} = (\sigma_x, \sigma_y, \sigma_z)$, and $c_{a,\sigma}^\dagger, c_{a,\sigma}$ are the fermionic creation and annihilation operators at the site $a$. $\hat{S}_a$ is the operator of the localized spin-S at the site a. Finally, $\mathcal{E}[\hat{S}_a^i]$ represents all the on-site energy terms due to the internal structure of the molecule, here we only contemplate anisotropic energies, and for simplicity on the expressions, we neglect it until the last equation due to the similarity with the Zeeman effect, in terms of how we deal with it. In later sections, we will simplify the above Hamiltonian to the case of interest. We have define the hopping matrix $\mathbb{T}$ in $H_e$ so we can include a spin-dependent hopping between the sites on the device, meaning that it will not be present for the monomer case. The matrix

$$\mathbb{T}_{\sigma\sigma'} = t_0 \mathbb{I}_{\sigma\sigma'} + t\hat{t} \cdot \vec{\tau}_{\sigma\sigma'}, \tag{2.7}$$

depends on an arbitrary vector $t$ that accounts for the spin-orbit coupling inside the system. With all these ingredients, we can write the probability density using the "path integral formalism" in the standard construction [33, 49, 2] from which we get an expression that depends on all the possible ways that itinerant electrons and the localized spin can interact, so we must integrate over the Grassmann variables for the fermionic state, and the unit vector for the spin's coherent state. Although robust, this usual construction does not include the non-equilibrium configuration that we are interested in here. Instead of the usual imaginary time integral for the action, our probability is defined over the close-contour path $\mathcal{C}^t$ we introduced in the first chapter. So now, the probability density is expressed in terms of the Grassmann vector field $\mathbf{\Psi}$ describing the electrons, and the unit vector fields $\hat{\Omega}_a$ that describe each localized spin's state at site $a$ and time t, i.e. $\hat{S}_a = S\hat{\Omega}_a$, like

$$\mathbb{P}[\Psi, \mathbf{\Omega}, t] = \int_{\Psi(t)=\Psi} \mathcal{D}^2\Psi \prod_a^N \int_{\mathbf{\Omega}_a(t)=\hat{\Omega}_a} \mathcal{D}\mathbf{\Omega}_a \delta(|\mathbf{\Omega}_a|^2 - 1) e^{\frac{i}{\hbar}\mathcal{S}_T}. \tag{2.8}$$

The total action $\mathcal{S}_T$, can be separated into an electronic action $\mathcal{S}_\Psi$, an spin action $\mathcal{S}_\Omega$ and interaction action $\mathcal{S}_I$, where each term is written as

$$S_\Omega = \sum_a \int_{\mathcal{C}^t} dt_c \left[ -\hbar S \frac{d\omega_a}{dt_c} + S\mathbf{\Omega}_a \cdot \boldsymbol{h} - \mathcal{E}[\boldsymbol{S}_a] \right], \tag{2.9}$$

$$\begin{aligned} S_\Psi = \int_{\mathcal{C}^t} dt_c \Big[ & i\hbar \sum_{\sigma,i} \left( \psi_{Li,\sigma}^* \partial_{t_c} \psi_{Li,\sigma} + \psi_{Di,\sigma}^* \partial_{t_c} \psi_{Di,\sigma} + \psi_{Ri,\sigma}^* \partial_{t_c} \psi_{Ri,\sigma} \right) + \\ & - H_R - H_L - H_{Rc} - H_{Lc} - H_e \Big], \end{aligned} \tag{2.10}$$

$$S_I = \sum_a \int_{\mathcal{C}^t} dt_c \Delta S \mathbf{\Omega}_a \cdot \boldsymbol{s}_a. \tag{2.11}$$

Where, in the action for the localized spins $\mathcal{S}_\Omega$, $\omega_a$ is the Berry phase for the spin variable [4], and in the action for the free or itinerant electrons $\mathcal{S}_\Psi$, the terms with contour-time derivative, $\psi^* \partial_{t_c} \psi$, are the Berry phases of the Grassmann fields [33]. Now we have all the pieces that characterize the system. We can start to manipulate them to obtain the spin's effective dynamics. Since the action in (2.9), (2.10), and (2.11) are quadratic in their fields, we could, in principle, directly perform the integral over the Grassmann variables $\psi$. However, due to the $s-d$ interaction, the resulting factor would depend on the spin direction field, and it would be of no use for us. Instead of that, we can use the standard Effective Field

Theory (EFT) methods to deal with more than one field and expand perturbatively over $\Delta$ that couple those fields. A common way to expand it is the Cumulant expansion [41] up to second order, like

$$\mathcal{S}_T \to \mathcal{S} = \mathcal{S}_\Omega + \langle \mathcal{S}_I \rangle + \frac{i}{2\hbar}(\langle \mathcal{S}_I^2 \rangle - \langle \mathcal{S}_I \rangle^2). \tag{2.12}$$

Where $\langle(\dots)\rangle$ represents the average value of an operator, obtained by integrating the Grassmann field due to the electronic degree of freedom, with only the electronic action $S_\Psi$ as a weight factor, i.e., without the ferromagnetic coupling with the localized spin, with this in mind, we define the integral kernel that keeps the localized-itinerant spin interaction information up to second order

$$K_{ab}^{ij}(t_c, t_c{}') \equiv \frac{i}{2\hbar}\left[\langle \mathcal{T} s_a^i(t_c) s_b^j(t_c{}')\rangle - \langle s_a^i(t_c)\rangle\langle s_b^j(t_c{}')\rangle\right] \tag{2.13}$$

So the effective action for the array of N localized sites, each with spin S, and approximated up to second order in $\Delta$ is

$$\mathcal{S} = \mathcal{S}_\Omega + \int_{\mathcal{C}_t} dt' \left( S\Delta \sum_a \mathbf{\Omega}_a \cdot \langle \boldsymbol{s}_a(t')\rangle + \int_{\mathcal{C}_t} dt'' S^2\Delta^2 \sum_{ij,ab} \Omega_a^i(t') K_{ab}^{ij}(t', t'') \Omega_b^j(t'') \right), \tag{2.14}$$

and the probability density only depends on the spin path integrals and its constraints that enforce each localized spin at the specific state $\hat{\Omega}_a$ at the time $t$, which define the contour time $\mathcal{C}_t$, so

$$\mathbb{P}[\hat{\Omega}_a, t] = \prod_a^N \int_{\mathbf{\Omega}_a(t)=\hat{\Omega}_a} \mathcal{D}\mathbf{\Omega}_a \delta(|\mathbf{\Omega}_a|^2 - 1) e^{\frac{i}{\hbar}\mathcal{S}}. \tag{2.15}$$

The remaining piece we have left is the change in perspective when analyzing the kernel $\mathcal{K}_{ab}^{ij}$ in terms of the correlation of 2 spin variables instead of the correlation of 4 electronic states. This change can seem useless or even make the problem harder, but if we define the electronic Green's function as the correlation between two sites ($a$ and $b$), and two spins ($\sigma$ and $\sigma'$), keeping in mind that there is no reason for not being the same, we get:

$$iG_{a\sigma;b\sigma'}(t, t') \equiv \langle \mathcal{T} \psi_{a\sigma}(t) \psi_{b\sigma'}^*(t')\rangle, \tag{2.16}$$

with the time-ordered operator along the Keldysh contour, we can use Wick's Theorem [35] to rewrite $\mathcal{K}_{ab}^{ij}$ in terms of $G_{a\sigma;b\sigma'}$ only by replacing the $s_a^i(t) = \frac{1}{2}\sum_{\sigma\sigma'} \psi_{a\sigma}^*(t)\tau_{\sigma\sigma'}^i \psi_{a\sigma'}$ so if we drop the Pauli matrices and analyze the first term in (2.13) like

$$\begin{aligned}\langle \mathcal{T}\psi_{a\sigma}^*(t)\psi_{a\sigma'}(t)\psi_{b\mu}^*(t')\psi_{b\mu'}(t')\rangle = &\langle \mathcal{T}\psi_{a\sigma}^*(t)\psi_{a\sigma'}(t)\rangle\langle \mathcal{T}\psi_{b\mu}^*(t')\psi_{b\mu'}(t')\rangle \\ &-\langle \mathcal{T}\psi_{a\sigma}^*(t)\psi_{b\mu'}(t')\rangle\langle \mathcal{T}\psi_{b\mu}^*(t')\psi_{a\sigma'}(t)\rangle\end{aligned} \tag{2.17}$$

So the two-terms definition of the integral kernel is reduced to a single term of the electronic Green's functions, like

$$K_{ab}^{ij}(t, t') \equiv \frac{i}{8\hbar} \sum_{\sigma\sigma'\mu\mu'} \tau_{\sigma\sigma'}^i \tau_{\mu\mu'}^j G_{a\sigma';b\mu}(t, t') G_{b\mu';a\sigma}(t', t). \tag{2.18}$$

From now on, we will study each case (monomer and dimer) separated, since they present their own peculiarities that are worth looking at individually. Aside from the fact that the monomer case is the simpler version of the problem, it also will be useful to develop a recipe to obtain the spin's dynamics and obtain comparable results for the dimer case.

## 2.3. Spin Monomer

The spin monomer system [34], as the name suggests, consists of a single molecule with total spin S and unit direction vector $\mathbf{\Omega}$, coupled to two leads by the connection Hamiltonians (2.4) and (2.3). Since we have a one-site-device to study, there is no need for the hopping matrix $\mathbb{T}_{\sigma\sigma'}$ in equation (2.5), and we can model the electronic Hamiltonian by means of spin-independent hoppings. Therefore, the electronic Green's function $G_{a\sigma;b\sigma'}(t,t')$ defined in (2.18), must be spin-independent as well:

$$iG_{a\sigma;b\sigma'}(t,t') = \delta_{ab}\delta_{\sigma\sigma'}iG(t,t') \tag{2.19}$$

That means that there is no preferred direction for the itinerant electron's spin to choose, i.e., $\langle \boldsymbol{s}(t)\rangle = 0$. This can be shown by applying the sum over spin and using the Pauli matrices have null trace. The integral kernel is clearly also affected by this property

$$\begin{aligned}
\mathcal{K}^{ij}_{ab} &= \frac{i}{8\hbar}\delta_{ab}G(t,t')G(t',t)\sum_{\sigma\sigma'\mu\mu'}\tau^i_{\sigma\sigma'}\tau^j_{\mu\mu'}\delta_{\sigma'\mu}\delta_{\mu'\sigma} \\
&= \frac{i}{8\hbar}\delta_{ab}G(t,t')G(t',t)\sum_{\sigma\mu}\tau^i_{\sigma\mu}\tau^j_{\mu\sigma} \\
&= \frac{i}{4\hbar}\delta_{ab}\delta^{ij}G(t,t')G(t',t) \qquad (2.20)\\
&= \delta_{ab}\delta^{ij}K(t,t'). \qquad (2.21)
\end{aligned}$$

Where we have defined the one particle integral kernel K(t,t'). Now we can write the one-site version of (2.14) and (2.15) as:

$$\mathbb{P}[\hat{\Omega},t] = \int_{\mathbf{\Omega}(t)=\hat{\Omega}}\mathcal{D}\mathbf{\Omega}\delta(|\mathbf{\Omega}|^2-1)e^{\frac{i}{\hbar}\mathcal{S}}, \tag{2.22}$$

where

$$\mathcal{S} = \int_{C^t}dt'\left[-S\hbar\frac{d\omega}{dt} + S\boldsymbol{h}\cdot\mathbf{\Omega} + \Delta^2S^2\int_{C^t}dt''K(t',t'')\mathbf{\Omega}(t')\cdot\mathbf{\Omega}(t'')\right], \tag{2.23}$$

is the *effective action* for the spin-monomer system in between the leads. This action and the time-ordered operator in (2.21) are defined over the Keldysh contour time, from which, as explained in the Introduction section 1.3, it is not very easy to extract physical insight. Therefore, we have to map it back to real time to understand the action and obtain relevant information about the system or an effective equation of motion for the localized spin. We

can map it back by separating the spin vector in the forward ($t_+$) and backward ($t_-$) paths of the Keldysh contour time $t_c$ . This separation between the branches of the close-contour time path defines the variables $t_+ : -\infty \to t$ and $t_- : t \to -\infty$ that lead to a change of variables from $\Omega(t_c)$ to $\Omega(t_\pm)$ and $\delta\Omega(t_\pm)$, the classical and fluctuation parts of the spin. The separation

$$\mathbf{\Omega}(t_\pm) = \mathbf{\Omega}(t) \pm \frac{1}{2}\delta\mathbf{\Omega}(t), \tag{2.24}$$

will allow us to map back to real time [39]. Here we notice that the change of variables has a unitary Jacobian up to first order in the perturbation $\delta\mathbf{\Omega}$. The delta functional in equation (2.22) enforce the unitary value of $\Omega(t_c)$, but to keep that restriction in the new time variables, we need to write it in a more manageable way. Luckily we can replace it with a functional integral of a Lagrangian multiplier $\lambda$ as

$$\delta(||\Omega||^2 - 1) = \int \mathcal{D}\lambda e^{\frac{i}{\hbar}\int_{C^t} dt' \lambda S^2(||\vec{\Omega}(t')||^2 - 1)}. \tag{2.25}$$

Therefore, we have to give the same treatment for $\lambda$ as for $\Omega$:

$$\lambda(t_\pm) = \lambda(t) \pm \frac{1}{2}\delta\lambda(t) \tag{2.26}$$

Once we have prepared the effective action to transform it into real-time construction, these two variables allow us to separate the time integral as follows

$$\int_{C^t} dt_c = \int_{-\infty}^{t} dt_+ + \int_{t}^{-\infty} dt_- = \int_{-\infty}^{t} dt_+ - \int_{-\infty}^{t} dt_-. \tag{2.27}$$

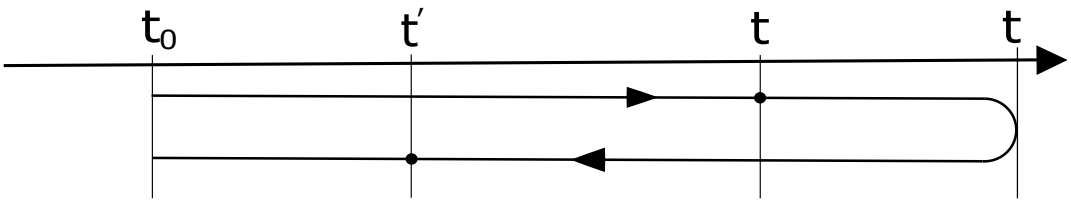


Figure 2.2: Sketch of the contour time illustrating how two times t and $t'$ can be one greater than the other in value, but the relation is inverted when we compare them in the contour time.

However, to map back to real-time, we must apply the decomposition presented in section 1.3 that introduces five new versions of the original kernel $K(t, t')$:

$$K(t,t') = \Theta(t-t')K^{>}(t,t') + \Theta(t'-t)K^{<}(t,t'), \tag{2.28}$$
$$K^{(\pm)}(t,t') = \pm\Theta\left(\pm(t-t')\right)\left[K^{>}(t,t') - K^{<}(t,t')\right], \tag{2.29}$$
$$K^{(K)}(t,t') = K^{>}(t,t') + K^{<}(t,t'). \tag{2.30}$$

With careful treatment on which function is defined in which branch, and applying the Heaviside function's properties: $\Theta(t-t')$: $\Theta(t-t')\Theta(t'-t) = 0$, $\Theta^2(t-t') = \Theta(t-t')$ we can finally obtain the action's real-time expression (2.23). A special note has to be taken here because the Heaviside function takes values from the contour time; the difference between time $t$ and $t'$ depends on which branch they lay on, as shown in figure 2.2. So even tough their actual value shows that $t > t'$, along the contour time $t'$ still can be greater than $t$: $t <_c t'$. After taking all these steps and ingredients into account, the effective action $\mathcal{S}$ is written in real-time as

$$\begin{aligned}\mathcal{S} = &\int dt' \left[\hbar S\epsilon^{\alpha\beta\gamma}\frac{d\Omega_\alpha}{dt'}\delta\Omega_\beta\Omega_\gamma + \left(h_\alpha + 2\lambda\Omega_\alpha\right)\delta\Omega_\alpha + \delta\lambda\left(||\Omega||^2 + \frac{1}{4}||\delta\Omega||^2 - 1\right)\right] \\ &+S^2\Delta^2\int dt'\int dt''\left[K^{(+)}(t',t'') + K^{(-)}(t'',t')\right]\delta\boldsymbol{\Omega}(t')\cdot\boldsymbol{\Omega}(t'') \\ &+\frac{1}{2}S^2\Delta^2\int dt'\int dt''\left[K^{(K)}(t',t'')\right]\delta\boldsymbol{\Omega}(t')\delta\boldsymbol{\Omega}(t'') + \mathcal{O}(\delta\boldsymbol{\Omega}^3).\end{aligned} \tag{2.31}$$

We have gotten a more extensive action than in 2.23, and the probability now is defined by several path integrals over spin, Lagrangian multiplier and their fluctuations :

$$\mathbb{P}[\hat{\Omega},t] = \int_{\boldsymbol{\Omega}(t)=\hat{\Omega}}(\mathcal{D}\Omega\mathcal{D}\delta\Omega\mathcal{D}\lambda\mathcal{D}\delta\lambda)\exp\left\{\frac{i}{\hbar}S[\Omega,\delta\Omega,\lambda,\delta\lambda]\right\}. \tag{2.32}$$

The significant advantage of these expressions is that we can directly integrate the Lagrangian multiplier fluctuation ($\mathcal{D}\delta\lambda$) since it only appears linearly in the action. The result is a delta function that enforces that the classical direction plus the fluctuation still lies in each site's unit sphere. That leaves us with the condition:

$$||\Omega||^2 = 1 - \frac{1}{4}||\delta\Omega||^2, \tag{2.33}$$

this result is simply the consequence of the original condition on the contour time. However, when we try to implement this condition in the effective real-time action, it only gives higher than second-order terms in $\delta\Omega$. Therefore, in the following sections, we neglect it and consider that the $\boldsymbol{\Omega}(t)$ lies in the unit sphere, i.e., $||\Omega(t)||^2 - 1 = 0$.

### 2.3.1. Equation of motion

The remaining fluctuation field $\delta\Omega$ makes it complicated to obtain insightful notions of the classical part dynamics since $K^{(\pm)}$ coupled them. This problem gets even more problematic due to the non-trivial kernel $K^{(K)}$ as weight factor of the quadratic term in $\delta\Omega$. This complication can be simplified if we transform the quadratic term, using the *Hubbard-Stratonovich* (H-S) transformation [22, 46] to replace the fluctuation field's quadratic term by adding a new pure imaginary auxiliary field $\frac{i}{\hbar}\boldsymbol{\eta}$. To apply the transformation, we need to define the

inverse of the Keldysh kernel as

$$\int_{-\infty}^{\infty} dt'' K^K(t,t'')[K^K(t'',t')]^{-1} = \delta(t-t'). \tag{2.34}$$

We can now perform the transformation that is, broadly speaking, a direct gaussian integration of the auxiliary field. Which results in the quadratic term that we want to replace. So, the last term in equation (2.31) can now be written as the path integral

$$\int \mathcal{D}\boldsymbol{\eta} \exp\Big\{\Big[-\frac{1}{2}\int_{-\infty}^{t}\int_{-\infty}^{t} dtdt' \eta^i(t)[-i\hbar S^2\Delta^2 K^{(K)}(t,t')\delta^{ij}]^{-1}\eta^j(t') + \frac{i}{\hbar}\int_{-\infty}^{t} dt \boldsymbol{\eta}\cdot\delta\boldsymbol{\Omega}\Big]\Big\}. \tag{2.35}$$

We can see that the "path integral" representation of the probability density got bigger, but easier. This simplification is due to the fluctuation field $\delta\boldsymbol{\Omega}$ appears only linearly, allowing us to integrate it into a delta-functional. From where we define a constraint vector $\boldsymbol{C}$ that imposes a relation between the rest of the fields. The final version of the probability density is

$$\mathbb{P}[\hat{\boldsymbol{\Omega}},\lambda,t] = \int \mathcal{D}\boldsymbol{\eta}\int_{\boldsymbol{\Omega}(t)=\hat{\Omega}}(\mathcal{D}\Omega\mathcal{D}\lambda)\delta(\boldsymbol{C})\exp\Big[-\frac{1}{2}\int dt\int dt'\eta^i(t)[-i\hbar S^2\Delta^2 K^{(K)}(t,t')\delta^{ij}]^{-1}\eta^j(t')\Big], \tag{2.36}$$

where the constrain vector is defined as

$$C^i \equiv \hbar S\epsilon^{ijk}\Omega^j\frac{d\Omega^k}{dt} + Sh^i + 2\lambda\Omega^i + \eta^i + S^2\Delta^2\int[\delta^{ij}K^{(+)}(t,t') + \delta^{ji}K^{(-)}(t',t)]\Omega^j(t')dt'. \tag{2.37}$$

This relation is what we have been looking for, but it still has the inconvenient Lagrangian multiplier $\lambda$. We no longer need this field because its primary purpose was to enforce that the spin direction in the contour time lies in the unit sphere, and at the end of the last section, we have already done it. We can apply the cross product to the above equation to get rid of it, using the classical direction's unitary condition. Therefore, the equation of motion for the spin direction is:

$$\hbar S\frac{d\boldsymbol{\Omega}(t)}{dt} = \boldsymbol{\Omega}(t)\times\left[(S\mathbf{h}+\boldsymbol{\eta}) + S^2\int_{-\infty}^{\infty} dt'\bar{K}(t,t')\boldsymbol{\Omega}(t')\right], \tag{2.38}$$

where for notation simplicity we define

$$\bar{K}(t,t') = -\Delta^2[K^{(+)}(t,t') + K^{(-)}(t',t)] = -2\Delta^2 K^{(+)}(t,t'). \tag{2.39}$$

The last equality comes from the symmetry of the kernel definition in (2.29) under interchange the sign $(+)\leftrightarrow(-)$ while interchanging $t\leftrightarrow t'$. From equation (2.38), we see that $\boldsymbol{\eta}$ plays the role of a stochastic magnetic field. The auxiliary field inherits its stochastic nature from the fluctuating field, and we can characterize its one and two-point correlation functions as

$$\langle\boldsymbol{\eta}(t)\rangle = 0, \tag{2.40}$$

$$\langle\eta^\alpha(t)\eta^\beta(t')\rangle = -i\Delta^2\hbar S^2 K^{(K)}(t,t')\delta^{\alpha\beta}. \tag{2.41}$$

Up to this point, we have not studied in much detail the kernel itself. Apart from its definition (2.21) and that it can be expressed in the usual Green's function decomposition (2.28), (2.29) and (2.30). It is not easy to obtain analytical information from the kernel in its current state. However, if we assume some considerations in the system's time scales, we can obtain some insight into the kernel behavior, at least in the low energy regime.

### 2.3.2. Low energy approximation

We can easily spot that the integral kernel $K(t,t')$ is the complicated term in equation 2.38, and we need a way to deal with it. This kernel has all the information about the interaction between the itinerant electrons and the localized spin. It covers the whole range of energies. With that in mind, it is clear that the kernel's full analytical expression and the effects on the system are far from easy to calculate. Nevertheless, to maintain consistency with our first approximation to get equations (2.36) and (2.38), weak s-d interaction, we can neglect the kernel's high energies processes. Besides the second approximation, where we neglect high order terms in the fluctuation part of the localized spin. So, we first need the energy representation of the integral kernel. To do it, we perform a Fourier transformation in the time domain the advanced, retarded, and Keldysh component in equations (2.29) and (2.30), we get:

$$K^{(\pm,K)}(t,t') \equiv \int_{-\infty}^{\infty} \frac{d(\epsilon)}{2\pi} e^{-\frac{i}{\hbar}\epsilon(t-t')} K^{(\pm,K)}(\epsilon) \tag{2.42}$$

$$K^{(\pm)}(\epsilon) = -\int \frac{d\epsilon'}{2\pi} \int \frac{d\epsilon''}{2\pi} \frac{[G^{<}(\epsilon')G^{>}(\epsilon'') - G^{>}(\epsilon')G^{<}(\epsilon'')]}{(\epsilon \pm i\eta + \epsilon'' - \epsilon')} \tag{2.43}$$

$$K^{(K)}(\epsilon) = -2i\pi \int \frac{d\epsilon'}{2\pi} \int \frac{d\epsilon''}{2\pi} \delta(\epsilon - \epsilon' + \epsilon'')[G^{<}(\epsilon')G^{>}(\epsilon'') + G^{>}(\epsilon')G^{<}(\epsilon'')] \tag{2.44}$$

In the above expressions, we have made use of the fact that for the steady-state regime, the kernels only depend on the time difference, which in the end, is the regime we want to study. Now we have reduced the problem to calculate and manage the electronic Green's function. We obtain them from the Dyson equation:

$$[\epsilon^{\pm} - 2\hbar\Sigma^{(\pm)}(\epsilon)]G^{(\pm)} = 1 \tag{2.45}$$

Where $\Sigma^{(\pm)}(\epsilon)$ in equation 2.45 are the advanced and retarded self-energies of a semi-infinite chain. These functions represent the lead's effects on the system, as shown in [12, 9, 10, 39]. To determine their analytical expression, we considered each lead to be in thermal equilibrium at temperature T, and chemical potential $\mu_L$ and $\mu_R$ for the left and right lead, respectively. A handy tool to gain interpretation of the equations in energy representation is the *spectral function* $A(\epsilon)$, defined as

$$A(\epsilon) = i[G^{(+)}(\epsilon) - G^{-}(\epsilon)], \tag{2.46}$$

this function allows as to express the needed components of the electronic Green's function as shown in [9, 10]

$$-iG^{<}(\epsilon) = \frac{A(\epsilon)}{2} \sum_{s\in\{L,R\}} n_F(\epsilon - \mu_s) \tag{2.47}$$

$$iG^{>}(\epsilon) = \frac{A(\epsilon)}{2} \sum_{s\in\{L,R\}} [1 - n_F(\epsilon - \mu_s)] \tag{2.48}$$

where $n_F(\epsilon)$ is the Fermi-Dirac distribution. The spectral function will allow us to dig deeper into finding an interpretative, analytical expression for the integral kernel $\bar{K}$ in equation (2.38). A Taylor expansion easily finds the low energy approximation up to first order for $\epsilon$ around 0 in equations (2.43) and (2.44). As explained in this chapter's introduction, our main goal is to study the dynamics mediated by the non-equilibrium electrons, so we introduce an imbalance between the chemical potential through an external voltage difference between them: $\mu_L = \mu_F + \frac{|e|V}{2}$ and $\mu_R = \mu_F - \frac{|e|V}{2}$. This unbalance gives us two control parameters, the band of voltage and the center of the band. Applying the above expressions, we find that equation (2.43) is, in terms of the spectral function, an expression more easily interpreted:

$$K^{(\pm)}(\epsilon) = K^{(\pm)}(\epsilon = 0) \mp \frac{i}{8\pi} \left( A^2(\mu_F + \frac{|e|V}{2}) + A^2(\mu_F - \frac{|e|V}{2}) \right) \epsilon. \tag{2.49}$$

We have used the approximation of a delta function for the derivative of the Fermi distribution, ${n'}_F(\epsilon) \approx -\delta(\epsilon)$. Since we think on a low energy approximation, a possible low-temperature experiment seems reasonable and justifies that approximation. Here we use the Cauchy Principal value identity to work the complex-valued denominator, due to $\pm i\delta$. Now we can come back to the integral in the equation of motion (2.38) and approximate it as:

$$\mathbf{\Omega}(t) \times \int_{-\infty}^{\infty} \bar{K}(t,t')\mathbf{\Omega}(t')dt' \simeq -\hbar\alpha(V)\mathbf{\Omega}(t) \times \frac{d\mathbf{\Omega}(t)}{dt} \tag{2.50}$$

We see that the energy-independent term in equation (2.49) plays no role in the spin direction dynamics. Replacing the above expression in the equation (2.38), we see that a Landau-Lifshitz-Gilbert equation (LLG) rules the spin direction dynamics with $\alpha(V)$ as the effective damping.

$$\alpha(V) = \frac{\Delta^2}{4\pi}[A^2(\mu_F + \frac{|e|V}{2}) + A^2(\mu_F - \frac{|e|V}{2})] \tag{2.51}$$

so the final form of 2.38 is

$$\hbar S\frac{d\mathbf{\Omega}(t)}{dt} = \mathbf{\Omega}(t) \times \left( S\boldsymbol{h} + \boldsymbol{\eta} - S^2\hbar\alpha(V)\frac{d\mathbf{\Omega}(t)}{dt} \right) \tag{2.52}$$

With this, we have found an elegant expression for the equation of motion that includes the interaction of the itinerant electrons with the localized spin as an effective damping and a stochastic magnetic field. This result presents a very interesting microscopic derivation of the Landau-Lifshitz-Gilbert equation and gives an analytical justification of the damping contribution rather than the usual phenomenological reasoning to include it. A significant detail that needs to be noted is that $\alpha(V) \geq 0$, meaning that this interaction can only extract energy from the molecule and give it to the electrons passing through. Applying the same mechanism explained for the advanced and retarded components to the Keldysh component,

we find that

$$K^{(K)}(\epsilon) = \frac{-i}{2}\int \frac{d\epsilon''}{2\pi} A^2(\epsilon'')\{n_F(\mu_L - \epsilon'') + n_F(\mu_R - \epsilon'')\}[n_F(\epsilon'' - \mu_L) + n_F(\epsilon'' - \mu_R)], \quad (2.53)$$

this expression is hardly as simple as the one we find for the advanced and retarded component, but if we see the equilibrium situation where $\mu_L = \mu_R = \mu_F$ for some illumination, we can see that the Keldysh component $K_0^{(K)}$ in the low energy approximation is

$$K_0^{(K)}(\epsilon \to 0) = 2\frac{k_B T}{i\Delta^2}\alpha_0. \quad (2.54)$$

Where $\alpha_0$ in the above equation is the equilibrium value of the effective damping. With this, we see that $K^{(K)}$ defines an effective temperature, just like $K^{(\pm)}$ define an effective damping. Another way to see this relationship between the Keldysh and the advanced and retarded Green's functions is through the Fluctuation-Dissipation theorem that connects the fluctuating part of a system, the Keldysh component, with the dissipation in the same system, the advanced and retarded components. Theorem's applicability has been shown to hold at equilibrium in [34] and further extended to non-equilibrium in [13]. In both cases, they show the same idea of the effective temperature from the Keldysh component as:

$$k_B T_{eff}(V) \equiv \frac{i\Delta^2}{2\alpha(V)} K^{(K)}(\epsilon) \quad (2.55)$$

We find a more detailed deduction of this relationship in the next chapter when studying the stochastic field's implications in the equation of motion. For now, we can see that the two-points correlation function of the auxiliary field in equation (2.41) is

$$\langle \eta^\alpha(t)\eta^\beta(t')\rangle = [-i\Delta^2\hbar^2 S^2 K^{(K)}(\epsilon \to 0)]\delta^{\alpha\beta}\delta(t - t'). \quad (2.56)$$

We see that the correlation, after the low-energy approximation, is local in time and is diagonal in its vector components, both essential characteristics that will simplify much work in the next chapter when we study the effects of the stochastic nature of equation (2.52).

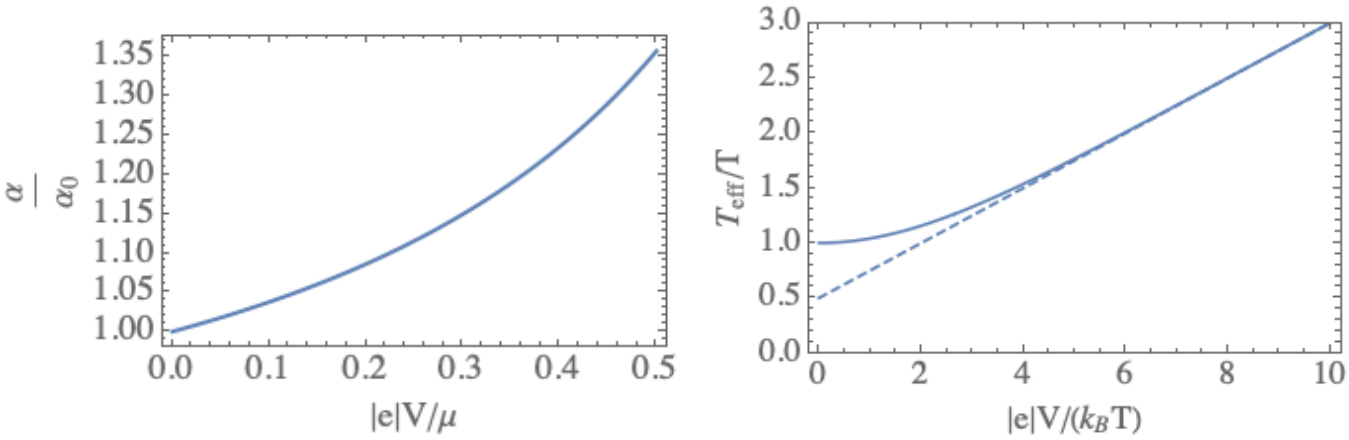


Figure 2.3: Effective damping and effective temperature, considering a symmetric case with $t_L = 1[meV]$ and $t_R = 1[meV]$, along with the hopping between electrodes sites $J = 1[meV]$, as presented in [34]. We can see that the effective temperature has an asymptotic value for high voltages as shown in equation 2.57.

### 2.3.3. Effective temperature and damping: Numerical analysis

Now that we have found the mathematical expressions for the effective temperature $T_{eff}(V)$ and damping $\alpha(V)$, we can explore in detail the numerical aspects of those expressions. We compare our results with the ones presented in [34], from where the authors developed the framework and presented a microscopic derivation of the stochastic Landau-Lifshitz-Gilbert equation for the spin direction of a molecule under the effects of electrical current. We study the effective temperature and damping as function of the bias voltage at a fixed value of the chemical potential $\mu_F = 1[meV]$.

A fascinating result for the effective temperature appears when we study the limit where the voltage is much larger than the system's temperature. In this limit, the authors of [34] found that $T_{eff}(V)$ has a simple asymptotic expression.

$$k_B T_{eff} \simeq \frac{|e|V}{4} + \frac{1}{2} k_B T \tag{2.57}$$

## 2.4. Spin dimer

The spin dimer system [12] is the natural extension of the monomer system. Since we only add another molecule, at first sight, it might not look like a very exciting system to work with. However we find some new phenomena that the monomer system can not include; effective interactions inside the device. Like the last case, this system consists of two leads connected to the device by the connection Hamiltonian for each one in equation (2.3) and (2.4), as shown in figure 2.4. Only now, the device consists of two molecules with total spin S and unit vector $\mathbf{\Omega}_a$, where $a \in \{1, 2\}$. Since now we have a two-site-device, we cannot reduce the full electronic Green's expression to a single function, like in equation (2.19). Instead, we

deal with a 4x4 matrix from the general expression (2.16) as:

$$iG_{a\sigma;b\sigma'}(t,t') \equiv \langle \mathcal{T}\psi_{a\sigma}(t)\psi^*_{b\sigma'}(t')\rangle. \tag{2.58}$$

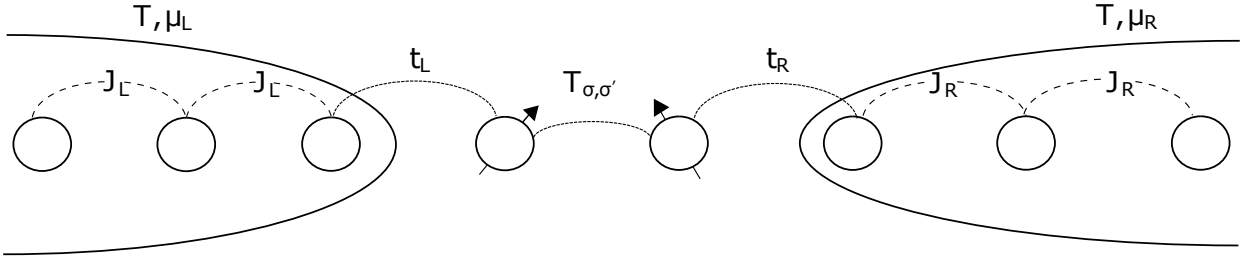


Figure 2.4: Sketch of a one-dimensional chain toy model that includes two semi-infinite leads and an N-sites device.

Clearly, in this case, due to the hopping matrix $\mathbb{T}$, more specifically, the spin-orbit coupling $t$, the system presents a preferred direction to interact with the itinerant electrons. So $\langle \boldsymbol{s}(t)\rangle \neq 0$, and we have to calculate it. For now, we can establish the framework using the general expression shown in equations (2.13) and (2.14) with $N = 2$, so we find that:

$$\mathcal{S} = \int_{C^t} dt \sum_a \{-\hbar S \frac{d\omega_a}{dt} - \mathcal{E}[\boldsymbol{\Omega}_a(t)] + S\Delta\langle \mathbf{s}_a\rangle \cdot \Omega_a(t)\} + \int_{C^t} dt \int_{C^t} dt' \sum_{abij} \Delta^2 S^2 K^{ij}_{ab}(t,t')\Omega^i_a(t)\Omega^j_b(t') \tag{2.59}$$

is the *effective action* for the spin dimer, where we already made the second-order approximation on $\Delta$. The probability keeps the same structure, but now includes two path integrals, one for each spin, like:

$$\mathbb{P}[\boldsymbol{\Omega}_1, \boldsymbol{\Omega}_2, t] = \int_{\boldsymbol{\Omega}_1(t)=\hat{\boldsymbol{\Omega}}_1} \int_{\boldsymbol{\Omega}_2(t)=\hat{\boldsymbol{\Omega}}_2} \mathcal{D}\boldsymbol{\Omega}_1 \mathcal{D}\boldsymbol{\Omega}_2 \delta(|\boldsymbol{\Omega}_1|^2 - 1)\delta(|\boldsymbol{\Omega}_2|^2 - 1) e^{\frac{i}{\hbar}\mathcal{S}}. \tag{2.60}$$

The above expressions for the action and the probability function are defined over the Keldysh contour time, so we have to map it back to real-time, just like for the monomer case. In order to do it, we have to define the components of the integral kernel $K^{ij}_{ab}(t,t')$ in the Keldysh contour using equations (1.12), (1.13) and (1.14). So we have that

$$K^{ij}_{ab}(t,t') = \Theta(t-t')K^{ij\ >}_{ab}(t,t') + \Theta(t'-t)K^{ij\ <}_{ab}(t,t'), \tag{2.61}$$

$$K^{ij\ (\pm)}_{ab}(t,t') = \pm\Theta\left(\pm(t-t')\right)\left[K^{ij\ >}_{ab}(t,t') - K^{ij\ <}_{ab}(t,t')\right], \tag{2.62}$$

$$K^{ij\ (K)}_{ab}(t,t') = K^{ij\ >}_{ab}(t,t') + K^{ij\ <}_{ab}(t,t'). \tag{2.63}$$

Here we notice the first advantage of our early study of the monomer case. We see that the calculations done to obtain the monomer case's real-time action are straightforwardly

applicable to the dimer case since, in essence, we only have to repeat the procedure for each field, $\mathbf{\Omega}_1$ and $\mathbf{\Omega}_2$. Although it is a bit more complicated than just that because the fields are coupled, it still follows the same steps. So, we split the contour time into the forward and backward paths like in (2.27). Along with the change of variables in equation (2.24) for both spins. We obtain that the action is written as

$$\begin{aligned}\mathcal{S} = \int dt' \sum_a \left[ \hbar S \epsilon_{\alpha\beta\gamma} \frac{d\Omega_a^\alpha}{dt'} \delta\Omega_a^\beta \Omega_a^\gamma + \delta\lambda_a \left( ||\mathbf{\Omega}_a||^2 + \frac{1}{4}||\delta\mathbf{\Omega}_a||^2 - 1 \right) \right] \\ \left( -\frac{d\mathcal{E}}{d\mathbf{\Omega}_a}[\mathbf{\Omega}_a] + S\Delta\langle \boldsymbol{s}_a \rangle \cdot \mathbf{\Omega}_a + 2\lambda_a \mathbf{\Omega}_a \right) \delta\mathbf{\Omega}_a + \\ S^2\Delta^2 \int dt' \int dt'' \sum_{abij} \delta\mathbf{\Omega}_a^i(t') \left[ K_{ab}^{ij\ (+)}(t', t'') + K_{ba}^{ij\ (-)}(t'', t') \right] \mathbf{\Omega}_b^j(t'') + \\ \frac{1}{2} S^2\Delta^2 \int dt' \int dt'' \sum_{abij} \delta\mathbf{\Omega}_a^i(t') \left[ K_{ab}^{ij\ (K)}(t', t'') \right] \delta\mathbf{\Omega}_b^j(t'') + \mathcal{O}(\delta\mathbf{\Omega}_a^3). \end{aligned} \tag{2.64}$$

Where again, we introduce the Lagrangian multipliers, $\lambda_a$, to enforce that the spin's direction $\mathbf{\Omega}_a$, in the Keldysh time, lies in the unit sphere, and the Lagrangian multiplier's fluctuation, $\delta\lambda_a$, to map it back to real-time. Following the same argument presented in the last section, we expand the action up to second order in $\delta\mathbf{\Omega}_a$, so we neglect the rapid fluctuation contribution to the spin's dynamics. We can see that, as before, the integration of $\delta\lambda_a$ presents higher-order contributions in terms of $\delta\mathbf{\Omega}_a$. So, even in the dimer configuration, we find that both spin vectors lie on the unit sphere under our approximations. We describe the probability $\mathbb{P}$ by several Path integrals over the spin direction, its fluctuation, and the Lagrangian multiplier

$$\mathbb{P}[\hat{\mathbf{\Omega}}_1, \hat{\mathbf{\Omega}}_2, t] = \prod_a \int_{\mathbf{\Omega}_a(t)=\hat{\Omega}_a} (\mathcal{D}\Omega_a \mathcal{D}\delta\Omega_a \mathcal{D}\lambda_a) \exp\left\{ \frac{i}{\hbar} S[\Omega_a, \delta\Omega_a, \lambda_a] \right\}. \tag{2.65}$$

This expression is more complicated than the former one, but it shows us that besides the extra indices from the sites, the non-zero average of the itinerant spin and the integral kernel is even more intricate than before, the structure of the probability remains unchanged.

### 2.4.1. Equation of motion

We see the same problem from equations (2.64) and (2.65) that the one we have encountered in the last section. The fluctuating part $\delta\mathbf{\Omega}_a$ makes it complicated to extract real information on the classical part $\mathbf{\Omega}_a$ due to the quadratic terms and the Keldysh Green's function $K^{(K)}$. Naturally, we apply the Hubbard-Stratonovich transformation to each field fluctuating part and obtain two auxiliary fields, $\boldsymbol{\eta}_a$. In the next chapter, we will study the implications of these new fields on the localized spins. This transformation adds one integral for each new auxiliary field, which is highly unrecommended because it makes a more extended-expression. Nevertheless, it simplifies the integration of the fluctuating part of each spin. The final form of the probability density is:

$$\mathbb{P}[\boldsymbol{\Omega}_1,\boldsymbol{\Omega}_2,t]=\prod_a\int\mathcal{D}\boldsymbol{\eta}_a\int\mathcal{D}\boldsymbol{\Omega}_a\mathcal{D}\lambda_a\delta(\boldsymbol{C_a})\exp\left\{-\frac{1}{2}\sum_{ab;ij}\int dt'\int dt''\eta_a^i(t')\left[\frac{(K_{ab}^{ij\ (K)}(t',t''))^{-1}}{-i\hbar S^2\Delta^2}\right]\eta_b^j(t'')\right\}. \tag{2.66}$$

We have defined the inverse of the Keldysh component, like in equation (2.34), and two constraint vectors, $\boldsymbol{C}_a$, from integrating each fluctuating parts at the site a,

$$C_a^i(t)\equiv\hbar S\epsilon_{ijk}\Omega_a^j\frac{d\Omega_a^k}{dt}-\frac{\partial\mathcal{E}}{\partial\Omega_a^i}[\boldsymbol{\Omega}_a]+S\Delta\langle s_a^i\rangle+2\lambda_a\Omega^i+\eta^i+S^2\Delta^2\int dt'\left[K_{ab}^{ij\ (+)}(t,t')+K_{ba}^{ji\ (-)}(t',t)\right]\Omega_b^j(t'). \tag{2.67}$$

As for the monomer case, this vector gives us the relations we are looking for, the equation of motion for each spin. Once we get rid of the Lagrangian multiplier, the equations of motion are:

$$\begin{aligned}\hbar S\frac{d\Omega_a^i(t)}{dt}=&\left(\hat{\Omega}_a\times\left[-\frac{\partial\varepsilon[\hat{\Omega}_a]}{\partial\hat{\Omega}_a}+S\Delta\langle\vec{s}_a(t)\rangle+\vec{\eta}_a(t)\right]\right)^i\\&+\sum_{bklm}\epsilon^{ikl}\Omega_a^k(t)\int dt'S^2\Delta^2\underbrace{\left[\mathcal{K}_{ab}^{lm\ (+)}(t,t')+\mathcal{K}_{ba}^{ml\ (-)}(t',t)\right]}_{\chi_{ab}^{lm}(t-t')=2\mathcal{K}_{ab}^{lm\ (+)}(t,t')}\Omega_b^m(t')\end{aligned} \tag{2.68}$$

here we can define the magnetic susceptibility $\chi_{ab}^{ij}(t-t')$, to simplify the notation. From this equation, we see that each auxiliary field, $\boldsymbol{\eta}_a(t)$, only affects the equation of their related site. This field inherits a stochastic nature from the fluctuating nature of the fluctuating part. We can characterize it by the one and two-point correlation functions defined by the Keldysh components, like

$$\langle\boldsymbol{\eta}_a(t)\rangle=0, \tag{2.69}$$

$$\langle\eta_a^\alpha(t)\eta_b^\beta(t')\rangle=-i\Delta^2\hbar S^2K_{ab}^{\alpha\beta\ (K)}(t,t'). \tag{2.70}$$

If we look closely at the structure of equation (2.68), we can see that the stochastic auxiliary fields appear in the same way as a magnetic field from the Zeeman interaction. This means that the fluctuating part of the spin direction in both sites adds random magnetic fields to each site.

Now we have to explore a little more in the integral kernel's nature. As shown in the last section, the simplest way is through the energy representation of the electronic Green's functions. Following the steps from section 2.3.2 and adapting it to the dimer configuration we can obtain a compute-able expression for $K^{(\pm)}$ and $K^{(K)}$. Using the same reasoning of section 2.3, we can restrict our analysis to a low energy range to satisfy the approximations done to obtain the equation of motion for the, now, localized classical spins at each site. Therefore, we can perform a Taylor expansion to obtain the low energy behavior and extract all the information that we need to understand the dynamics of the system. To focus on the relevant results and the physics behind them, we left the step by step deduction of each equation in

Appendix A. Here we only show the relevant expressions and final results to analyze.

Applying the decomposition of equations (2.61), (2.62), and (2.63) to the electronic Green's function, we find the relation between the advanced, retarded ,and Keldysh components of $K_{ab}^{ij}$ in the energy representation, with the Greater and Lesser components of $G_{a\sigma;b\sigma'}(\epsilon)$. So we have that

$$K_{ab}^{ij\ (\pm)}(\epsilon) = \frac{-1}{8\hbar}\sum_{\sigma\sigma'\mu\mu'}\tau^{i}_{\sigma\sigma'}\tau^{j}_{\mu\mu'}\int\frac{d\epsilon'}{2\pi}\frac{d\epsilon''}{2\pi}\frac{G^{>}_{a\sigma';b\mu}(\epsilon')G^{<}_{b\mu';a\sigma}(\epsilon'') - G^{<}_{a\sigma';b\mu}(\epsilon')G^{>}_{b\mu';a\sigma}(\epsilon'')}{\epsilon^{\pm}-\epsilon'+\epsilon''} \tag{2.71}$$

$$\begin{aligned}K_{ab}^{ij\ (K)}(\epsilon) = -\frac{i\pi}{4\hbar}\sum_{\sigma\sigma'\mu\mu'}\tau^{i}_{\sigma\sigma'}\tau^{j}_{\mu\mu'}\int\frac{d\epsilon'}{2\pi}\frac{d\epsilon''}{2\pi}\delta(\epsilon-\epsilon'+\epsilon'')[G^{>}_{a\sigma';b\mu}(\epsilon')G^{<}_{b\mu';a\sigma}(\epsilon'')+\\ +G^{<}_{a\sigma';b\mu}(\epsilon')G^{>}_{b\mu';a\sigma}(\epsilon'')].\end{aligned} \tag{2.72}$$

Where $\epsilon^{\pm} = \epsilon \pm i\delta$ is added for convergence in the integration as usual [2, 33]. Here we can see that equations (2.71) and (2.72) are the clear extension of equations (2.43) and (2.44) with the addition of site and spin dependence on $G(t,t')$. With the Dyson equation and the steady-state kinetic equation [9, 10, 12], we find the exact solution for $G^{\lessgtr}$ from the device's Hamiltonian and the self-energies of the leads. When we analyze that solution for $G^{\lessgtr}$, we see that the intricate site and spin dependence in the 4x4 matrix, can be decomposed into four new 2x2 matrices as

$$G^{\lessgtr}_{a\sigma;b\sigma'}(\epsilon) = G_{ab}^{(s)\ \lessgtr}(\epsilon)\mathbb{I}_{\sigma\sigma'} + G_{ab}^{(t)\ \lessgtr}(\epsilon)[\boldsymbol{t}\cdot\boldsymbol{\tau}]_{\sigma\sigma'}. \tag{2.73}$$

This decomposition is actually a direct result of the symmetry on the original theory over spin. When we replace equation (2.73) in equation (2.71) it shows an essential separation because it allow us to work out the spin indices independently of the site indices. Using the Pauli matrices' properties, we see that $K_{ij}^{(\pm)}$ have three very characteristic tensors that work the spatial indices; a fully symmetric part ($\delta^{ij}$), an antisymmetric part ($\epsilon^{ijk}\hat{t}^{k}$), and asymmetric part ($\hat{t}^{i}\hat{t}^{j}$). So we can write the advanced and retarded components as:

$$K_{ab}^{ij\ (\pm)}(\epsilon) = -\frac{1}{4}\int\frac{d\epsilon'}{2\pi}\frac{d\epsilon''}{2\pi}\frac{\left[\mathcal{J}_{ab}(\epsilon',\epsilon'')\delta^{ij} + i\mathcal{D}_{ab}(\epsilon',\epsilon'')\epsilon^{ijk}\hat{t}^{k} + 2\bar{\Gamma}_{ab}(\epsilon',\epsilon'')\hat{t}^{i}\hat{t}^{j}\right]}{\epsilon^{\pm}-\epsilon'+\epsilon''}. \tag{2.74}$$

Therefore, we tentatively call their weight factors: the symmetric $\mathcal{J}_{ab}$, antisymmetric $\mathcal{D}_{ab}$, and anisotropic $\bar{\Gamma}_{ab}$ full interactions. In a later section, we will check if they follow the expected symmetries. In Appendix A, we present a detailed derivation of the analytical expression of these interactions. We treat them as "full interactions" because up to now, we have not made the low energy approximation, so they contain the kernels' full behavior and information from the interaction with the itinerant electrons. However, as we argue at the beginning of the section, we are not interested in their full behavior, nor are we allowed to describe the full range of energies. Here we call the result shown in Appendix A, where we obtain that from each full interaction we get a low energy effective interaction and damping as: $\mathcal{J}_{ab} \mapsto \{J_{ab}, \alpha_{ab}\}$, $\mathcal{D}_{ab} \mapsto \{D_{ab}, \beta_{ab}\}$ and $\bar{\Gamma}_{ab} \mapsto \{\Gamma_{ab}, \gamma_{ab}\}$, respectively. With those definitions we can come back to the equation of motion and obtain:

$$\hbar S\frac{d\boldsymbol{\Omega}_a}{dt}(t) = \boldsymbol{\Omega}_a \times \left[-\frac{\partial}{\partial \boldsymbol{\Omega}_a}\mathcal{E}^a_{eff}[\hat{\Omega}_a(t), \hat{\Omega}_b(t)] + \boldsymbol{\eta}_a(t) - \hbar S^2 \sum_b \bar{\boldsymbol{\alpha}}_{ab}\frac{d\boldsymbol{\Omega}_b}{dt}(t)\right]. \tag{2.75}$$

We have defined the effective energy at site $a$ due to the spin direction of both spins at time t, $\mathcal{E}^a_{eff}$, and the effective damping tensor,$\bar{\boldsymbol{\alpha}}_{ab}$, as

$$\begin{aligned}\mathcal{E}^a_{eff}[\hat{\Omega}_a(t), \hat{\Omega}_b(t)] = \mathcal{E}[\hat{\Omega}_a] - S\Delta\langle \boldsymbol{s}_a(t)\rangle \cdot \boldsymbol{\Omega}_a(t) - \hbar S^2\Delta^2 \sum_b \Big[J_{ab}\boldsymbol{\Omega}_a \cdot \boldsymbol{\Omega}_b + \\ + iD_{ab}\boldsymbol{t}\cdot(\boldsymbol{\Omega}_a \times \boldsymbol{\Omega}_b) + 2\Gamma_{ab}(\boldsymbol{\Omega}_a \cdot \boldsymbol{t})(\boldsymbol{\Omega}_b \cdot \boldsymbol{t}) - \frac{1}{2}\Gamma_{aa}(\boldsymbol{\Omega}_a \cdot \boldsymbol{t})^2\Big], \end{aligned} \tag{2.76}$$

$$\bar{\alpha}^{ij}_{ab} = \Delta^2\left[\alpha_{ab}\delta^{ij} + i\beta_{ab}\epsilon^{ijk}\hat{t}^k + 2\gamma_{ab}\hat{t}^i\hat{t}^j\right]. \tag{2.77}$$

Here we notice the resemblance with equation 2.52, but due to the spin-orbit coupling, the expression is more challenging, and the damping is now a non-diagonal tensor. On the other hand, if we apply equation (2.73) in the Keldysh component $K^{ij\ (K)}_{ab}$, along with the low energy approximations, we find that up to first order in $\epsilon$, the Keldysh component is

$$K^{ij\ (K)}_{ab}(\epsilon) = j_{ab}\delta^{\alpha\beta} + id_{ab}\epsilon^{\alpha\beta k}\hat{t}^k + 2g_{ab}\hat{t}^\alpha\hat{t}^\beta. \tag{2.78}$$

Where we see that $K^{(K)}$ has the same vectorial structure as the advanced and retarded functions, but in contrast with those expressions, the Keldysh component is constant in energy. Therefore, with equations (2.78) and (2.70), we find the final version of the two-point correlation function for the stochastic magnetic field as

$$\langle \eta^\alpha_a(t)\eta^\beta_b(t')\rangle = -i\Delta^2\hbar S^2\left[j_{ab}\delta^{\alpha\beta} + id_{ab}\epsilon^{\alpha\beta k}\hat{t}^k + 2g_{ab}\hat{t}^\alpha\hat{t}^\beta\right]\delta(t-t'). \tag{2.79}$$

This correlation function is far from the diagonal one we found for the monomer configuration. This complication comes essentially from the spin-orbit coupling rather than the addition of another molecule. When we look at the antisymmetric and the asymmetric damping's analytical expressions, it is clear that those terms drop to zero for a neglectable spin-orbit coupling, and the Keldysh component is a diagonal again. The antisymmetric and the asymmetric interactions drop to zero as well when there is no spin-orbit coupling. The physical reasoning of all these comes from the loss of a preferred direction. Therefore, the only possible interaction between the spin has to be a symmetric interaction.

### 2.4.2. One spin fixed

When we look at equation (2.75), we can anticipate a much longer and harder treatment to obtain the steady-state probability density than the one needed to deal with equation (2.52). However, if we study the case where we somehow manage to fix one of the localized spin's directions, the equation of motion for the free spin simplifies considerably. Due to the symmetry in the system, we can set the localized spin at site 1 as fixed along $\hat{m}$. Later it will be parallel to the external magnetic field, and let $\boldsymbol{\Omega}_2$ evolve in time. Now, instead of two coupled Langevin equations, we only contemplate effective interactions with a fixed localized spin. We can drop the sub-index in the $\boldsymbol{\Omega}_a$ vectors, and re-name them as $\hat{m}$ for $\boldsymbol{\Omega}_1$, and $\boldsymbol{\Omega}$ for the spin's direction of site 2. Therefore, the final effective energy of the localized spin at

site 2 is

$$\mathcal{E}'[\Omega,\hat{m},\hat{t}] = \mathcal{E}[\Omega] - S\Delta\langle s\rangle\cdot\Omega - \hbar S^2\Delta^2\Big[J_{21}\Omega\cdot\hat{m} + D_{21}\hat{t}\cdot(\Omega\times\hat{m}) + 2\Gamma_{21}(\Omega t)(\hat{m}\cdot\hat{t}) + \Gamma_{22}(\Omega t)^2\Big]. \tag{2.80}$$

When we study the damping tensor, we see that the relevant component turns out to be $\bar{\boldsymbol{\alpha}}_{22}$, and we can define the damping factors

$$i\hbar\Delta^2\{\alpha_{22},\beta_{22},\gamma_{22}\}\to\{\alpha,\beta,\gamma\}, \tag{2.81}$$

for simplicity in notation. Therefore, the final Langevin equation is

$$\hbar S\frac{d\boldsymbol{\Omega}}{dt} = \boldsymbol{\Omega}\times\left[\boldsymbol{H}+\boldsymbol{\eta} - \hbar S\{S\alpha\frac{d\boldsymbol{\Omega}}{dt} + S\beta(\frac{d\boldsymbol{\Omega}}{dt})\times\hat{\boldsymbol{t}} + S\gamma\hat{\boldsymbol{t}}(\hat{t}\cdot\frac{d\Omega}{dt})\}\right]. \tag{2.82}$$

where we have defined the effective field $\boldsymbol{H} = -\frac{\partial\mathcal{E}'}{\partial\boldsymbol{\Omega}}$. Now we can see that, even though equation (2.82) still depends on the spin's direction at site 1, it is a much simpler equation. The effect of the damping factors and how we can keep extracting information from this equation of motion will be studied in the next chapter. In the above equation, we notice that the relevant stochastic magnetic field, one is at site 2, i.e., $\boldsymbol{\eta}_2$. We can define the correlation terms as

$$-i\Delta^2\hbar S^2\{j_{22},id_{22},2g_{22}\}\to\{j,d,g\}, \tag{2.83}$$

as for the damping tensor for simplicity. Before we continue with the analysis of the equation of motion and its implication to an average value of the spin direction, we have to study different relations between the hopping parameters. These configurations will allow us to understand a little more the low energy representation of the system's electrical current effects.

### 2.4.3. Analysis of effective interactions

When we see the final equations for the effective interactions in Appendix A, we see that they are meant to be numerically calculated. However, if we define the spectral function (2.46) in a similar way as for the monomer case, we see that a little more information can be obtained but only for very characteristic cases, like equilibrium ($V=0$), symmetric comparison ($F(V)\sim F(-V)$) or index permutation. Those are the cases that we should pay special attention to because it will help us verify our assumptions of the kind of interaction we are looking at, with the aid of section 1.2. It also will help us to verify that we are computing each term right. First, we have to define the *partial spectral functions*:

$$A^{(s)}_{c;ab} = -2\hbar\left[G^{(s)(+)}_{ac}\,\mathrm{Im}\left(\Sigma^{(+)}_c\right)G^{(s)(-)}_{cb} + G^{(t)(+)}_{ac}\,\mathrm{Im}\left(\Sigma^{(+)}_c\right)G^{(t)(-)}_{cb}\right], \tag{2.84}$$

$$A^{(t)}_{c;ab} = -2\hbar\left[G^{(s)(+)}_{ac}\,\mathrm{Im}\left(\Sigma^{(+)}_c\right)G^{(t)(-)}_{cb} + G^{(t)(+)}_{ac}\,\mathrm{Im}\left(\Sigma^{(+)}_c\right)G^{(s)(-)}_{cb}\right], \tag{2.85}$$

so we can write the effective interactions in equations (A.23), (A.24) and (A.25), as:

$$\mathcal{J}_{ab}(\epsilon',\epsilon'') = \sum_{cd}[n_F(\epsilon''-\mu_d) - n_F(\epsilon'-\mu_c)]\left(A^{(s)}_{c;ab}(\epsilon')A^{(s)}_{d;ba}(\epsilon'') - A^{(t)}_{c;ab}(\epsilon')A^{(t)}_{d;ba}(\epsilon'')\right), \tag{2.86}$$

$$\mathcal{D}_{ab}(\epsilon',\epsilon'') = \sum_{cd}[n_F(\epsilon''-\mu_d) - n_F(\epsilon'-\mu_c)]\left(A^{(s)}_{c;ab}(\epsilon')A^{(t)}_{d;ba}(\epsilon'') - A^{(t)}_{c;ab}(\epsilon')A^{(s)}_{d;ba}(\epsilon'')\right), \tag{2.87}$$

$$\Gamma_{ab}(\epsilon',\epsilon'') = \sum_{cd}[n_F(\epsilon''-\mu_d) - n_F(\epsilon'-\mu_c)]A^{(s)}_{c;ab}(\epsilon')A^{(s)}_{d;ba}(\epsilon''). \tag{2.88}$$

The significant advantage of those expressions over the original ones comes from the separation of the site dependence and the non-equilibrium parameters $\{\mu_F, V\}$, through the spectral function and the Fermi distribution, respectively. Now we can study each interaction and its symmetries. We can deduce the most relevant symmetries by studying the parity symmetry under energy exchanges, i.e. $\epsilon' \leftrightarrow \epsilon''$

$$\mathcal{J}_{ab}(\epsilon',\epsilon'') = -\mathcal{J}_{ba}(\epsilon'',\epsilon'), \tag{2.89}$$

$$\mathcal{D}_{ab}(\epsilon',\epsilon'') = \mathcal{D}_{ba}(\epsilon'',\epsilon'), \tag{2.90}$$

$$\bar{\Gamma}_{ab}(\epsilon',\epsilon'') = -\bar{\Gamma}_{ba}(\epsilon'',\epsilon'). \tag{2.91}$$

Therefore, when we evaluate the expression for $J_{21}$ we find that only for the equilibrium situation, i.e. $V = 0$, it presents the symmetry $J_{12} = J_{21}$. From that, we see that only in equilibrium we have symmetric interactions between the spins. With the same reasoning, we can see that $\Gamma_{21} = \Gamma_{12}$ for $V = 0$, but that relation does not hold for the non-equilibrium configuration. On the other hand, the antisymmetric interaction has the special property that, at equilibrium, $D_{21} = 0$. All this equilibrium-symmetries can be understood from the symmetry that breaks the voltage. Since the voltage sets an imbalance between the sites the interaction between them cannot be equal, one must react different from the other. Therefore, they only interact symmetrically when their occupancies are filled symmetrically, and clearly the antisymmetric interaction has to vanish for such configuration.

With relations (2.89), (2.90), and (2.91) we can also study the damping terms $\{\alpha_{22}, \beta_{22}, \gamma_{22}\}$. Even more, we can analyze and reduce the number of integrals. All this since $\mathcal{J}_{22}$ and $\bar{\Gamma}_{22}$ are completely antisymmetric under energies switch, i.e. $\epsilon' \leftrightarrow \epsilon''$. Another significant result from the study of these symmetries comes from the correlation functions, particularly the antisymmetric correlation. Since it presents a relation similar to equation (2.90):

$$\bar{d}_{ab}(\epsilon',\epsilon'') = -\bar{d}_{ba}(\epsilon'',\epsilon'). \tag{2.92}$$

With this relation, it is very clear that the $id_{22}$ integral is zero. So the system does not present an antisymmetric part in the correlation function. In purely physical interpretation we can see that this contribution must be zero. Since it make no sense that the two-point correlation function for the stochastic magnetic field would not commute. So we have that the correlation functions of the $\eta_2(t)$ are:

$$\langle \boldsymbol{\eta}_2(t)\rangle = 0, \tag{2.93}$$

$$\langle \eta_2^{\alpha}(t)\eta_2^{\beta}(t')\rangle = \left[j\delta^{\alpha\beta} + g\hat{t}^{\alpha}\hat{t}^{\beta}\right]\delta(t-t'). \tag{2.94}$$

With these results and those of the last sections, we see that each interaction can be identified as:

- **Exchange:** $-J_{21}\Omega \cdot \hat{m}$.

  This interaction minimizes the system's energy when the spin at site 2 is parallel ($J_{21} > 0$) or anti-parallel ($J_{21} < 0$) with respect to the spin at site 1 $\hat{m}$. Therefore, this interaction makes the system tend to the ferromagnetic/antiferromagnetic configuration according to the sign of $J_{21}$.

- **DM:** $-iD_{21}\hat{t} \cdot (\Omega \times \hat{m})$.

  In contrast to $J_{21}$, this interaction minimizes the energy of the system when the spins are orthogonal to each other. In fact, it makes the spin at site 2 to align with $\hat{m} \times \hat{t}$, forming a right-handed triad with $\{\hat{t}, \Omega, \hat{m}\}$.

- **Asymmetric Exchange:** $\Gamma_{21}(\Omega t)(mt)$ and $\Gamma_{22}(\Omega t)^2$.

  Here the energy is minimized when both spins align ($\Gamma_{21} > 0$) or anti-align ($\Gamma_{21} < 0$) with a preferred direction $\hat{t}$. However, the second contribution $\Gamma_{22}$ only considers the alignment between the dynamic spin $\Omega$ and the spin-orbit direction $\hat{t}$.

All this agrees with what we have shown in Section 1.2. We can see that the vector-like of the DM interaction in equation (1.5) turns to be $\boldsymbol{D}_{21} = iD_{21}\hat{t}$, and the anisotropic interaction in equation (1.4) is the exterior product of the spin-orbit direction, i.e. $\mathbb{A}_{ij} = \Gamma_{ij}\hat{t} \otimes \hat{t}$. A final note on these interactions is that $\Gamma_{21}$ does not contribute to our's case's dynamics since we have chosen $\hat{m}$ and $\hat{t}$ to be orthogonal to each other. This interaction would be relevant if we study the case where those vectors align or even if they are not orthogonal, i.e. $\hat{m} \cdot \hat{t} \neq 0$. However, we are interested in the DMI effects, so we choose that configuration in order to maximize that effect. Another exciting configuration could be where those effects are mixed and balanced, but we leave that configuration for future work. Therefore, in the next section, we study the numerical value of both interactions.

### 2.4.4. Effective interactions, damping, and correlation: Numerical analysis

To better understand each interaction, damping, and correlation strength, we can explore the numerical value for a certain relation between the hoppings. From the mathematical expression presented in the last section and at the end of Appendix A, we can see that the explicit form of each effective term is highly dependent of the external parameters, the chemical potential of each lead, and the bias voltage. We can explore the space parameter of combinations between the center-band chemical potential $\mu_F$ that sets the equilibrium behavior and the bias voltage V that sets an imbalance between the leads, as shown in figure 2.5. This section is devoted to analyze those results and discuss the interesting features of each one. The numerical calculations were done using *Mathematica* to integrate the expressions in Appendix A.

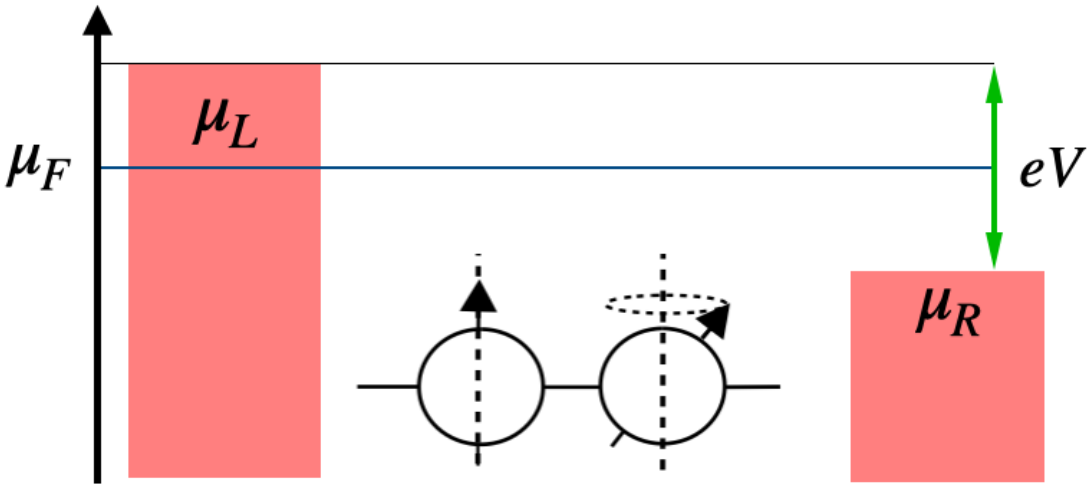


Figure 2.5: Sketch of the relation between the center-band chemical potential, $\mu_F$, and the bias voltage, $eV$. Along with the illustration of which spin is fixed and which is free to move.

To identify the spin-dependent hopping effect in the system and the effects of the electrical current, we propose to study three different strength of the spin-orbit coupling (SOC). At first, we establish main contribution of the electrical current by setting a neglected SOC, i.e., $t = 0$ [meV]. With this configuration, we aim to set the ground results in order to compare them with non-neglectable SOC configurations. We can understand the system's sensitivity to the SOC with a perturbative inclusion of the spin-dependent hopping, $t = 0.05$ [meV]. However, the full effect of including a spin-dependent hopping can be found for strong coupling $t = 1$ [meV].

### Without spin-orbit coupling

We begin the numerical analysis with the null SOC configuration, for which we have seen in the analysis of the former section and Appendix A that from all the interaction, damping, and correlation strengths, the only non-zero terms are: the symmetric interaction $J_{21}$, the symmetric damping $\alpha_{22}$ and the symmetric correlation factor $j_{22}$. These results are shown in figure 2.6. Those figures consider the hopping parameters for the intra-lead hopping of $J = 100[meV]$, the lead-device hopping of $t_{L/R} = 10[meV]$, and the intra-device hopping of $t_0 = 2[meV]$, as shown in [12]. We choose the relation between the hoppings so the approximation we have done in this chapter are valid.

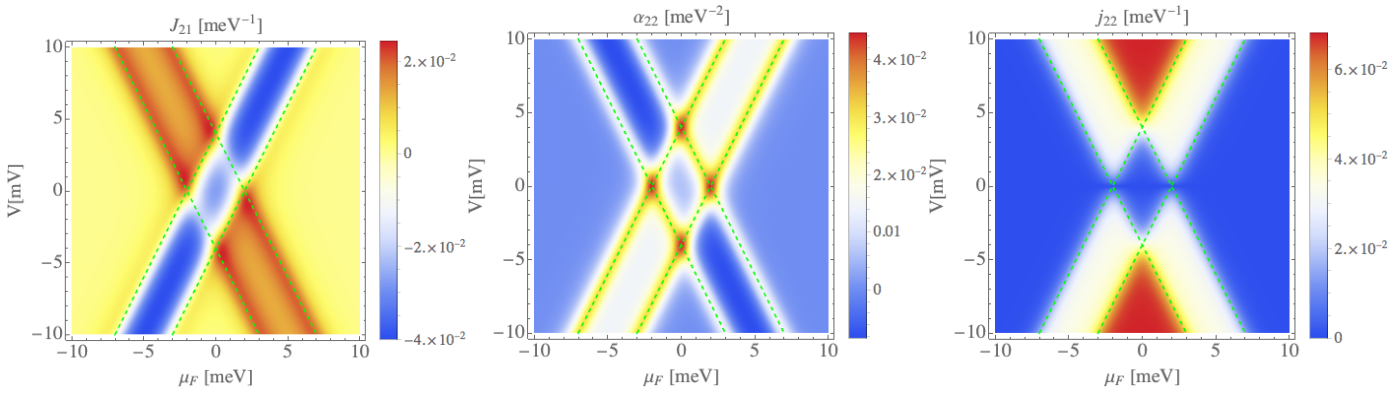


(a) $J_{21}$ (b) $\alpha_{22}$ (c) $j_{22}$

Figure 2.6: Effective terms in absence of the spin-orbit coupling, considering symmetric relation between the leads. Where the effective exchange interaction $J_{21}$ is shown in (a), the effective symmetric damping is shown in (b), and the symmetric correlation strength is shown in (c). In every figure, we show the reference lines $\mu_L = \pm t_0$ and $\mu_R = \pm t_0$ to illustrate the cross-like structure. These lines show a more profound and underlying relation between the hoppings.

In figure (2.6), we show the three effective terms for the spin dimer in the absence of the spin-orbit coupling. All three plots share the same underlying cross-like structure, that indicate a deeper relationship between the bias voltage and the chemical potential of each lead. When we analyze those figures, we can see that the characteristic lines are:

$$||\mu_{L/R}|| = t_0, \tag{2.95}$$

where we remember that $\mu_L = \mu_F + \frac{|e|V}{2}$ and $\mu_R = \mu_F - \frac{|e|V}{2}$, as shown in figure 2.5. These lines are shown in all three plots of figure 2.6. It is important to note that these lines show the characteristic cross-like line, but slightly different lines represent different aspects of each term, such as the local minima/maxima or possible zeros.

The effective exchange interaction $J_{21}$ in figure 2.6a shows many interesting features; to us, the most important one is the sign switch. When we look at the definition and consequences of the symmetric exchange interaction in section 1.2, we find that the system can present either a ferromagnetic or an antiferromagnetic configuration due to this sign change. Even more, this switch can be achieved by adjusting the center-band $\mu_F$ and the bias voltage $|e|V$. The big advantage here is that both parameters can be tuned externally. We do not have to settle to a magnetic configuration restricted by the properties of the components in the system. As we mentioned in the last section, the symmetric interaction is not symmetric for a voltage inversion. It is very interesting that the parameter space where the interaction is negative ($J_{21} < 0$) is approximately restricted by $|\mu_L| > t_0$ and $|\mu_R| > t_0$. We can only express an approximate expression of the characteristic lines because of the complex form of each effective term's expression. Even though those lines can not predict the zeros of the function, they surely set the local maxima along $|\mu_L| = t_0$ and $|\mu_R| = t_0$. Besides, the global maxima of the function is found for slightly outside of the intersection, along $|\mu_R| > t_0$.

In figure 2.6b, we present the numerical value of the effective damping $\alpha_{22}$. Unlike the monomer case, the dimer in the absence of the spin-orbit coupling has effective damping with a negative value for a certain combination of the external parameters. The fact that $\alpha_{22}$ is negative shows that the localized spin at site two is gaining energy instead of dissipating it to the nearest lead. This region in the parameter space is roughly characterized by $|\mu_L| < t_0$ and $|\mu_R| > t_0$. Similarly to the exchange interaction, the effective damping presents their local maxima along the lines $|\mu_L| = t_0$ and $|\mu_R| = t_0$, where the latter one is greater than the first. Even more, in this case, the global maxima are precisely at the intersection of those lines.

Finally, in figure 2.6c, we present the symmetric correlation strength. This effective term is inherently different from the former factors. Although the same characteristic lines can analyze it, the cross-like form does not follow the local maxima, but instead, the mid-point of the step-like increase along with an increasing absolute value of the voltage. Unlike the former terms, the correlation strength presents a perfect symmetry meaning that an stochastic magnetic field does not care of the direction of the current but the intensity.

**Weak spin-orbit coupling**

As we can see from the explicit expressions of the interactions, damping, and correlation strengths, as soon as we include the SOC ($t \neq 0$), the anomalous terms; $D_{ab}$, $\Gamma_{ab}$, $\gamma_{ab}$ and $g_{ab}$, are no longer zero-valued. So, as explained at the beginning of this section, we will study the inclusion of this new interaction by comparing the results of weak coupling ($t = 0.0$ [meV]) with a strong coupling ($t = 1$ [meV]), so we can understand the main effects of the SOC qualitatively.

Unlike the former configuration, when we include the SOC, the number of effective terms increases significantly, so we separate them by their common role. We present the numerical results of the interactions, damping, and correlation strength that are relevant to the dynamics of the spin at site two, in figures 2.7, 2.8, 2.9, and 2.10. In those figures, we can see that the earlier characteristic lines in equation (2.95) still seem very accurate. However, by a closer look and comparison between the symmetric terms shown in figure 2.6, under both configurations, we can see that the characteristic lines for this system are:

$$||\mu_L|| = t_0 - t, \tag{2.96}$$
$$||\mu_R|| = t_0 + t. \tag{2.97}$$

We can see that those results seem similar because of the low value of $t$. Although these lines are highly motivated by the *pole-like* value of the explicit electronic Green's function shown in Appendix A, we still have to check the validity of these lines with the strong SOC case.

The effective interactions $J_{21}$, $D_{21}$, $\Gamma_{21}$, and $\Gamma_{22}$ are shown in figures 2.7 and 2.8. When we compare the symmetric interaction $J_{21}$ in figure 2.7a with its counterpart in without SOC in 2.6a, we can see that all the relevant characteristics are preserved. The low sensitivity under an additional hopping comes from the fact that this particular interaction is mainly affected and originated by the electrical current, therefore the system-lead interaction. As

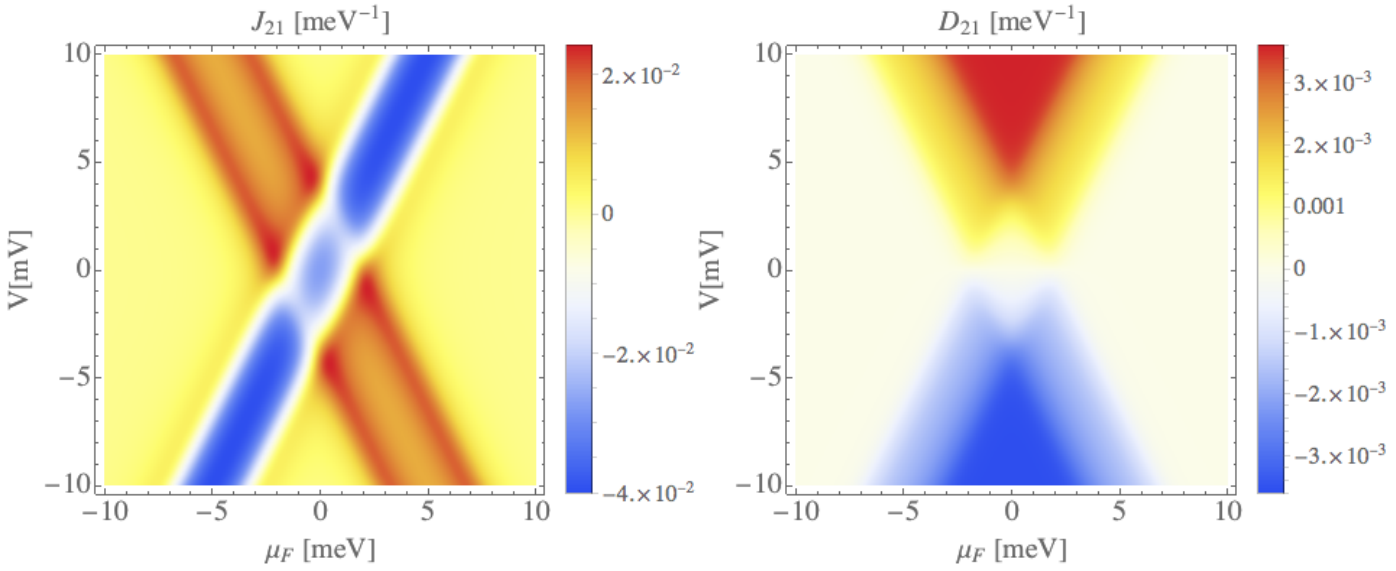


(a) $J_{21}$ (b) $D_{21}$

Figure 2.7: Effective interactions for weak spin-orbit coupling, considering symmetric relation between the leads. The effective exchange interaction $J_{21}$ is shown in (a), and the DM interaction is shown in (b). Here we can see that $J_{21}$ allows a ferromagnetic or antiferromagnetic interaction for certain combinations of the external parameters. The DM shows a step-like behavior that resembles the structure of the correlation factor in 2.6c. The spin's direction dynamics would be ruled by the relation between these interactions and the corresponding correlation factors.

we can see from the characteristic lines $||\mu_R|| = t_0 + t$, the local maxima that enclose the negative-valued region are separated by the inclusion of the SOC compare with the former case. Nevertheless, the more interesting result comes by comparing the global maxima and minima, because both values are slightly smaller/bigger, indicating that it is affected by the SOC.

Between the new interactions that appear with the inclusion of the SOC, we are more interested in the effective DM interaction $D_{21}$ in figure 2.7b. This interaction is exceptionally different from $J_{21}$. Even though it is still represented by characteristic lines in equations (2.96) and (2.97), it follows a similar step-like form as for the symmetric correlation strength rather than a cross-like form denoted by its local maxima. However, unlike $j_{22}$, the DM interaction turns to be an odd function of the voltage, which follows the regular physical interpretation of a DM interaction. It is important to note that this interaction is lower than $J_{21}$, but not for that much, even for a weak SOC. In the end, this close relation between them will provide interesting effects in the dynamics.

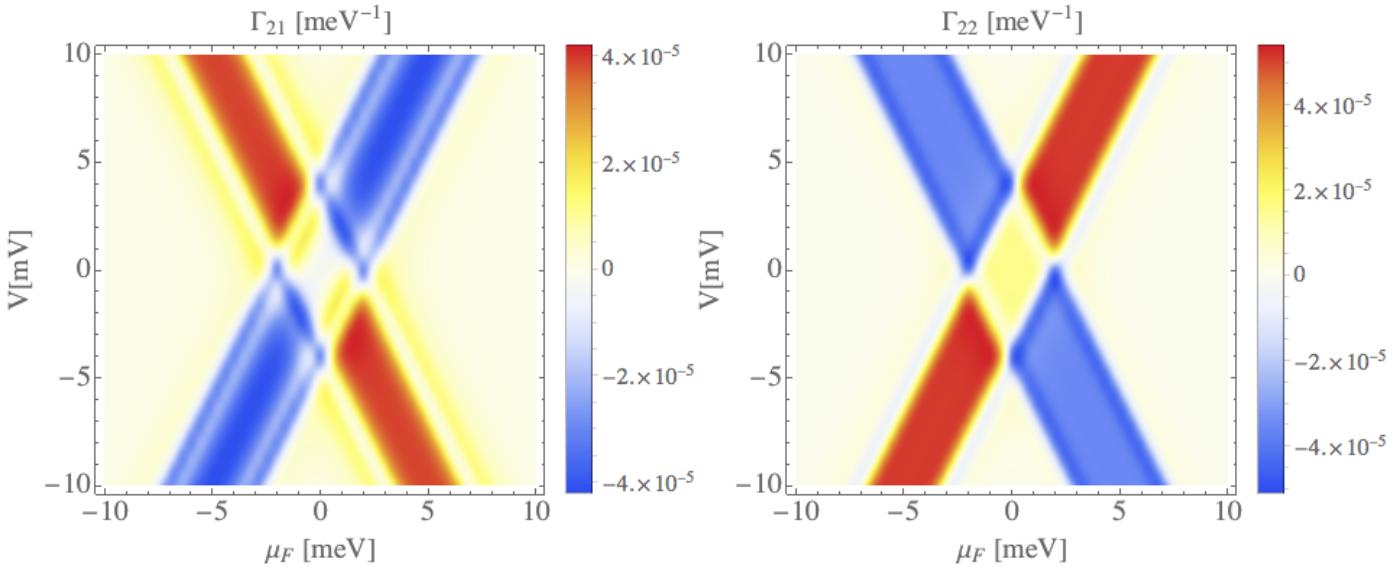


(a) $\Gamma_{21}$ (b) $\Gamma_{22}$

Figure 2.8: Effective interactions for weak spin-orbit coupling, considering symmetric relation between the leads. Where the effective anisotropic interactions $\Gamma_{21}$ and $\Gamma_{22}$ are shown in (a) and (b), respectively. We can see the oppositve response in sign to the characteristic lines of constant value of each lead chemical potential.

At last, the anisotropic interactions $\Gamma_{21}$ and $\Gamma_{22}$ are shown in figures 2.8a and 2.8b, respectively. First, we see that $\Gamma_{21}$ is very similar to $J_{21}$, however, this interaction is three orders of magnitude smaller, and the local maxima along $||\mu_L|| = t_0 - t$ is swapped by minima and the global maximum appear along the $||\mu_L|| = 0$. The anisotropic "self-interaction" $\Gamma_{22}$, like $J_{21}$ and $\Gamma_{22}$, also follow the cross-like form of local maxima/minima, but it presents the inverse positive-negative relation. These interactions tell us the response to an alignment with the spin-orbit unit vector $\hat{t}$. So $\Gamma_{21}$ says that as long as the localized spin at site one, as some alignment with that unit vector, it will increase the likelihood toward that direction. However, $\Gamma_{22}$ represents the aim of the system to oppose to that alignment under the same configuration. Still, both effective interactions are much lesser than the symmetric interaction $J_{21}$, and we would not expect to see a significant influence to the dynamics, at least for the weak SOC.

The damping factors, $\alpha_{22}$ and $\gamma_{22}$, are shown in figure 2.9. When we compare the symmetric damping in figure 2.6b without SOC, with the figure 2.9a that includes that effect, we can see that the latter one has the local maxima slightly moved, following equations (2.96) and (2.97). That displacement is added to a little reduction in the maximum values at the local maxima. Besides that little changes, the cross-like form is preserved, along with the global maxima that appears at the intersection of the local maxima lines. Furthermore, the negative-value region is still defined by the relations between the chemical potential with the additional spin-dependent hopping changing the symmetry, $|\mu_L| < t_0 - t$ and $|\mu_R| > t_0 + t$. The relation between the local maxima is also preserved, with the $\alpha_{22}$ is bigger at $|\mu_R| = t_0 + t$.

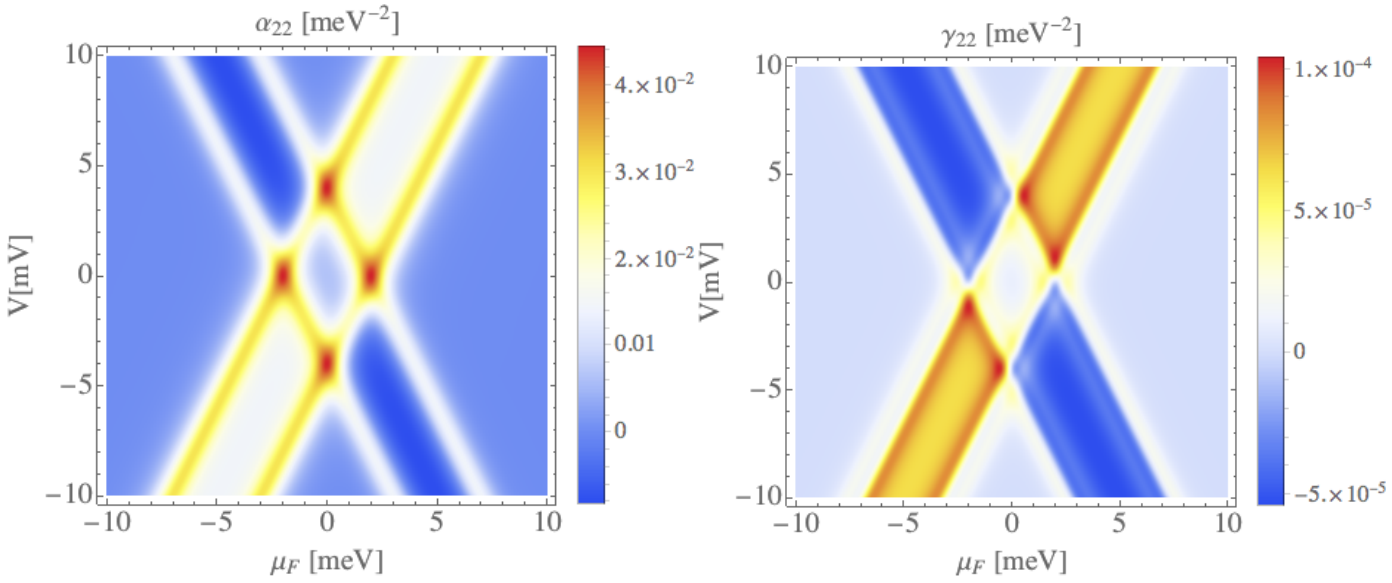


(a) $\alpha_{22}$ (b) $\gamma_{22}$

Figure 2.9: Effective damping factors, considering the symmetric case relation between the lead and a weak SOC. Both damping factors show the same cross-like form for the local maxima lines. However, the global maxima of $\gamma_{22}$ are slightly out of the intersection.

On the other hand, now we have the additional anisotropic damping $\gamma_{22}$ in figure 2.9b. This new damping presents the same cross-like form that resembles the anisotropic interaction $\Gamma_{22}$. It is very interesting that, even though $\gamma_{22}$ is much lesser than $\alpha_{22}$, it has a wider range of negative values. We can see that the global minima, as for the symmetric damping, is located at $|\mu_L| = 0$ [meV], but the global maxima, as for $\Gamma_{22}$ are precisely at the intersection of the local maxima, which do not entirely follow the same equations as for $\alpha_{22}$.

The correlation strengths are shown in figure 2.10. Following the same analysis as for $j_{22}$ in figure 2.6c, we can see that in figure 2.10a the same features are presented. The resemblances between them confirm that along with $J_{21}$ and $\alpha_{22}$, the main contribution to these effective terms come from the electrical current, and the spin-dependent hopping does not change the structure with a weak coupling. However, when we look closer, we can see that the inclusion of the SOC slows the step-like change, making it softer.

In the end, we have the anisotropic correlation strength in figure 2.10b. This new correlation that appears as we include the SOC, follows the same step-like form as for $j_{22}$, but with additional local minima following the equations (2.96) and (2.97), making it present a cross-like form similar to the earlier effective terms but with local minima instead of maxima. This correlation presents a bigger region for the first step value but a smaller global maxima region. We can see that both effective anisotropic terms, $\gamma_{22}$ and $g_{22}$, are much smaller than their symmetric counterparts, which leads us to understand that the main contribution to both factors come from the spin-dependent hopping rather than the electrical current.

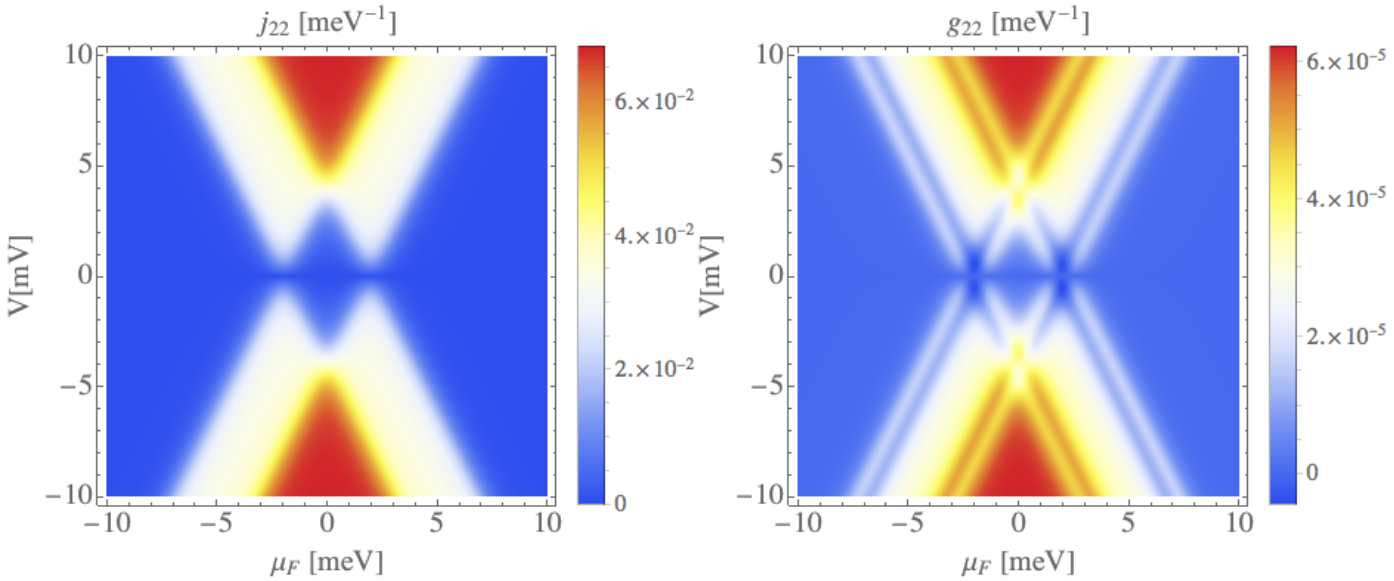


(a) $j_{22}$ (b) $g_{22}$

Figure 2.10: Effective correlation strengths, considering the symmetric case relation between the lead and a weak SOC. Here we see that the step-like form of the correlation in figure 2.6c is preserved. Even more, the anisotropic correlation presents the same structure, with the addition of extra local minima at the transition of each step.

### Strong spin-orbit coupling

Up to this point we have presented the results in absence of the spin-dependent hopping and those for a perturbative inclusion of SOC. Now we can study what happens when we consider a strong SOC, $t = 1$ [meV]. Here, we aim to determine the validity of the aforementioned line equations, and how sensitive are our earlier results to the specific configuration. One way to quantify that response is in terms of the maximum and minimum values that the effective factors present, and compare it with the case of a weak coupling.

The effective interactions for strong SOC are shown in figures 2.11 and 2.12. In this case, the symmetric interaction $J_{21}$ has lost the status of the dominant interaction against the DM interaction $D_{21}$, as we can see by comparing figures 2.11a and 2.11b. However, most features discussed for previews configurations are preserved, such as the negative valued region that now is enclose by $|\mu_L| < t_0 - t$ and $|\mu_R| > t_0 + t$, approximately. Furthermore, the local maxima follow the lines $|\mu_L| = t_0$ and $|\mu_R| = t_0 + t$. We can see that for this high-value SOC, the region where $J_{21} < 0$ is reduced, and the global maximum and minimum are smaller, which is reasonable since the rest of the interactions have increased their numerical values.

The DM interaction in figure 2.11b shows many interesting factors, such as the already mentioned comparable scale with $J_{21}$. However, the numerical increase is not the only characteristic effect of the increase in the SOC. The step-like form of $D_{21}$, compared with 2.7b, is smoother. Because the range,$|\mu_{L,R}| < t_0 - t$, for the step valued is narrower and the increase range,$|\mu_{L,R}| > t_0 - t$ and $|\mu_{L,R}| < t_0 + t$ , is wider. This smoother behavior allowed

is accompanied with a smaller zero diamond-like region at the center of the space parameters.

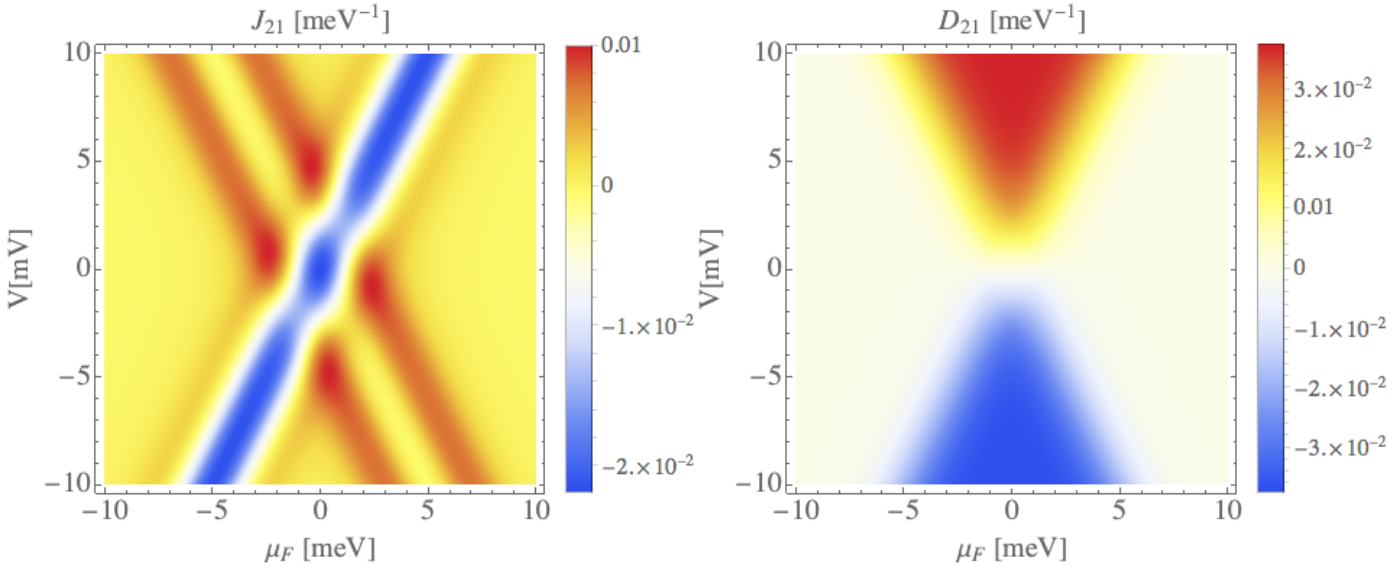


(a) $J_{21}$ (b) $D_{21}$

Figure 2.11: Effective interactions for strong spin-orbit coupling, considering symmetric relation between the leads. Here the effective exchange interaction $J_{21}$ is shown in (a) and the DM interaction is shown in (b). We can see that $J_{21}$ preserve the sign switch that allows modifying the Ferromagnetic or antiferromagnetic preferred configuration for certain combinations of the external parameters. The DM preserved the step-like, although this time is much smoother than what was presented in 2.7b. Unlike the case for the weak SOC, the dynamics of the spin direction would mostly rule by the DM interaction, meaning that we should expect a significant increase in the tendency towards $(\hat{m} \times \hat{t})$, rather than exclusively to $(\hat{m})$.

With the above explained lines, we can see that both anisotropic interactions $\Gamma_{21}$ and $\Gamma_{22}$ in figure 2.12 follow them. Similar to the DM interaction, these interactions increase their values to be comparable with $J_{21}$. However they do not overcome the symmetric interaction. It is very interesting to note that the global maxima and minima of $\Gamma_{21}$ are enclosed by $|\mu_{L,R}| < t_0 - t$, and are located at $\mu_{L,R} = 0$, respectively. On the other hand, $\Gamma_{22}$ follows the same relation; however, where the former interaction has the global minimum, now it is the global maximum and vice versa.

In figure 2.13, we present both symmetric $\alpha_{22}$ and asymmetric damping $\gamma_{22}$. With figure 2.13a, we can see that one big effect of the spin-dependent hopping inclusion, as we expected, is the inevitable loss of symmetry This comes directly from the fact that the maxima do not follow the same equation for both chemical potential-like relations between the external parameters. Although the features that characterize the symmetric damping are not lost, they are rearranged. For example, the negative valued zone is now in the region where the condition $|\mu_L| > t_0 - t$ and $|\mu_R| < t_0 + t$ are simultaneously fulfilled, and the global minimum is located

along $\mu_R = 0$. However, the global maxima still appears at the local maxima intersection, even though they do not follow the same lines.

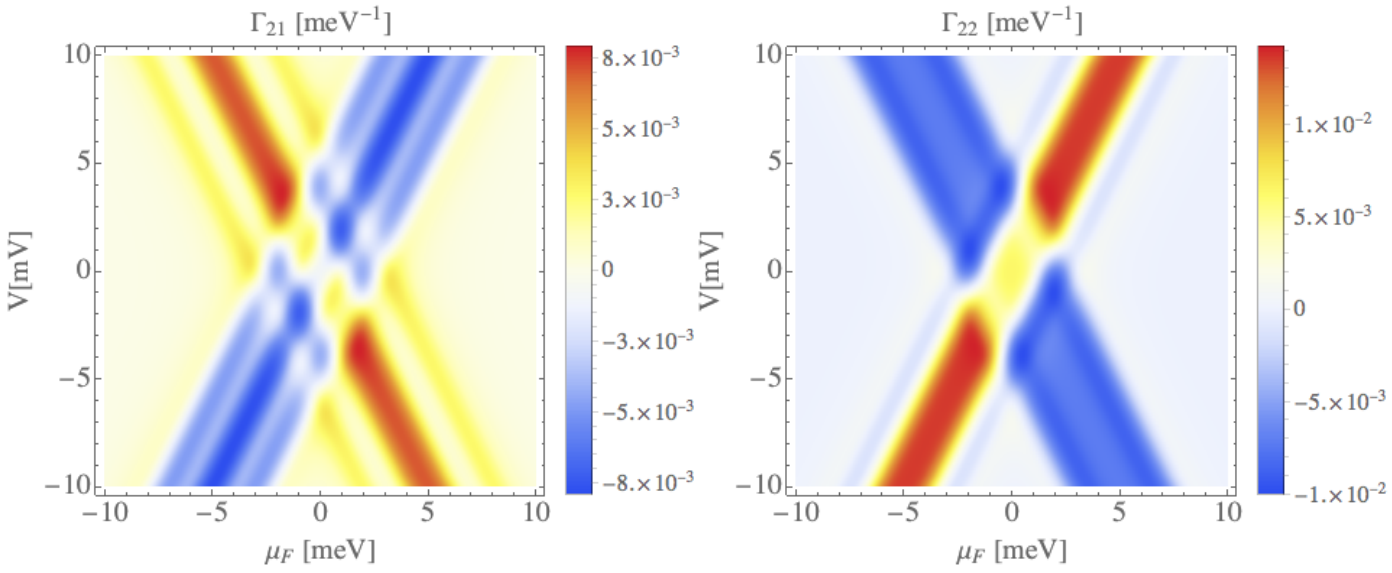


(a) $\Gamma_{21}$ (b) $\Gamma_{22}$

Figure 2.12: Effective interactions for strong spin-orbit coupling, considering symmetric relation between the leads. Here we show the effective anisotropic interactions $\Gamma_{21}$ and $\Gamma_{21}$ in (a) and (b), respectively. In this case, the interactions come to be comparable with $J_{21}$ and $D_{21}$, so we expect that although they still are lesser than them, the dynamics will be affected towards the SOC polarization, $\hat{t}$.

The asymmetric damping $\gamma_{22}$ is presented in figure 2.13b. This new damping presents the remarkable feature that allows us to identify the meaning of the extra minima and maxima that we commented for the weak coupling. Those new minima and maxima that are not present in the symmetric damping, differ between them in value. Nevertheless, we can note that the maxima that follows equations $|\mu_L| = t_0 + t$ and $|\mu_R| = t_0 - t$ are bigger than their counterparts with the inverse relation with $t$. However, the deeper, physical interpretation of these values can only be found through a more thorough analytical analysis. At this point, we can see that for strong SOC, the values of both damping are now comparable, either because the symmetric damping is decreased and/or the asymmetic damping is enhanced.

The correlation strengths are shown in figure 2.14. As we have seen for all the correlation figures, in figure 2.14a, we can see that $j_{22}$ follows a similar step-like structure. However, with the aid of equations (2.96) and (2.97), we can see that the first step-like value range is wider, and the second value is narrower than before. This smoothing of the curve comes from the increase in the spin-orbit factor $t$.

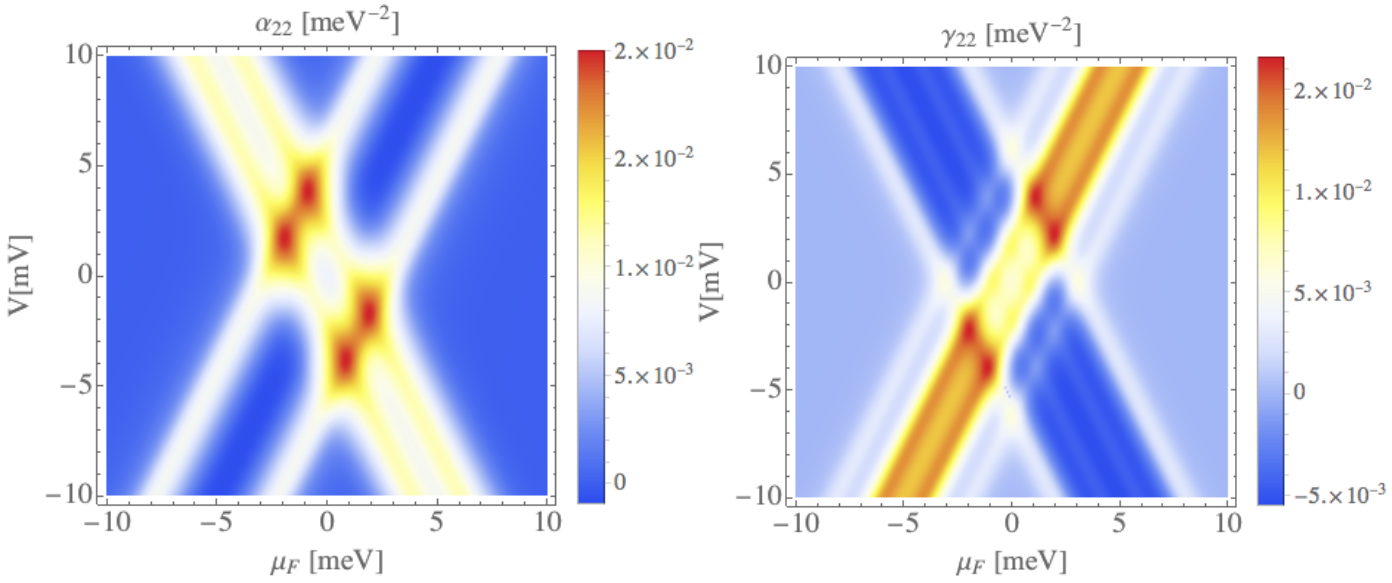


(a) $\alpha_{22}$ (b) $\gamma_{22}$

Figure 2.13: Effective damping factors, considering the symmetric relation between the leads and a strong SOC. We can see that the symmetric damping in figure (a) is highly affected by the SOC. Due to the decrease in magnitude and the displacement of the maxima towards $\mu_L = t_0 - t$ and $\mu_R = t_0 + t$. Another important feature of $\alpha_{22}$ with $t = 1$ [meV], is that the negative region is now enclosed by the lines of $\mu_R$, rather than $\mu_L$ as for former cases.On the other hand, the anisotropic damping in figure (b) has increased its maximum value at the point to be comparable with $\alpha_{22}$. Unlike the symmetric damping, $\gamma_{22}$ preserve all the features as for figure 2.9b.

When we study the anisotropic correlation strength $g_{22}$ in figure 2.14b, we see that the extra minima that appear in 2.10b are very well described by the new characteristic lines that interchange the t-dependence in equations (2.96) and (2.97). The most important fact here is the comparable numerical value between $j_{22}$ and $g_{22}$. Besides that, they share the increase and decrease in their first and second step-like values.

**Summary**

With the above results where we investigated how the effective interactions, damping, and correlation strengths are affected when we increase the SOC, we can summarize the relevant conclusions from each kind of term.

When we compare each interaction with its respective counterpart at different SOC strength, we see that while the symmetric interaction decreases with the SOC, the non-symmetrical interactions are highly enhanced. We interpret this behavior as the system's increasing lack of symmetry is preferring an antisymmetric magnetic configuration ruled by the SOC. This change can be seen from the strong spin-orbit coupling configuration, where

the DM interaction surpasses the symmetric interaction and become the dominant interaction in the system. Another relevant feature that appears as we increase the SOC is the narrowing down of the region in the parameter space where the symmetric interaction is negative, allowing an antiferromagnetic configuration.

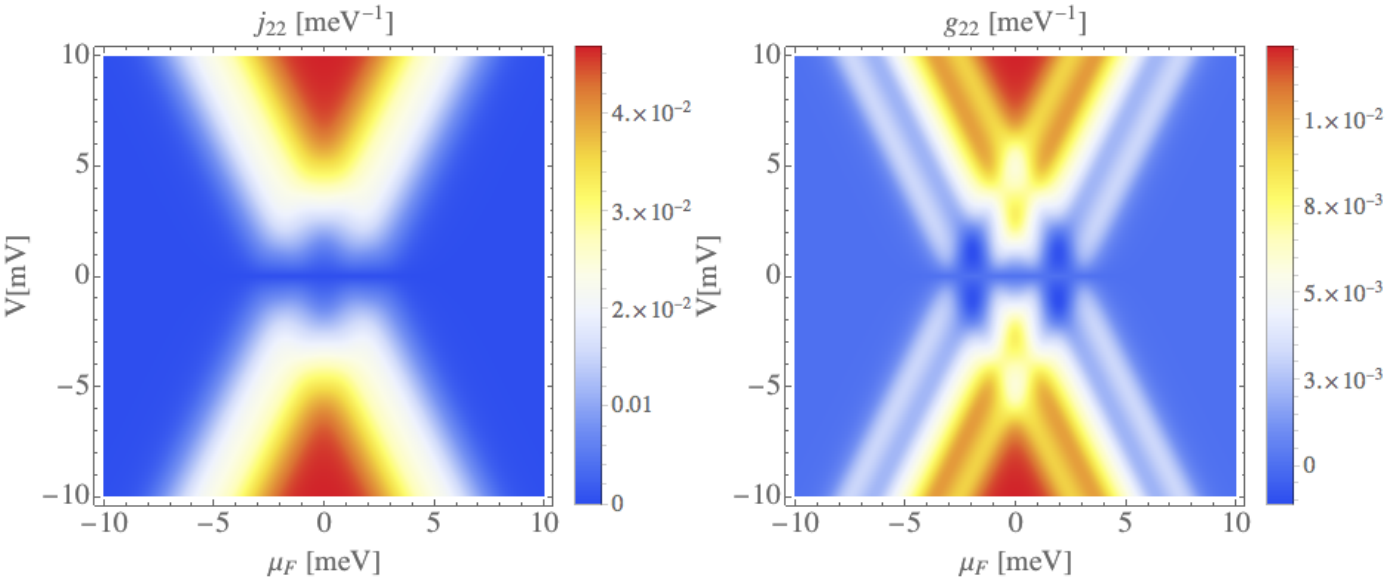


(a) $j_{22}$ (b) $g_{22}$

Figure 2.14: Effective correlation strengths, considering the symmetric relation between the leads and strong SOC. The symmetric correlation preserved the step-like form with a much smoother increase between the values. This is most relevant impact on $j_{22}$, since even though its maximum value is now smaller than 2.10a, it is not a significant decrease. As for the anisotropic correlation, the value is significantly increased. This increase means that both correlations are comparable for this case, and we should see a preferred direction for the stochastic magnetic field $\eta$.

As for the damping factors, we see very little change in terms of the strength of the symmetric damping, although the parameters relation for the local maxima lines is directly affected by the increase of the SOC can see in figure (2.11a). However, the anisotropic damping's strength is severely enhanced by the same increase that reduces the maximum value of the symmetric damping, and it presents an opposite reaction to the position of its local maxima and minima compared to the symmetric damping.

For the correlation strengths, we see that both functions' step-like forms get smoother as we increase the SOC. However, contrasting with the interactions and damping factors, the correlation functions cooperate at each point in the parameter space. So, even though the SOC increase reduces the stochastic magnetic field's statistical strength in the isotropic component, it intensifies the same magnetic field towards the SOC's direction.

# Chapter 3

# Fokker-Planck Analysis

## 3.1. Introduction

In this chapter, we focus our attention on, somehow, solving the equations of motion for the spin direction of the monomer and dimer configurations. When we look closely at equations (2.52) and (2.75), it is clear that in order to obtain information from them, we first need to understand the effects of the stochastic magnetic field and what it means to have a differential equation with a stochastic variable. In the last chapter, we introduced the stochastic variable from the fluctuating part of the spin direction and found out that it behaves as a stochastic magnetic field. Moreover, we called those equations, Langevin equations. These equations consist of a simple ordinary differential equation, usually of first-order derivatives in time, that includes a rapidly and fluctuating random function called stochastic force.

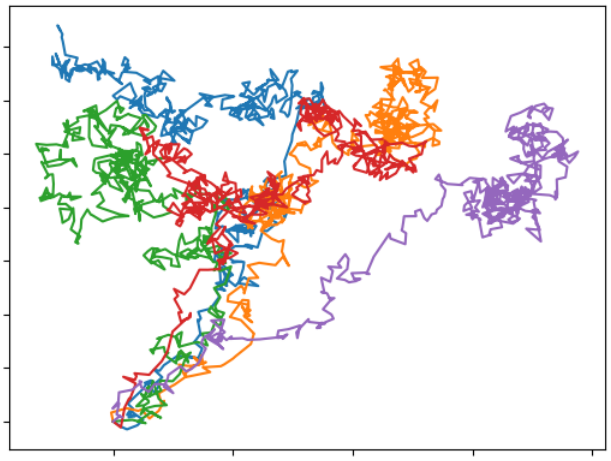

Figure 3.1: Motion of five point particles undergoing Brownian motion from the same initial point. Where we can see the randomness of the trajectory due to many collisions in unpredictable directions.

The original Langevin equation was presented as an alternative method to understand the Brownian motion, besides Einstein's original derivation. Historically, it was one of the

firsts applications of a stochastic differential equation. Here, instead of a discretized time interval as in Einstein's deduction, this method studies the correlation functions of the stochastic force to obtain the system variable's average value throughout many realizations of the experiment. Hence this differential equation, in some sense, works with random functions.

The relevance of this new kind of equation, ruled by random variables, is when we deal with a many-body system such as a fluid. Where we cannot follow each particle position, the interactions with the test particle, electron, or molecule must be treated statistically. Since at each implementation of the experiment, the interaction, therefore the force on the test particle, will be different. We must treat the particle's position as a stochastic process. For example, in the Brownian motion, we follow a specific particle on a fluid. In this scenario, the particle has multiple collisions with the fluid molecules that can happen at any time and in any direction. Therefore, the solution must be a stochastic process. In our system, we see that the stochastic magnetic field comes from the interaction between the localized spin and the itinerant electrons' random spin direction from the electrodes. This kind of equation can seem as hard to obtain any real information from it. However, using the stochastic force's relatively simple information, we can obtain some measurable results, but always on average. In general, a Langevin equation is rarely solvable under normal conditions, such as very strong or non-uniform interactions. The study of stochastic differential equations is a vast and complicated branch of mathematics. In this thesis, we do not try to give more than a simple summary of how to deal with our specific case to make this thesis as self-contained as possible.

There is an alternative way to deal with a system under the effects of a random force. If we agree not to study the dynamical variable itself, and instead study the conditional probability density of that variable being restricted to a sharp-value at a given time. In that case, we can redirect our calculations to study the so-called Fokker-Planck equation. Then, we may find a more solvable equation. Even though this equation can be solved analytically in some specific cases, it is not easy to obtain a solution for most cases. The first section of this chapter will present a general recipe to obtain the Fokker-Planck equation from a Langevin equation in the "canonical form". [18, 28, 41].

## 3.2. From Langevin to Fokker-Planck equation

The generic Langevin equation consists of studying the influence of a "fast" variable on a "slow" variable. For example, in the Brownian motion, we study the slowly moving particle's position under the effect of the faster fluid molecules. So, as we can see from the earlier chapter's equations of motion, the Langevin equation we have to study is of the form:

$$\dot{\xi}_i = a_i + R_{ij}\Gamma_i, \tag{3.1}$$

where we have a first-order time derivative for the slow variable $\xi$ and a linear dependence of the stochastic part $\Gamma$. This expression is called the canonical Langevin equation and will be the starting point for our deduction of the Fokker-Planck equation. We can clearly separate the above equation into deterministic parts, $a_i$ and $R_{ij}$, from the stochastic force. This force presents the major deal in solving the equation. However, luckily enough, in this thesis, we focus on the specific (and simplest) case of a $\delta$-correlated Gaussian distributed force:

$$\langle \Gamma \rangle = 0, \tag{3.2}$$

$$\langle \Gamma^i(t)\Gamma^j(t')\rangle = b^{ij}\delta(t-t'). \tag{3.3}$$

We will leave $b^{ij}$ without any restriction, so it would be case dependent, as we have seen from the previous Chapter results (monomer and dimer). The general procedure to obtain the Fokker-Planck from a Langevin equation consists of obtaining the Kramers-Moyal coefficients $D^{(\nu)}_{i_1\ldots i_\nu}$, from

$$D^{(\nu)}_{i_1\ldots i_\nu} = \frac{1}{\nu!}\lim_{\tau\to 0}\frac{1}{\tau}\langle[\xi_{i_1}(t+\tau)-x_{i_1}]\ldots[\xi_{i_\nu}(t+\tau)-x_{i_\nu}]\rangle \tag{3.4}$$

where $\xi_i(t+\tau)$ with $\tau > 0$, is a solution of (3.1) and $\xi_i(t) = x_i$. For a process that is described by a Langevin equation like (3.1), with a $\delta$-correlated Gaussian force $\Gamma$, (3.2) and (3.3), it can be shown that all coefficients with $\nu \geq 3$ are identically zero [41]. The remaining non-zero coefficients $D^{(1)}_i$ and $D^{(2)}_{ij}$ are known as drift vector and diffusion tensor. We can see that the time evolution of the probability density is described by

$$\frac{\partial}{\partial t}P = \left(-\partial_\mu A^\mu + \partial_\mu\partial_\nu D^{\mu\nu}\right)P, \tag{3.5}$$

where we have defined

$$A^\mu = a^\mu + \frac{1}{2}b^{mn}(\partial_k R^\mu{}_m)R^k{}_n \tag{3.6}$$

$$D^{\mu\nu} = \frac{1}{2}b^{mn}R^\mu{}_m R^\nu{}_n \tag{3.7}$$

Since we aim to study the steady-state solution of equation (3.5), we define the probability current $J^\mu$ by a conservation of probability equation:

$$\partial_t\mathbb{P} + \partial_\mu J^\mu = 0. \tag{3.8}$$

The above equation allows us to work with the divergence of the current instead of the partial derivative with respect to the time variable. We can see that, for the generic case described earlier, the current in terms of the characteristic functions of the Langevin equation is

$$J^\mu = \left[a^\mu - \frac{1}{2}b^{mn}R^\mu{}_m(\partial_\nu R^\nu{}_n)\right]\mathbb{P} - \frac{1}{2}b^{mn}R^\mu{}_m R^\nu{}_n(\partial_\nu\mathbb{P}) \tag{3.9}$$

Using this mechanism, we can transform the Langevin equations found for the monomer (2.52) and dimer (2.75) configurations, into a canonical form (3.1). From there, we obtain their respective Fokker-Planck equation to study the probability density and the average value for the spin's direction $\langle\boldsymbol{\Omega}\rangle$.

## 3.3. Monomer

The monomer case presents the ideal starting point since the equation (2.52) becomes a simple Landau-Lifshitz-Gilbert equation with no effective extra interaction due to the s-d interaction. This equation gives us a more straightforward way to obtain the Fokker-Planck equation than the dimer case in the presence of the spin-orbit coupling.

$$\hbar S\frac{d\boldsymbol{\Omega}}{dt}(t) = \boldsymbol{\Omega}(t)\times[S\mathbf{h}+\boldsymbol{\eta}(t)] - \hbar S^2\alpha(V)\boldsymbol{\Omega}(t)\times\frac{d\boldsymbol{\Omega}(t)}{dt}. \tag{3.10}$$

To apply the routine presented at the beginning of this chapter, we need the Langevin equation in the canonical form. This transformation is generally known as constant renormalization from where we get a Landau-Lifshitz equation without the damping term but a damping-like torque as:

$$\frac{d\boldsymbol{\Omega}}{dt} = \boldsymbol{\Omega}\times\left[\boldsymbol{H}+\tilde{\boldsymbol{\eta}} - S\alpha\boldsymbol{\Omega}\times(\boldsymbol{H}+\tilde{\boldsymbol{\eta}})\right], \tag{3.11}$$

from where we re-define the fields variables as

$$\boldsymbol{H} = \frac{S\boldsymbol{h}}{\hbar S(1+(S\alpha)^2)}, \tag{3.12}$$

$$\tilde{\boldsymbol{\eta}} = \frac{\boldsymbol{\eta}}{\hbar S(1+(S\alpha)^2)}. \tag{3.13}$$

The second condition of the procedure is that the stochastic field's correlation is zero for the one-point correlation and a delta function in time with a Kronecker delta relation between the vector indices for the two points correlation, known as white noise. We immediately notice that (2.40) and (2.41) do not satisfy such condition. However, after the the low energy approximation (2.56), we find that the two-point correlation function is delta correlated. Now we can see that the characteristic functions of 3.1 are

$$\boldsymbol{a} = \boldsymbol{\Omega}\times\left[\boldsymbol{H} - S\alpha\boldsymbol{\Omega}\times\boldsymbol{H}\right], \tag{3.14}$$

$$R^{\mu}{}_{m} = A[\epsilon^{\mu am}\Omega_a - S\alpha(\Omega^{\mu}\Omega_m - \delta^{\mu}{}_{m})], \tag{3.15}$$

$$b^{ij} = j\ \delta^{ij}, \tag{3.16}$$

here we remind the reader that we have defined $j = -i\Delta^2\hbar^2S^2K^{(k)}(\epsilon\to 0)$ and $A = 1/\hbar S(1+(S\alpha)^2)$. From (3.9), we get that $J^{\mu}$ is

$$\boldsymbol{J} = A\boldsymbol{\Omega}\times\left[(S\boldsymbol{h} - S\alpha\boldsymbol{\Omega}\times S\boldsymbol{h})\mathbb{P} + \frac{j}{2\hbar S}\boldsymbol{\Omega}\times\frac{\partial\mathbb{P}}{\partial\boldsymbol{\Omega}}\right]. \tag{3.17}$$

The main reason to calculate $J^{\mu}$, as said, is to study the steady-state solution of the Fokker-Plank equation (3.11), which means that we are interested only in what happens to the system after the transient regime has no effects. We can argue that we have always contemplated this situation throughout our calculations; therefore, studying the transient part of equation (3.11) has no sense. Nevertheless, the physical reasoning to do it comes from the assumption that the characteristic times in which the multiple electrons, responsible for the

transients, interact with the system is much shorter than the localized spin characteristic times.

Finally, we want to solve the conservation of probability equation in the steady-state regime, i.e., $\partial_\mu J^\mu = 0$. The Boltzmann distribution, $\mathbb{P} = N \exp\{-\beta\mathcal{E}\}$, gives the stationary probability distribution that solves this equation, from which we find the final expression of the effective temperature $(1/\beta)$ as:

$$\beta = \frac{2S\alpha(V)\hbar S}{j}, \tag{3.18}$$

this temperature was predicted when we study the relationship between the Keldysh component and the effective damping at equilibrium configuration (2.54). So, the specific form of the probability distribution in the stationary regime is given by

$$\mathbb{P}[\boldsymbol{\Omega}] = N \exp\left\{\frac{2S\alpha\hbar S}{j}(S\boldsymbol{h}\cdot\boldsymbol{\Omega})\right\}. \tag{3.19}$$

It turns out that this solution holds for any Effective field $\boldsymbol{H} = -\frac{\partial\mathcal{E}}{\partial\boldsymbol{\Omega}}[\boldsymbol{\Omega}]$ as long as the energy is quadratic in the spin direction $\boldsymbol{\Omega}$, like the anisotropic energies that we left out for simplicity. In principle, we can extract all the information needed to study the localized spin's dynamics from equation (3.11) and (3.19). However, due to the voltage and chemical potential dependence of the effective damping, we preferred to extract the equilibrium orientation and the torques that affect the spin from the numerical calculation and show them in figures 3.2 and 3.3. We calculate the following results considering the center-band chemical potential $\mu_F = 1[meV]$, the temperature $T = 0.01[K]$, an inter-lead hopping $J = 3[meV]$, a connection hopping $t_{L/R} = 1[meV]$, and a s-d interaction factor $\Delta = 1$ [meV].

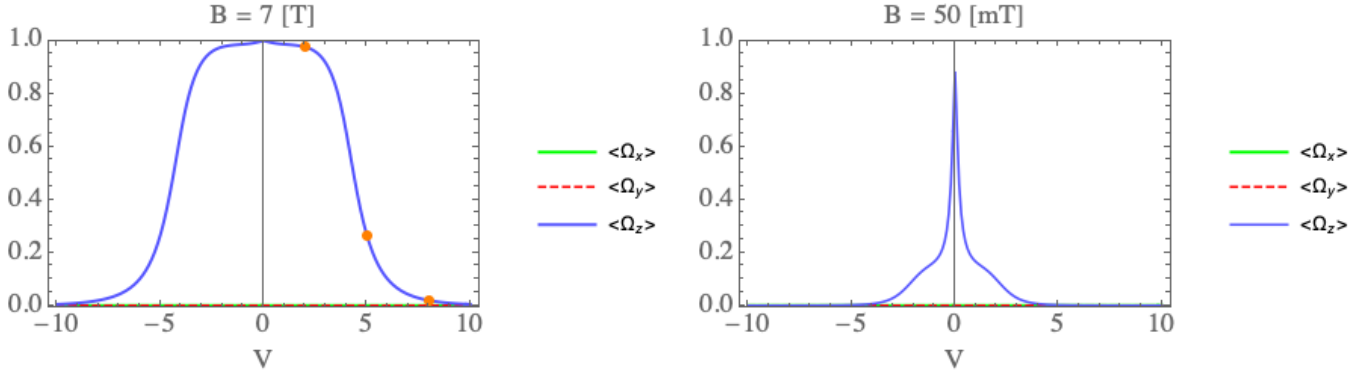


Figure 3.2: The average value of the localized spin's direction for each component considers two cases — one where the magnetic field is strong enough to maintain the equilibrium direction near the z-axis before decay to a full delocalized state over the unit sphere for high voltages. The second case shows that the average can not maintain a well defined preferred direction at high voltages for low magnetic fields.

In the high voltage case in figure (3.2), we show three points to explore the torques of equation (3.11) in figure (3.3). Due to the zero-average of the x and y-components, we take the liberty to illustrate the different average spin direction values by different azimuth angles

to have a less cluttered illustration. We stressed that although one may think it is precessing and decaying towards the magnetic field, this is not a time-varying process. We show the probability distribution projection in the unit sphere in figure 3.4 for these three points. Here we can see that although the positive z-axis represents the maximum of the probability for each case. Simultaneously, we increase the voltage, the probability becomes more and more homogeneous, explaining the decrease of the z-component average.

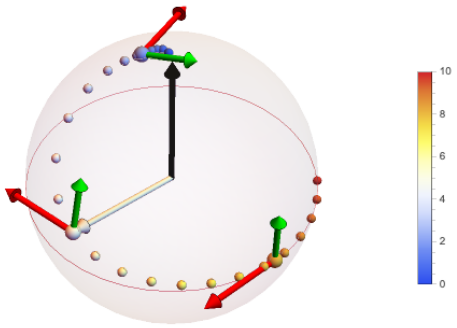


Figure 3.3: Illustration of the torques at the three points remarked in figure (10). The black, red, and green arrows represent the magnetic field, the precessional torque, and the damping-like torque's direction. Each sphere illustrates a point in figure (3.2), and we represent the Voltage value by the sphere's color.

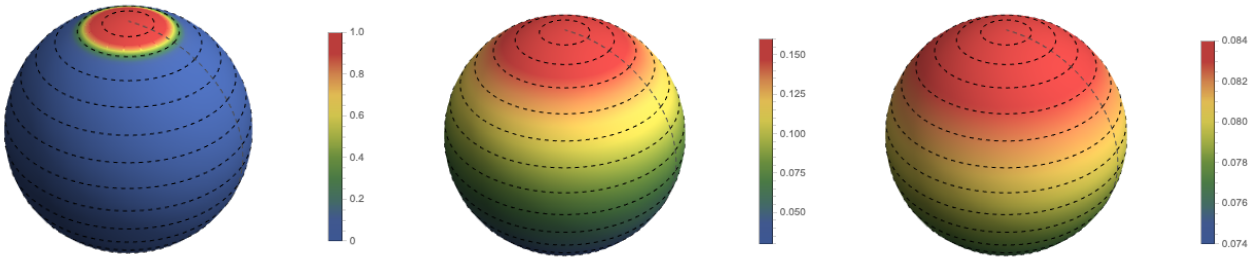


Figure 3.4: The probability density illustration of the localized spin's direction for the three points remarked in figure (3.2). The left plot represents the point at 2 [mV] and shows a higher probability density for the positive z-axis, explaining the average value shown in figure (3.2). We can see the delocalization of the spin's direction for higher values of the voltage in the central (5 [mV]) and the right(8 [mV]) plots by looking into the range of values.

## 3.4. Dimer

The dimer case is more complicated to handle than the monomer case. The complication comes mostly from the spin-orbit coupling since, as argued in section 2.4.3, the anomalous terms drop to zero as the spin-orbit coupling is neglected. This configuration generates additional damping terms compared to equation (3.10), along with an effective energy that depends on the effective interactions $J_{ab}$, $D_{ab}$, and $\Gamma_{ab}$ from the s-d interaction $\Delta$. Therefore, we must deal with these additional terms to obtain the canonical form of this Langevin equation:

$$\hbar S\frac{d\boldsymbol{\Omega}}{dt} = \boldsymbol{\Omega}\times[\boldsymbol{H}+\boldsymbol{\eta}]-\hbar S\left\{S\alpha\ \boldsymbol{\Omega}\times\frac{d\boldsymbol{\Omega}}{dt}+S\beta\ \boldsymbol{\Omega}\times(\frac{d\boldsymbol{\Omega}}{dt}\times\hat{t})+S\gamma\ \boldsymbol{\Omega}\times\hat{t}\ (\hat{t}\cdot\frac{d\boldsymbol{\Omega}}{dt})\right\}. \quad (3.20)$$

We have defined $\boldsymbol{H} = -\frac{\partial\mathcal{E}_2^{eff}}{\partial\boldsymbol{\Omega}}$ with $\mathcal{E}^{eff}$ from (2.80) to simplify the notation and keep the monomer case's similarities. We see that the first additional damping term, $\beta\boldsymbol{\Omega}\times\frac{d\boldsymbol{\Omega}}{dt}\times\hat{t}$, is easier to treat, but the second one presents a bigger problem, although not impossible. Even though $\beta = 0$, we present a deduction of the canonical Langevin equation in Appendix B that include that factor, and impose that condition at the end. Equation (3.20) is written as:

$$\hbar S\frac{d\boldsymbol{\Omega}}{dt} = A\boldsymbol{\Omega}\times\left[\tilde{\boldsymbol{H}}+\tilde{\boldsymbol{\eta}}-S\alpha\left(\tilde{\boldsymbol{H}}+\tilde{\boldsymbol{\eta}}\right)\right], \quad (3.21)$$

where we have defined the "tilde transformation" for a generic vector field $\Lambda$ as:

$$\tilde{\boldsymbol{\Lambda}} = \boldsymbol{\Lambda} - ACS\gamma\ \hat{t}\cdot\Omega\times[\Lambda - S\alpha\Omega\times\Lambda]\,\hat{\boldsymbol{t}}. \quad (3.22)$$

We defined the A-factor as for the monomer case, the C-factor in equation (B.13), and the deduction of the "tilde transformation" in Appendix B. With the low energy approximation for the Keldysh component, we can see that the two-points correlation function in equation (2.94), matches the condition of being delta-correlated. However, the correlation is not an isotropic relation between the indices. Instead, we have an anisotropic correlation, $g_{ab}$, with the spin-orbit vector $\hat{\boldsymbol{t}}$ as a preferred direction besides the Kronecker delta $j_{ab}$ relation we had for the monomer case. Equation (3.21) is much more complicated than equation (3.11), for many reasons. The first one is that now, we have space-dependent factors besides the cross products. The second one is that the stochastic field's matrix in the two-point correlation function (3.3) is far from simple, and that will give us a much more complicated probability current. Now we can see that the characteristic functions of the canonical form of the Langevin equation are:

$$a^{\mu} = \frac{A}{\hbar S}(\delta^{\mu\nu} - ACS\bar{\gamma}\mathcal{O}^{\mu c}t_c t_{\nu})\mathcal{O}^{\nu b}H_b, \quad (3.23)$$

$$R^{\mu}{}_{m} = \frac{A}{\hbar S}(\delta^{\mu\nu} - ACS\bar{\gamma}\mathcal{O}^{\mu c}t_c t_{\nu})\mathcal{O}^{\nu b}\delta_{bm}, \quad (3.24)$$

$$b^{ij} = j\ \delta^{ij} + g\ t^i t^j. \quad (3.25)$$

It is interesting to notice that the operator $\mathcal{O}$ is equal to the operator $R^{\mu}{}_{\nu}$ in the monomer case. If we take the limit with null spin-orbit coupling, the dimer equation is identical to the monomer, since $\gamma$ is zero for that case. Therefore, it has to have the same solution for that case. With the exception that now, we have an effective interaction that accounts for an exchange interaction between the two localized spins, as presented by [12], which does not vanish with a neglected spin-orbit coupling. As shown in the beginning of this chapter, when we have the Langevin equation in the canonical form, is straightforward to find the Fokker-Planck equation. We have to apply the formulae for the drift vector (3.6) and diffusion tensor (3.7). So, we find that the probability current $J^{\mu}$ is

$$\begin{aligned}
\boldsymbol{J} = &-\boldsymbol{h}\mathbb{P} + \frac{1}{2}a^2C^2(\Omega t)[jS\gamma(\boldsymbol{\Omega}\times\boldsymbol{t})\{1-2AS\gamma S\alpha(1-(\Omega t)^2)[1+C]\} - (\boldsymbol{\Omega}\times\boldsymbol{\Omega}\times\boldsymbol{t})S\alpha[3+2C]) \\
&-gS\alpha[1+C][(\boldsymbol{\Omega}\times\boldsymbol{t}) - S\alpha(\boldsymbol{\Omega}\times\boldsymbol{\Omega}\times\boldsymbol{t})]]\mathbb{P} + \frac{1}{2}a^2j[1+(S\alpha)^2](\boldsymbol{\Omega}\times\boldsymbol{\Omega}\times\boldsymbol{\partial_\nu}\mathbb{P}) + \\
&\frac{1}{2}a^2j[1+(S\alpha)^2]ACS\gamma\{C(\boldsymbol{\Omega}\times\boldsymbol{\Omega}\times\boldsymbol{t})(\Omega\times t)^\nu\partial_\nu\mathbb{P} + ACS\gamma(1-(\Omega t)^2)(\boldsymbol{\Omega}\times\boldsymbol{t})(\Omega\times\Omega\times t)^\nu\partial_\nu\mathbb{P} \\
&-(1+C)S\alpha(\boldsymbol{\Omega}\times\boldsymbol{\Omega}\times\boldsymbol{t})(\Omega\times\Omega\times t)^\nu\partial_\nu\mathbb{P} + ACS\gamma(1-(\Omega t)^2)(\boldsymbol{\Omega}\times\boldsymbol{t})(\Omega\times t)^\nu\partial_\nu\mathbb{P}]\} \\
&+\frac{1}{2}a^2gC^2[(\boldsymbol{\Omega}\times\boldsymbol{t} - S\alpha(\boldsymbol{\Omega}\times\boldsymbol{\Omega}\times\boldsymbol{t})]\{(\Omega\times\hat{t})^\nu\partial_\nu\mathbb{P} - S\alpha(\Omega\times\Omega\times\hat{t})^\nu\partial_\nu\mathbb{P}\}. \qquad (3.26)
\end{aligned}$$

This current is hardly solvable due to many factors, such as, the number of terms, the intricate structure of mixed derivatives, and the space dependent factors. Here we recall the deduction and definition of the C-factor in Appendix B, because it is a function of $(\Omega t)^2$, therefore the above expression is even harder than it looks. Nevertheless, if we look at the previews section, we can see that the solution could come from a new effective energy that includes the effects of the anisotropic part of equation (2.94). As for the monomer case, we can look for a solution like equation (3.19), with an energy as the "primitive" of the effective field in equation (3.21), like $\tilde{H} = -\frac{\partial}{\partial\Omega}\mathcal{E}''$. We could obtain $\mathcal{E}''$ by Helmholtz's theorem, but it seems to be an impossible task due to the multiple cross products, even for a numerical calculation. However, when we study the weak spin-orbit coupling limit in the numerical results of section 2.4.4, we see that $S\alpha \gg S\gamma$ and $j \gg g$. In this limit, we can neglect higher than linear terms in $\{S\gamma, g\}$, so the probability current take a much more treatable expression:

$$\begin{aligned}
J^\mu = &-a(\boldsymbol{\Omega}\times\boldsymbol{H})^\mu\mathbb{P} + aS\alpha(\boldsymbol{\Omega}\times\boldsymbol{\Omega}\times\boldsymbol{H})^\mu\mathbb{P} + \frac{1}{2}a^2j\{1+(S\alpha)^2\}\,(\boldsymbol{\Omega}\times\boldsymbol{\Omega}\times\boldsymbol{\partial}\mathbb{P})^\mu \; + \\
&+(\boldsymbol{\Omega}\times\boldsymbol{t})^\mu\Big[\frac{1}{2}a^2(\Omega t)\{jS\gamma - 4gS\alpha\}\mathbb{P} - AaS\gamma[(\Omega\times t)\cdot H + S\alpha(\Omega\times\Omega\times t)\cdot H]\mathbb{P} + \\
&\quad+\frac{1}{2}a^2g(\Omega\times t)\cdot\partial\mathbb{P} + \frac{1}{2}a^2\{jS\gamma - gS\alpha\}(\Omega\times\Omega\times t)\cdot\partial\mathbb{P}\Big] \\
&+(\boldsymbol{\Omega}\times\boldsymbol{\Omega}\times\boldsymbol{t})^\mu\Big[-\frac{1}{2}a^2S\alpha\{5jS\gamma - 4gS\alpha\}\mathbb{P} + AaS\gamma S\alpha[(\Omega\times t)\cdot H + S\alpha(\Omega\times\Omega\times t)\cdot H]\mathbb{P} + \\
&\quad+\frac{1}{2}a^2\{jS\gamma - gS\alpha\}(\Omega\times t)\cdot\partial\mathbb{P} - \frac{1}{2}a^2S\alpha\{2jS\gamma - gS\alpha\}(\Omega\times\Omega\times t)\cdot\partial\mathbb{P}\Big]. \qquad (3.27)
\end{aligned}$$

From the above expression, we can see that the number of direction-dependent factors have been reduced. However, we still have to solve $\boldsymbol{\nabla\cdot J} = 0$, which still is far too complicated. Nevertheless, when we follow our earlier proposal for the solution as a Boltzmann distribution,

we find an approximate steady-state solution for the above current. So the probability density is:

$$\mathbb{P} = N \exp\Big\{-\beta \mathcal{E}'_{eff}\Big\}, \tag{3.28}$$

where we have defined the *effective temperature* $(1/\beta)$ and the *effective energy* $(\mathcal{E}'_{eff})$ as

$$\beta = 2\frac{S\hbar S\alpha}{j}, \tag{3.29}$$

$$\mathcal{E}'_{eff} = \mathcal{E}[\Omega] - S\Delta\langle s\rangle \cdot \Omega - \hbar S^2\Delta^2\Big[J_{21}\Omega\cdot\hat{m} + D_{21}\hat{t}\cdot(\Omega\times\hat{m}) + \Gamma_{21}(\Omega t)(\hat{m}\cdot\hat{t}) + \frac{1}{2}\Gamma_{22}(\Omega t)^2\Big]. \tag{3.30}$$

where $\mathcal{E}[\Omega]$ contains the Zeeman and anisotropic energies. As we mentioned, this solution is not an exact solution of equation (3.27), and we have to analyze the results that we get accordingly.

## Numerical Analysis

As we said in the last chapter, we aim to study the effects of the electrical current over the dimer system. More precisely, we are interested in the consequences of the spin-dependent hopping between the dimer molecules. So, in order to distinguish between the effects of both factors, electrical current and spin-dependent hopping, we compare the average value of the spin' direction for three different SOC values and the same hopping configuration. We can identify those configurations as: null, perturbative, and strong SOC.

The first configuration establishes the ground effects, i.e., the electrical current effects. It is clear that, with a null SOC ($t = 0$), the approximate solution becomes an exact solution of equation (3.26). In section 2.4.3, we discuss that all the non-symmetric interaction, damping, and correlations drop to zero under that condition, and we recover the equations presented in [12]. From which we can solve as we did for the monomer. Only now, with an additional voltage-dependent magnetic field from the effective exchange interaction: $S^2\Delta^2 J_{21}$. The probability density for this case is:

$$\mathbb{P} = N \exp\left\{-2\frac{S\hbar S\alpha}{j}\Big(\mathcal{E}[\mathbf{\Omega}] - S^2\Delta^2 J_{21}\hat{m}\cdot\mathbf{\Omega}\Big)\right\}. \tag{3.31}$$

This expression is all we need to study the average value of the spin's direction under the influence of the non-equilibrium electrons from the leads. The above expression is very similar to equation (3.19), with the interesting addition of the exchange interaction between the originally not interacting spins. In figure 3.5, we show the average value of the spin's direction for the three components. We calculate that average value using the values used in section 2.4.4, where we have an inter-lead hopping $J = 100$ [meV], connection hopping $t_{L/R} = 10$ [meV], an inter-device hopping $t_0 = 2$ [meV], the anisotropic energies $E = 0.007$ [meV] and $D = -0.039$ [meV], and an external magnetic field $B = 7$ [T] as presented in [12, 29] for the anisotropic and Zeeman interactions.

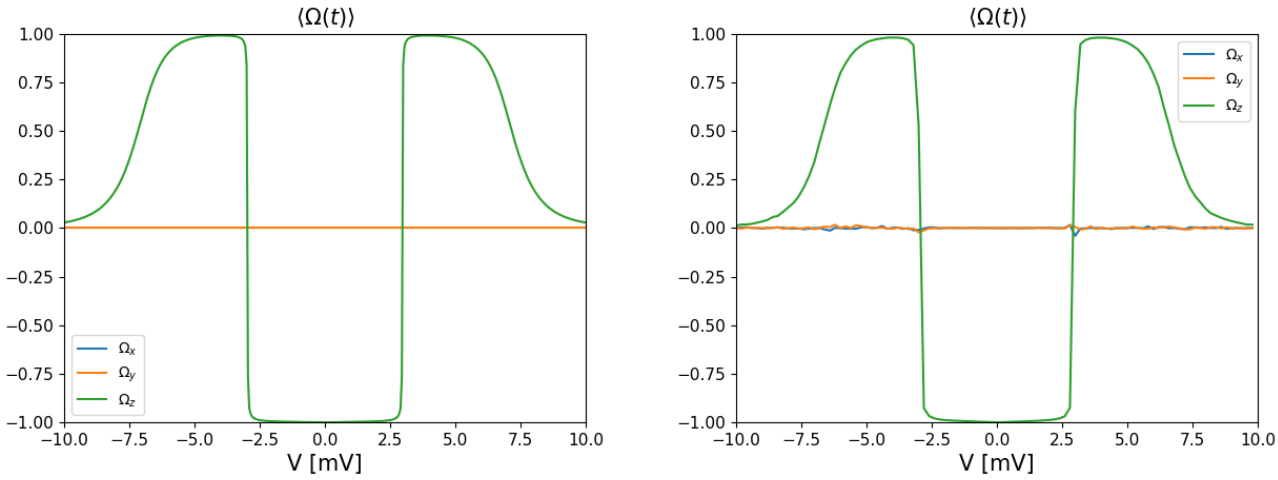


(a) Fokker-Planck method

(b) Langevin method

Figure 3.5: The average value of the localized spin's direction for each component at $\mu_F = 0[meV]$, using the FP method in (a) and the Langevin method in (b). The calculations were done considering that the fixed spin's direction is $\hat{z}$ in the absence of the SOC, $t = 0$ [meV], and the configuration explored in section 2.4.4. We can see that the system presents an antiferromagnetic configuration for $|V| < 3$ [mV]. However, as the voltage increase, the average value switches to a ferromagnetic configuration. At higher voltage, the spin's direction is fully degenerated by the increase in temperature. Both methods agree in every relevant result but differ in the decay of the z-component at high voltages.

Unlike the former case, now we study the non-equilibrium case with a center-band $\mu_F = 0$ as a function of the bias voltage for a fixed external magnetic field. We note that in this case, the system presents a switch in the spin orientation. At voltage $V = 0$, the average value of the spin's direction is negative due to the negative value of the effective interaction $J_{21}$. This result tells us that the system preferred an antiferromagnetic configuration between the localized spins. This negative average value persists until approximately $V = \pm 3$ [mV] where, as we saw in section 2.4.4, the sign of the effective interaction switches from negative to positive. We see that $\langle \Omega_z \rangle$ is positive for $|V| \geq 3$ [mV], meaning that the localized spins are aligned. Therefore, the system preferred a ferromagnetic configuration for high voltages.

We can see that, even though the interaction does not change in the sign for a voltage greater/lower that $V = \pm 6$ [mV], the average value decay to zero. This decay is approximately completed at $V = \pm 8$ [mV], where the system presents null polarization, i.e., the direction is completely degenerate. When we compare the numerical values presented in section 2.4.4 for this configuration, it is clear that the relation between the inverse temperature (3.30) that depends on the damping $S\alpha$ and the correlation $j$, and the effective exchange interaction in the effective energy (3.30), tends the system to decay at a zero-value polarization. Therefore,

this decay is due to a theoretical high temperature, so the system has enough energy to overrule the effects of either the external magnetic field and the exchange interaction between the spins.

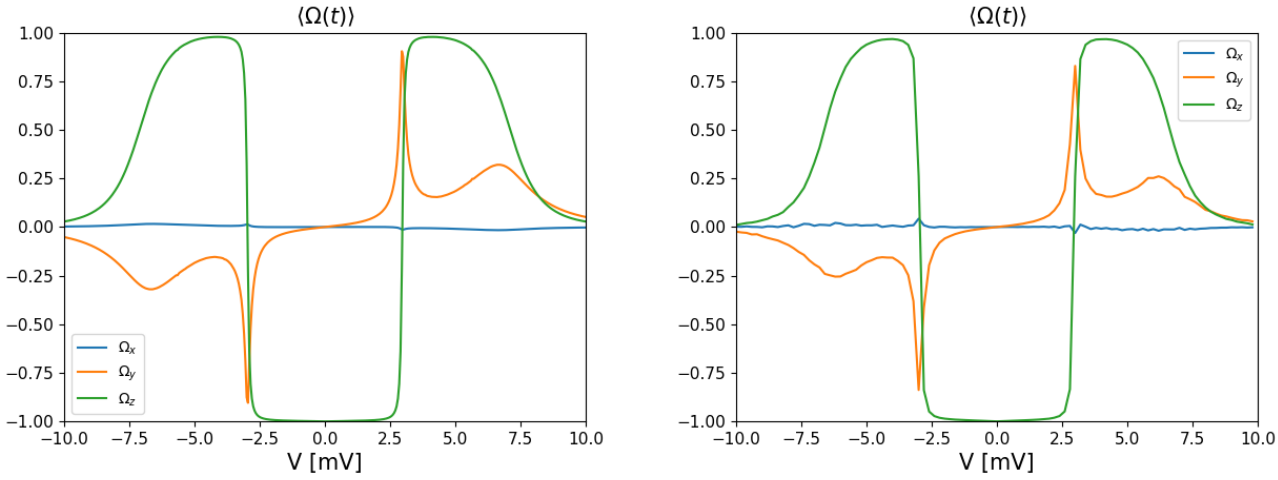


(a) Fokker-Planck method

(b) Langevin method

Figure 3.6: The average value of the localized spin's direction for each component at $\mu_F = 0[meV]$, using the FP method in (a) and the Langevin method in (b). The calculations were done considering that the fixed spin's direction is $\hat{z}$ in the absence of the SOC, $t = 0.05$ [meV], and the configuration explored in section 2.4.4. We can see that the z-component preserves the spin-inversion feature as for the case without SOC. However, the y-component is no longer fully degenerated due to the DM interaction. We can see that the maximum/minimum value is at the inversion point $V \sim 3$ [mV]. In this case, although both methods share the same structure, the FP method overestimates the effects of the DM interaction; therefore, the maximum and minimum values of the y-component.

As shown in figure 3.5, we have established that the electrical current introduces a fixed voltage that switches between an antiferromagnetic configuration to a ferromagnetic configuration. An important feature of this configuration is the degeneracy on the x-y plane, inherited from the symmetry of the system without spin-orbit coupling. Now we can study the inclusion of the SOC as a perturbation ($t = 0.05$) of the above configuration. The probability density now is not symmetric in the x-y plane due to the DM and the anisotropic interaction. These results are shown in figure 3.6.

Comparing the z-component shown in figures 3.5 and 3.6, it is very clear that SOC is, in fact, a small perturbation since it preserves the switching property. The only change between those configurations for $\langle \Omega_z \rangle$ is that the inversion is softer than before. The range of voltage for which the system preferred a ferromagnetic configuration is wider with the SOC. These modifications can be seen from the little change in the numerical values of $J_{21}$ between both cases. However, as we expected from the loss of symmetry in the x-y plane, when we include

the spin-dependent hopping the y-component is no longer zero. Instead, it reacts to the spin-switching point $V =\sim \pm 3$ [mV], and again at the decay range, $|V| \geq 6$ [mV]. To understand which interaction is responsible for this new effect, we can look at the end of Appendix B and see that the DM interaction is the only one that can contribute to the y-component. This observation is confirmed due to the opposite reaction for a negative voltage, matching the behavior of the DM interaction in figure 2.7b. The x-component remains almost zero, which can be seen by comparing the anisotropic interaction with respect to the other interactions along $\mu_F = 0$.

As said at the beginning of this chapter, the Fokker-Planck equation is a very useful mathematical tool to study the Langevin equation, but without an exact solution, we cannot say how far we are from the solution to the Langevin equation. That is why, even though the results presented at this point follow the intuition of what a weak extra interaction should do to the average spin's direction, we have to verify the validity of our approximate solution. When we compare the symmetric interaction $J_{21}$ with the anti-symmetric interaction $D_{21}$ in figure 2.7, it is clear that the approximate solution overestimates the effect of $D_{21}$. To check how far from the exact solution we are, we can study the absolute value of the difference between the approximate solution and the real theoretical solution, which satisfies $\boldsymbol{\nabla} \cdot \boldsymbol{J}^* = 0$ for each point, and is integrated over the unitary sphere. So the error would be:

$$\delta_{\mathbb{P}} \equiv \frac{1}{4\pi} \int ||\boldsymbol{\nabla} \cdot \boldsymbol{J}(\mathbb{P})|| dS. \tag{3.32}$$

The error of the results shown in figure 3.6 for weak SOC is shown in figure 3.7.

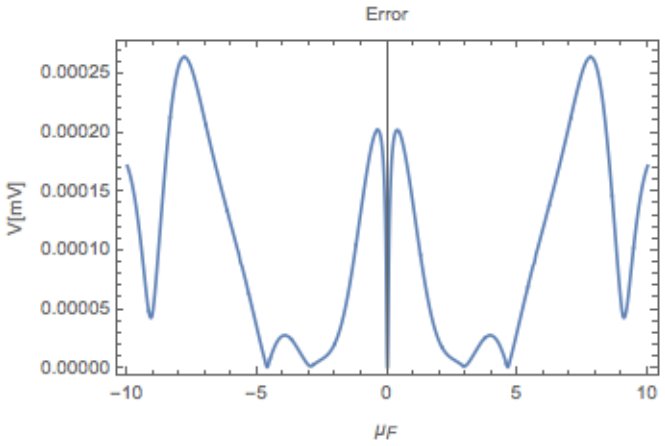


Figure 3.7: Integral error of the approximate solution to the FP equation. Calculated for the strong coupling configuration and weak SOC, $t = 0.05$ [meV].

We could argue that the error is low simply because the maximum value is small ($\sim 10^{-4}$) and lower than other possible solutions. However, this procedure lacks a real comparable framework. A clearer and direct way to know if our approximate solution is trustworthy is to compare it with the original stochastic equation's numerical solution equations numerical solution. We use a Montecarlo method that preserves the norm of the vector in *Python*. This approach is numerically demanding, so we use it as a last resource to check the approximate FP solution results. In figures 3.5 and 3.6, we have shown the FP result (left) and the Lan-

gevin equation's direct numerical solution (right). With this, we notice that our approximate solution is indeed an excellent approximation. However, as we predicted, it overestimates the DM interaction's effect. When we compared both solutions in figure 3.6, we can see that the error in figure 3.7 has the maxima approximately at the voltages that those methods differ.

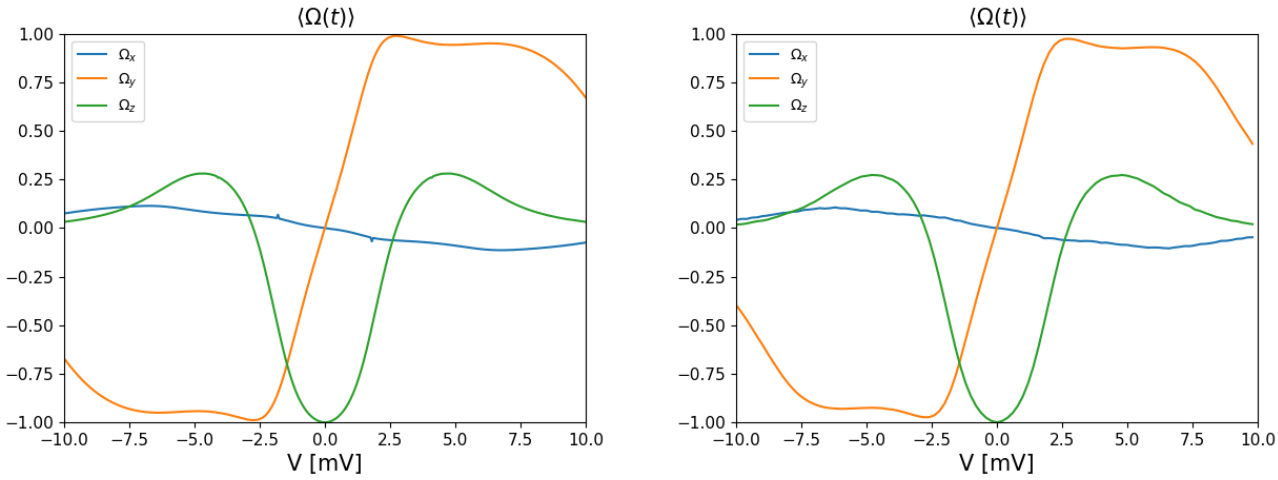


(a) Fokker-Planck method

(b) Langevin method

Figure 3.8: The average value of the localized spin's direction for each component at $\mu_F = 0[meV]$, using the FP method in (a) and the Langevin method in (b). The calculations were done considering that the fixed spin's direction is $\hat{z}$ in the absence of the SOC, $t = 1$ [meV], and the configuration explore in section 2.4.4. We can see that the spin-inversion of the z-component is now incomplete in both methods. This change can be explained by the numerical relation of $J_{21}$ with $D_{21}$ in figure 2.11. With this configuration, the dominant component is $\Omega_y$ and the x-component is not fully degenerated as for low SOC. We can see that although both methods predict the same raw behavior, they-component is highly overestimated in (a) and does not decay to zero, as shown with the Langevin method (b).

Due to the small differences between both methods, we have can study the strong SOC case. As we can see from section 2.4.4, when we consider $t = 1$ [meV], the conditions $S\alpha \gg S\gamma$ and $j \gg g$, that we impose to study the approximate form of the probability current, is no longer valid. Therefore, it is a suitable configuration to study the limitation of solution the (3.28). The spin's direction's average value is shown in figure 3.8, and the error of the FP method is shown in figure 3.9.

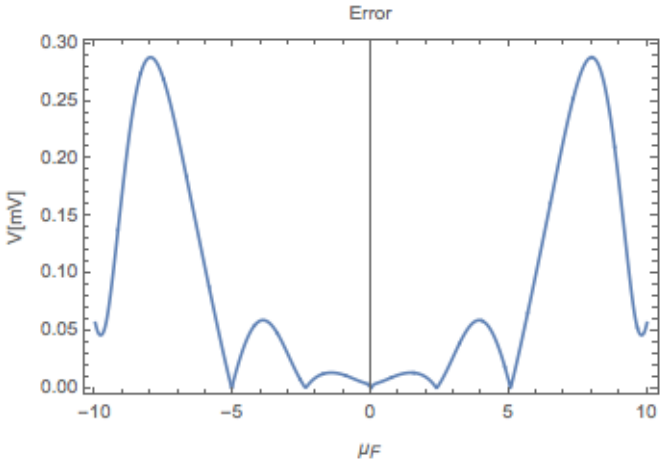


Figure 3.9: Integral error of the approximate solution to the FP equation. Calculated for the strong coupling configuration and strong SOC, $t = 1$ [meV]

Unlike the weak SOC results, when we study the average value $\langle\Omega\rangle$ with both methods, we can see more obvious differences. Although they are still reasonably similar since they present the same attenuation of the z-component, the FP method (left) fails to estimate the effect over the y and x-component. The fact that the y-component does not drop to zero as the Langevin method does presents a complication since it can not predict correctly the range of voltage for which $\langle\Omega_y\rangle$ could be used as $\langle\Omega_x\rangle$ for the case without SOC. In this case, the error shown in figure 3.9 indicates that the bigger problem is precisely at high voltages, where the FP method fails to estimate the decay zero-average.

# Chapter 4

# Conclusion

In this thesis, we work out the effective theory to study the time evolution of the spin's direction in two cases, the monomer and dimer configuration, previously presented in [34] and [12] respectively. Both configurations were studied with an electronic environment characterized by two infinite leads that inject and drain electrons. Using the Path integral techniques we were able to integrate both leads, so that we could focus on the dynamics of the spin's direction of the molecules in the system.

In the second chapter, we developed the mathematical framework to obtain each localized spin equation of motion. However, since we were interested in the effects of the bias voltage effects over the system, i.e., an electrical current passing through the leads, we had to implement the Keldysh formalism to include the non-equilibrium effects in the Path integral technique and the quantum many-body formalism. With these mathematical tools, we found the semiclassical equations of motion.

The most remarkable results come from the inclusion of a spin-dependent hopping in between the lead. This new interaction is attributed to a spin-orbit interaction present in the system. For the system, the consequence of the SOC was the loss of symmetry, thus introducing non-symmetrical effective interactions, such as the DM and the anisotropic interactions. Along with those interactions, a microscopic deduction of the Gilbert damping was presented for the monomer and dimer case. However, similar to the non-symmetric interactions, in the dimer configuration, we found anisotropic damping in addition to the symmetric Gilbert damping.

Furthermore, when we studied the stochastic magnetic field's correlation functions, we found the same additional structure. These new interactions, damping, and correlation strength are susceptible to the strength of the SOC. At the end of the chapter, we deduce the equation of motion that considers one of the two localized spins being fixed in a particular direction, which turns to resemble the Landau-Lifshitz-Gilbert equation with a stochastic magnetic field and anomalous non-symmetrical terms.

In the third chapter, the spin's direction's average value is studied using the Fokker-Planck equation and a direct numerical solution of the Langevin equation. Here the effects of the spin-dependent hopping were established for weak and strong coupling. Although we restricted the analysis to an approximate solution to the Fokker-Planck equation due to the

equations' high complexity, the comparison between the two methods showed remarkable resemblance.

In contrast with the monomer, the dimer configuration provides exceptional results when studying the average value of the one localized spin. The polarization of the given molecule can be electrically control between a Ferromagnetic and an Antiferromagnetic configuration by the bias voltage between the leads, with the restriction of the other spin being fixed in certain direction. This result has been predicted before for a similar configuration in [12, 43] among many others. However, we see that with the inclusion of strong SOC, that inversion is suppressed. For strong SOC, we showed that the dominant component is induced by the DM interaction rather than the exchange interaction or the Zeeman effect as for the same system in the absence of SOC. This effect can be understood when we analyze the canonical Langevin equation by means of the SOT, which is the most remarkable result of this thesis.

Future work would be the natural extension of the two-sites system towards an N-sites system where we could study the dynamics of magnetic textures like domain walls and, even more, how the spin-orbit coupling can affect the texture and its dynamics. We left pending the calculation of an exact solution for the Fokker-Planck equation if there is one. However, with the same framework developed in this thesis, we could study other exciting effects like the spin Hall effect by changing the connection between the leads and the dimer. It has been shown that a thermal gradient along the electronic device can introduce spin densities that can lead to the asymmetry needed to induced the STT or even modify the SOT, and this effect can be studied with the configuration presented in this thesis.

# Bibliography


[1] Amikam Aharoni et al. *Introduction to the Theory of Ferromagnetism*, volume 109. Clarendon Press, 2000.

[2] Alexander Altland and Ben D Simons. *Condensed matter field theory*. Cambridge university press, 2010.

[3] Philip W Anderson. More is different. *Science*, 177(4047):393–396, 1972.

[4] Assa Auerbach. *Interacting electrons and quantum magnetism*. Springer Science & Business Media, 2012.

[5] Mario Norberto Baibich, Jean Marc Broto, Albert Fert, F Nguyen Van Dau, Frédéric Petroff, P Etienne, G Creuzet, A Friederich, and J Chazelas. Giant magnetoresistance of (001) fe/(001) cr magnetic superlattices. *Physical review letters*, 61(21):2472, 1988.

[6] Supriyo Bandyopadhyay and Marc Cahay. *Introduction to spintronics*. CRC press, 2015.

[7] Luc Berger. Emission of spin waves by a magnetic multilayer traversed by a current. *Physical Review B*, 54(13):9353, 1996.

[8] Grünberg Binasch, Peter Grünberg, F Saurenbach, and W Zinn. Enhanced magnetoresistance in layered magnetic structures with antiferromagnetic interlayer exchange. *Physical review B*, 39(7):4828, 1989.

[9] Supriyo Datta. *Electronic transport in mesoscopic systems*. Cambridge university press, 1997.

[10] Supriyo Datta. *Quantum transport: atom to transistor*. Cambridge university press, 2005.

[11] Fernando Delgado, JJ Palacios, and Joaquín Fernández-Rossier. Spin-transfer torque on a single magnetic adatom. *Physical review letters*, 104(2):026601, 2010.

[12] Sebastián Díaz and Álvaro S Núñez. Current-induced exchange interactions and effective temperature in localized moment systems. *Journal of Physics: Condensed Matter*, 24 (11):116001, 2012.

[13] Sebastián Alejandro Díaz Santiago. Controlling spin interactions with electric currents. 2010.

[14] Mikhail I Dyakonov and VI Perel. Current-induced spin orientation of electrons in semiconductors. *Physics Letters A*, 35(6):459–460, 1971.

[15] Albert Fert, Vincent Cros, and Joao Sampaio. Skyrmions on the track. *Nature nanotechnology*, 8(3):152–156, 2013.

[16] Shunsuke Fukami, Hideo Sato, Michihiko Yamanouchi, Shoji Ikeda, Fumihiro Matsukura, and Hideo Ohno. Advances in spintronics devices for microelectronics—from spin-transfer torque to spin-orbit torque. In *2014 19th Asia and South Pacific Design Automation Conference (ASP-DAC)*, pages 684–691. IEEE, 2014.

[17] Ion Garate and Allan H MacDonald. Influence of a transport current on magnetic anisotropy in gyrotropic ferromagnets. *Physical Review B*, 80(13):134403, 2009.

[18] GW Gardiner. Handbook of stochastic processes for physics. *2002.,()*, 2002.

[19] Dante Gatteschi, Roberta Sessoli, and Jacques Villain. *Molecular nanomagnets*, volume 5. Oxford University Press on Demand, 2006.

[20] Murray Gell-Mann and Francis Low. Bound states in quantum field theory. *Physical Review*, 84(2):350, 1951.

[21] JF Gregg, I Petej, E Jouguelet, and C Dennis. Spin electronics—a review. *Journal of Physics D: Applied Physics*, 35(18):R121, 2002.

[22] John Hubbard. Calculation of partition functions. *Physical Review Letters*, 3(2):77, 1959.

[23] John David Jackson. *Classical electrodynamics*. John Wiley & Sons, 2007.

[24] Vinod Kumar Joshi. Spintronics: A contemporary review of emerging electronics devices. *Engineering Science and Technology, an International Journal*, 19(3):1503 – 1513, 2016. ISSN 2215-0986. doi: https://doi.org/10.1016/j.jestch.2016.05.002. URL http://www.sciencedirect.com/science/article/pii/S2215098615300501.

[25] Hosho Katsura, Alexander V Balatsky, Zohar Nussinov, and Naoto Nagaosa. Voltage dependence of landau-lifshitz-gilbert damping of spin in a current-driven tunnel junction. *Physical Review B*, 73(21):212501, 2006.

[26] Charles Kittel and Paul McEuen. *Introduction to solid state physics*, volume 8. Wiley New York, 1976.

[27] Jun Kondo. Resistance minimum in dilute magnetic alloys. *Progress of theoretical physics*, 32(1):37–49, 1964.

[28] Flor Langouche, Dirk Roekaerts, and Enrique Tirapegui. *Functional integration and semiclassical expansions*, volume 10. Springer Science & Business Media, 2013.

[29] Sebastian Loth, Kirsten Von Bergmann, Markus Ternes, Alexander F Otte, Christopher P Lutz, and Andreas J Heinrich. Controlling the state of quantum spins with electric currents. *Nature Physics*, 6(5):340–344, 2010.

[30] Aurelien Manchon and Shufeng Zhang. Theory of nonequilibrium intrinsic spin torque in a single nanomagnet. *Physical Review B*, 78(21):212405, 2008.

[31] Aurélien Manchon and Shufeng Zhang. Theory of spin torque due to spin-orbit coupling. *Physical Review B*, 79(9):094422, 2009.

[32] Nevill Francis Mott. The electrical conductivity of transition metals. *Proceedings of the Royal Society of London. Series A-Mathematical and Physical Sciences*, 153(880): 699–717, 1936.

[33] John W Negele. *Quantum many-particle systems*. CRC Press, 2018.

[34] Alvaro S Núñez and RA Duine. Effective temperature and gilbert damping of a current-driven localized spin. *Physical Review B*, 77(5):054401, 2008.

[35] Michael Peskin. *An introduction to quantum field theory*. CRC press, 2018.

[36] Gary A Prinz. Magnetoelectronics. *Science*, 282(5394):1660–1663, 1998.

[37] Daniel C Ralph and Mark D Stiles. Spin transfer torques. *Journal of Magnetism and Magnetic Materials*, 320(7):1190–1216, 2008.

[38] Rajagopalan Ramaswamy, Jong Min Lee, Kaiming Cai, and Hyunsoo Yang. Recent advances in spin-orbit torques: Moving towards device applications. *Applied Physics Reviews*, 5(3):031107, 2018.

[39] Jørgen Rammer. *Quantum field theory of non-equilibrium states*, volume 22. Cambridge University Press Cambridge, 2007.

[40] E. I. Rashba. *Sov. Phys. Solid State*, vol. 2:p. 1109, 1960.

[41] Hannes Risken. Fokker-planck equation. In *The Fokker-Planck Equation*, pages 63–95. Springer, 1996.

[42] S Das Sarma, Jaroslav Fabian, Xuedong Hu, and Igor Zutic. Spin electronics and spin computation. *Solid State Communications*, 119(4-5):207–215, 2001.

[43] T Saygun, J Bylin, Henning Hammar, and Jonas Fransson. Voltage-induced switching dynamics of a coupled spin pair in a molecular junction. *Nano Letters*, 16(4):2824–2829, 2016.

[44] Steven H Simon. *The Oxford solid state basics*. OUP Oxford, 2013.

[45] John C Slonczewski et al. Current-driven excitation of magnetic multilayers. *Journal of Magnetism and Magnetic Materials*, 159(1):L1, 1996.

[46] R. L. Stratonovich. On a method of calculating quantum distribution functions. 1957.

[47] Evgeny Y Tsymbal and Igor Žutić. *Spintronics Handbook: Spin Transport and Magnetism: Volume One: Metallic Spintronics*. CRC Press, 2019.

[48] Xuhui Wang and Aurelien Manchon. Diffusive spin dynamics in ferromagnetic thin films with a rashba interaction. *Physical review letters*, 108(11):117201, 2012.

[49] Xiao-Gang Wen. *Quantum field theory of many-body systems: from the origin of sound to an origin of light and electrons*. Oxford University Press on Demand, 2004.

[50] Xichao Zhang, Yan Zhou, Motohiko Ezawa, GP Zhao, and Weisheng Zhao. Magnetic skyrmion transistor: skyrmion motion in a voltage-gated nanotrack. *Scientific reports*, 5:11369, 2015.

[51] Michael Ziese and Martin J Thornton. *Spin electronics*, volume 569. Springer, 2007.

[52] Igor Žutić, Jaroslav Fabian, and S Das Sarma. Spintronics: Fundamentals and applications. *Reviews of modern physics*, 76(2):323, 2004.

# Appendix A

# Electronic Green's functions calculations

For the first half of Section 2.4, we avoid a detailed calculation of the integral kernel $K^{ij}_{ab}(t,t')$ that contains the information from the electronic interaction between the leads and the spin dimer device. Besides the relation with the electronic Green's function 2.18, the decomposition over the Keldysh contour (2.62) and (2.63), and a useful symmetry 2.68. The primary reason for this is to focus on the complicated deduction and the physical aspect, and not get lost with all the calculations. In this Appendix, we explain a bit more step by step procedure to obtain a low energy approximation of the integral kernel. Even though this deduction is standard and can be found in [9, 13]. Up to now, the best we know about $K^{ij}_{ab}(t,t')$ is that it relates to the electronic Green's function by equation (2.18), but if we apply the greater and lesser decomposition for $G$, to replace it in equation (2.18) we see that

$$\begin{aligned} G_{b\sigma';a\mu}(t,t')G_{b\mu';a\sigma}(t',t) = \Theta(t-t')\left[G^{>}_{b\sigma';a\mu}(t,t')G^{<}_{b\mu';a\sigma}(t',t)\right] \\ +\Theta(t'-t)\left[G^{<}_{b\sigma';a\mu}(t,t')G^{>}_{b\mu';a\sigma}(t',t)\right] \end{aligned} \tag{A.1}$$

Where we have used the properties of the $\Theta$ function: $\Theta(t)\Theta(-t) = 0$ and $\Theta^2(t) = \Theta(t)$. With these result, we can come back to equation (2.18) and identify the greater and lesser components of the integral kernel:

$$K^{ij\ >}_{ab} = \frac{i}{8\hbar}\sum_{\sigma\sigma'\mu\mu'} \tau^{i}_{\sigma\sigma'}\tau^{j}_{\mu\mu'}G^{>}_{a\sigma';b\mu}(t,t')G^{<}_{b\mu';a\sigma}(t',t) \tag{A.2}$$

$$K^{ij\ <}_{ab} = \frac{i}{8\hbar}\sum_{\sigma\sigma'\mu\mu'} \tau^{i}_{\sigma\sigma'}\tau^{j}_{\mu\mu'}G^{<}_{a\sigma';b\mu}(t,t')G^{>}_{b\mu';a\sigma}(t',t) \tag{A.3}$$

Applying the Fourier transformation (2.42), we find the energy representation of the dimer kernel in terms of the electronic Green's function components.

$$K_{ab}^{ij\ (\pm)}(\epsilon) = \frac{-1}{8}\sum_{\sigma\sigma'\mu\mu'}\tau^i_{\sigma\sigma'}\tau^j_{\mu\mu'}\int\frac{d\epsilon'}{2\pi}\frac{d\epsilon''}{2\pi}\frac{G^{>}_{a\sigma';b\mu}(\epsilon')G^{<}_{b\mu';a\sigma}(\epsilon'') - G^{<}_{a\sigma';b\mu}(\epsilon')G^{>}_{b\mu';a\sigma}(\epsilon'')}{\epsilon^{\pm}-\epsilon'+\epsilon''} \tag{A.4}$$

$$K_{ab}^{ij\ (K)}(\epsilon) = -\frac{i\pi}{4}\sum_{\sigma\sigma'\mu\mu'}\tau^i_{\sigma\sigma'}\tau^j_{\mu\mu'}\int\frac{d\epsilon'}{2\pi}\frac{d\epsilon''}{2\pi}\delta(\epsilon-\epsilon'+\epsilon'')[G^{>}_{a\sigma';b\mu}(\epsilon')G^{<}_{b\mu';a\sigma}(\epsilon'')+ \\ +G^{<}_{a\sigma';b\mu}(\epsilon')G^{>}_{b\mu';a\sigma}(\epsilon'')] \tag{A.5}$$

where $\epsilon^{\pm} = \epsilon \pm i\delta$ is added for convergence in the integration as usual [2, 33]. We have reduced the problem to characterize the lesser and greater electronic Green's functions, however, we do not have an explicit expression for them. On the other hand, we can compute the advanced and retarded Green's functions from

$$\begin{bmatrix} (\epsilon-\hbar\Sigma_1^{\pm}(\epsilon))\mathbb{I}_{\sigma\mu} & \mathbb{T}_{\sigma\mu} \\ \mathbb{T}_{\sigma\mu} & (\epsilon-\hbar\Sigma_2^{\pm}(\epsilon))\mathbb{I}_{\sigma\mu} \end{bmatrix}_{ac} G^{(\pm)}_{c\mu;b\sigma'} = \mathbb{I}_{a\sigma;b\sigma'} \tag{A.6}$$

where we have set a zero on-site energy for both leads, this may be used to add an extra set-able parameter like in [43]. We also have introduce the self-energy $\Sigma^{\pm}_{1,2}$ of each lead in order to account for their interaction with the system in the Hamiltonian. When we solve the above equation for $G^{(\pm)}_{c\mu;b\sigma'}$ , we find that it present a very useful and characteristic form

$$G^{(\pm)}_{a\sigma;b\sigma'}(\epsilon) = G^{(s)(\pm)}_{ab}(\epsilon)\mathbb{I}_{\sigma\sigma'} + G^{(t)(\pm)}_{ab}(\epsilon)[\boldsymbol{t}\cdot\boldsymbol{\tau}]_{\sigma\sigma'} \tag{A.7}$$

where we define the *Singlet* function $G^{(s)(\pm)}_{ab}(\epsilon)$ due to be related to the symmetric part in spin space, and the *Triplet* function $G^{(t)(\pm)}_{ab}(\epsilon)$ due to the trace-less part of the full electronic GF in spin space. The components of the singlet retarded and advanced function are

$$G^{(\pm)(s)}_{11}(\epsilon) = \frac{g_2^{\pm}}{2}\left[\frac{1}{g_1^{\pm}g_2^{\pm}-(t_0+t)^2} + \frac{1}{g_1^{\pm}g_2^{\pm}-(t_0-t)^2}\right] \tag{A.8}$$

$$G^{(\pm)(s)}_{12}(\epsilon) = G^{(\pm)(s)}_{21}(\epsilon) = -\frac{1}{2}\left[\frac{t_0+t}{g_1^{\pm}g_2^{\pm}-(t_0+t)^2} + \frac{t_0-t}{g_1^{\pm}g_2^{\pm}-(t_0-t)^2}\right] \tag{A.9}$$

$$G^{(\pm)(s)}_{22}(\epsilon) = \frac{g_1^{\pm}}{2}\left[\frac{1}{g_1^{\pm}g_2^{\pm}-(t_0+t)^2} + \frac{1}{g_1^{\pm}g_2^{\pm}-(t_0-t)^2}\right] \tag{A.10}$$

and the triplet retarded and advanced function

$$G^{(\pm)(t)}_{11}(\epsilon) = \frac{g_2^{\pm}}{2}\left[\frac{1}{g_1^{\pm}g_2^{\pm}-(t_0+t)^2} - \frac{1}{g_1^{\pm}g_2^{\pm}-(t_0-t)^2}\right] \tag{A.11}$$

$$G^{(\pm)(t)}_{12}(\epsilon) = G^{(\pm)(t)}_{21}(\epsilon) = -\frac{1}{2}\left[\frac{t_0+t}{g_1^{\pm}g_2^{\pm}-(t_0+t)^2} - \frac{t_0-t}{g_1^{\pm}g_2^{\pm}-(t_0-t)^2}\right] \tag{A.12}$$

$$G^{(\pm)(t)}_{22}(\epsilon) = \frac{g_1^{\pm}}{2}\left[\frac{1}{g_1^{\pm}g_2^{\pm}-(t_0+t)^2} - \frac{1}{g_1^{\pm}g_2^{\pm}-(t_0-t)^2}\right] \tag{A.13}$$

where we have define $g_i^{\pm} = \epsilon - \hbar\Sigma_i^{\pm}(\epsilon)$. The problem comes when we try to invert equation (2.62) to obtain the lesser and greater components from the advanced and retarded. Gladly,

we can do it by using the steady-state kinetic equation [9, 10, 12],

$$G^{\lessgtr}(\epsilon) = G^{(+)}(\epsilon)\hbar\Sigma^{\lessgtr}(\epsilon)G^{(-)}(\epsilon) \tag{A.14}$$

where $\Sigma^{\lessgtr}$ is a 4x4 matrix that tell us the rate at which electrons come in from each lead by the *in-scattering* function $\Sigma^{<}$, or the rate at which the electrons come out from each lead by the *out-scattering* function $\Sigma^{>}$. The matrix representation of $\Sigma^{\lessgtr}$ is

$$\Sigma^{\lessgtr}(\epsilon) = \begin{bmatrix} \Sigma_1^{\lessgtr}\mathbb{I} & 0 \\ 0 & \Sigma_2^{\lessgtr}\mathbb{I} \end{bmatrix} \tag{A.15}$$

a similar deduction has to be done to obtain equation (2.46) in the monomer case. It seems that we are complicating things rather than making them simpler, but since we are dealing with leads at equilibrium, the advanced and retarded self-energies can be written as

$$\Sigma_a^{<}(\epsilon) = -n_F(\epsilon - \mu_a)[\Sigma_a^{(+)}(\epsilon) - \Sigma_a^{(-)}(\epsilon)] \tag{A.16}$$
$$\Sigma_a^{>}(\epsilon) = \{1 - n_F(\epsilon - \mu_a)\}[\Sigma_a^{(+)}(\epsilon) - \Sigma_a^{(-)}(\epsilon)] \tag{A.17}$$

with this we have finally found an explicit expression of $G^{\lessgtr}_{a\sigma;b\sigma'}$ in term of the system variables and the self-energies, therefore the kernels' expressions (A.4) and (A.5), can be evaluated in those variables. However, with the decomposition into singlet and triplet components (A.7), and the properties of the Pauli matrices, we can see that the greater and lesser components of $G^{\lessgtr}_{a\sigma;b\sigma'}$ follows the same structure of singlet and triplet, only a bit more complicated.

$$G^{\lessgtr}_{a\sigma;b\sigma'}(\epsilon) = G^{(s)\ \lessgtr}_{ab}(\epsilon)\mathbb{I}_{\sigma\sigma'} + G^{(t)\ \lessgtr}_{ab}(\epsilon)[\boldsymbol{t}\cdot\boldsymbol{\tau}]_{\sigma\sigma'} \tag{A.18}$$

where we have define the lesser and greater singlet function and triplet function as

$$G^{(s)\lessgtr}_{ab} = \sum_c [G^{(s)(+)}_{ac}\hbar\Sigma^{\lessgtr}_c G^{(s)(-)}_{cb} + G^{(t)(+)}_{ac}\hbar\Sigma^{\lessgtr}_c G^{(t)(-)}_{cb}] \tag{A.19}$$
$$G^{(t)\lessgtr}_{ab} = \sum_c [G^{(s)(+)}_{ac}\hbar\Sigma^{\lessgtr}_c G^{(t)(-)}_{cb} + G^{(t)(+)}_{ac}\hbar\Sigma^{\lessgtr}_c G^{(s)(-)}_{cb}] \tag{A.20}$$

at this point we can define a spectral function like we have done for (2.46) and work accordingly, but since we are now dealing with matrices, the expressions only get bigger and no simple analytical interpretation can be obtain from it. Although one may gain some insight when analyze special cases like the zero voltage, symmetry under $V \leftrightarrow -V$, or local maximum and minimum values along characteristics lines. This analysis can be equally done by studying the numerical results and fit the special lines if there are any, therefore we focus on that path. When we replace the relation (A.18) into (A.4) and (A.5), we found that it follows a regular structure that we represent, for simplicity, in the function:

$$\mathbb{G}^{\{p,q\}}_{ab\ \pm}(\epsilon', \epsilon'') \equiv G^{(p)\ >}_{ab}(\epsilon')G^{(q)\ <}_{ba}(\epsilon'') \pm G^{(p)\ <}_{ab}(\epsilon')G^{(q)\ >}_{ba}(\epsilon'') \tag{A.21}$$

where $(p, q) \in \{s, t\}$. This new function and expression (A.18), allow us to separate the site-dependent Green's function from vector nature of the kernels (A.4) and (A.5). Furthermore, we actually see that both expressions has only three very characteristic relations between the

vector indices. The advanced and retarded components can be written as:

$$K_{ab}^{ij\ (\pm)}(\epsilon) = -\frac{1}{4\hbar}\int \frac{d\epsilon'}{2\pi}\frac{d\epsilon''}{2\pi}\frac{\left[\mathcal{J}_{ab}(\epsilon',\epsilon'')\delta^{ij} + i\mathcal{D}_{ab}(\epsilon',\epsilon'')\epsilon^{ijk}\hat{t}^k + 2\bar{\Gamma}_{ab}(\epsilon',\epsilon'')\hat{t}^i\hat{t}^j\right]}{\epsilon^{\pm} - \epsilon' + \epsilon''} \tag{A.22}$$

where

$$\mathcal{J}_{ab}(\epsilon',\epsilon'') = \mathbb{G}^{\{s,s\}}_{ab\ (-)}(\epsilon',\epsilon'') - \mathbb{G}^{\{t,t\}}_{ab\ (-)}(\epsilon',\epsilon'') \tag{A.23}$$

$$\mathcal{D}_{ab}(\epsilon',\epsilon'') = \mathbb{G}^{\{s,t\}}_{ab\ (-)}(\epsilon',\epsilon'') - \mathbb{G}^{\{t,s\}}_{ab\ (-)}(\epsilon',\epsilon'') \tag{A.24}$$

$$\bar{\Gamma}_{ab}(\epsilon',\epsilon'') = \mathbb{G}^{\{t,t\}}_{ab\ (-)}(\epsilon',\epsilon'') \tag{A.25}$$

here we clearly anticipate that $\mathcal{J}_{ab}$, $\mathcal{D}_{ab}$, $\bar{\Gamma}_{ab}$ will give the effective symmetric exchange-like interaction, the effective antisymmetric exchange-like interaction and an effective anisotropic-like interaction, respectively. Nevertheless, we still have some analysis to do before confirm the above interpretation. Analogously for the Keldysh component in (A.5) we find

$$K_{ab}^{ij\ (K)}(\epsilon) = -\frac{i\pi}{2\hbar}\int \frac{d\epsilon'}{2\pi}\frac{d\epsilon''}{2\pi}\left[\bar{j}_{ab}(\epsilon',\epsilon'')\delta^{ij} + i\bar{d}_{ab}(\epsilon',\epsilon'')\epsilon^{ijk}\hat{t}^k + 2\bar{g}_{ab}(\epsilon',\epsilon'')\hat{t}^i\hat{t}^j\right]\delta(\epsilon - \epsilon' + \epsilon'') \tag{A.26}$$

where we define $\bar{j}_{ab}$, $\bar{d}_{ab}$ and $\bar{g}_{ab}$ by the same structure as for $\{\mathcal{J}_{ab}, \mathcal{D}_{ab}, \bar{\Gamma}_{ab}\}$, but replacing $(-) \mapsto (+)$ in (A.21). Now that we have make the connection of the advanced, retarded and Keldysh components to the singlet and triplet advanced and retarded electronic Green's functions, we can perform a Taylor expansion for $\epsilon \sim 0$ up to first order, and find that

$$(J_{ab}, iD_{ab}, \Gamma_{ab}) = -\frac{1}{2}\int \frac{d\epsilon'}{2\pi}\frac{d\epsilon''}{2\pi}\frac{1}{\epsilon'' - \epsilon' + i\delta}(\mathcal{J}_{ab}, i\mathcal{D}_{ab}, \bar{\Gamma}_{ab})(\epsilon',\epsilon'') \tag{A.27}$$

$$(\alpha_{ab}, i\beta_{ab}, \gamma_{ab}) = \frac{i}{2}\int \frac{d\epsilon'}{2\pi}\frac{d\epsilon''}{2\pi}\frac{\partial}{\partial\epsilon}\left(\frac{1}{\epsilon + i\delta - \epsilon' + \epsilon''}\right)_{\epsilon=0}(\mathcal{J}_{ab}, i\mathcal{D}_{ab}, \bar{\Gamma}_{ab})(\epsilon',\epsilon'') \tag{A.28}$$

So we have define the effective interactions and dampings as: $\mathcal{J}_{ab} \mapsto \{J_{ab}, \alpha_{ab}\}$, $\mathcal{D}_{ab} \mapsto \{D_{ab}, \beta_{ab}\}$ and $\bar{\Gamma}_{ab} \mapsto \{\Gamma_{ab}, \gamma_{ab}\}$. With this definitions, we can come back to equation (2.68) and work out the time integral. So the final expression for the equation of motion of $\mathbf{\Omega}_a$ is:

$$\hbar S\frac{d\mathbf{\Omega}_a}{dt}(t) = \mathbf{\Omega}_a \times \left[-\frac{\partial}{\partial\mathbf{\Omega}_a}\mathcal{E}^a_{eff}[\hat{\Omega}_a(t), \hat{\Omega}_b(t)] + \boldsymbol{\eta}_a(t) - \hbar S^2\sum_b \bar{\boldsymbol{\alpha}}_{ab}\frac{d\mathbf{\Omega}_b}{dt}(t)\right] \tag{A.29}$$

Where we have define the effective energy at site $a$ $\mathcal{E}^a_{eff}$ and the effective damping tensor $\bar{\boldsymbol{\alpha}}_{ab}$, as

$$\mathcal{E}^a_{eff}[\hat{\Omega}_a(t),\hat{\Omega}_b(t)] = \mathcal{E}[\hat{\Omega}_a] - S\Delta\langle \boldsymbol{s}_a(t)\rangle\cdot\boldsymbol{\Omega}_a(t) - \hbar S^2\Delta^2\sum_b\Big[J_{ab}\boldsymbol{\Omega}_a\cdot\boldsymbol{\Omega}_b+ \\ +D_{ab}\boldsymbol{t}\cdot(\boldsymbol{\Omega}_a\times\boldsymbol{\Omega}_b)+2\Gamma_{ab}(\boldsymbol{\Omega}_a\cdot\boldsymbol{t})(\boldsymbol{\Omega}_b\cdot\boldsymbol{t})-\Gamma_{aa}(\boldsymbol{\Omega}_a\cdot\boldsymbol{t})^2\Big] \quad (A.30)$$

$$\bar{\alpha}^{ij}_{ab} = \hbar\Delta^2\left[\alpha_{ab}\delta^{ij}+i\beta_{ab}\epsilon^{ijk}\hat{t}^k+2\gamma_{ab}\hat{t}^i\hat{t}^j\right] \quad (A.31)$$

When we analyze the Keldysh component, we notice that up to first order in $\epsilon$, the expression is constant, so the two-point correlation functions for the stochastic magnetic fields are written as:

$$\langle\eta^\alpha_a(t)\eta^\beta_b(t')\rangle = -i\Delta^2\hbar S^2\left[j_{ab}\delta^{\alpha\beta}+id_{ab}\epsilon^{\alpha\beta k}\hat{t}^k+2g_{ab}\hat{t}^\alpha\hat{t}^\beta\right]\delta(t-t') \quad (A.32)$$

where we can see that due to the spin-orbit coupling, the strength of $\boldsymbol{\eta}$ is far from the diagonal one found for the monomer configuration.

At the end of section 2.4, we specialize in the case where the spin at the first site is fixed. Therefore, we find that only a few components are relevant for the equation of motion of the free spin. These components are:

$$(J_{21},iD_{21},\Gamma_{21},\Gamma_{22}) = -\frac{1}{2}\int\frac{d\epsilon'}{2\pi}\frac{d\epsilon''}{2\pi}\frac{1}{\epsilon''-\epsilon'+i\delta}(\mathcal{J}_{21},i\mathcal{D}_{21},\bar{\Gamma}_{21},\bar{\Gamma}_{22})(\epsilon',\epsilon'') \quad (A.33)$$

$$(\alpha_{22},\gamma_{22}) = -\frac{1}{4}\int\frac{d\epsilon'}{2\pi}\frac{\partial}{\partial\epsilon}\Big((\mathcal{J}_{22},\bar{\Gamma}_{22})(\epsilon',\epsilon+\epsilon')\Big) \quad (A.34)$$

$$i\beta_{22} = -\frac{1}{2}\int\frac{d\epsilon'}{2\pi}\frac{d\epsilon''}{2\pi}\mathcal{P}\left(\frac{\frac{\partial}{\partial\epsilon''}\left[i\mathcal{D}_{22}(\epsilon',\epsilon'')\right]}{\epsilon''-\epsilon'}\right) \quad (A.35)$$

$$(j_{22},g_{22}) = -\frac{i}{4\hbar}\int\frac{d\epsilon'}{2\pi}(\bar{j}_{22},\bar{g}_{22})(\epsilon',\epsilon') \quad (A.36)$$

$$id_{22} = 0 \quad (A.37)$$

# Appendix B

# Dimer's canonical Langevin equation: Calculations

From equation (3.20) we now have three damping-like torques. As said in section 3.4, the $\beta$-term is the easier to treat, even though as we see in section 2.4.3, that term is actually zero for our configuration. However, we deduce the canonical form of the Langevin equation for the free spin in the dimer configuration, including that term for generality. Since we have the unitary condition for $\mathbf{\Omega}$, we can re-write that damping-like torque as

$$\beta\mathbf{\Omega} \times \frac{d\mathbf{\Omega}}{dt} \times \hat{t} = \beta(\Omega t)\frac{d\mathbf{\Omega}}{dt}. \tag{B.1}$$

Therefore, the original three-damping equation can be written as a two-damping equation with an simple parameter-transformation

$$\hbar S\frac{d\mathbf{\Omega}}{dt} = \mathbf{\Omega} \times [\bar{H} + \bar{\eta}] - S\bar{\alpha}\mathbf{\Omega} \times (\hbar S\frac{d\mathbf{\Omega}}{dt}) - S\bar{\gamma}\mathbf{\Omega} \times \hat{t}(\hat{t} \cdot \hbar S\frac{d\mathbf{\Omega}}{dt}), \tag{B.2}$$

where we have defined the "bar transformation" as:

$$\bar{\Lambda} = \frac{\Lambda}{(1 + S\beta(\hat{\Omega} \cdot \hat{t}))}. \tag{B.3}$$

Here we present $\Lambda$ as a generic variable so we can write the explicit form of the transformation. We will keep using it for simplicity in following definitions. Now we have to deal with the $\gamma$-term. The main complication of dealing with this kind of term comes from the inner product between the spin-orbit unitary vector and the time derivative of the spin's direction. But, if we replace the expression for $\hbar S\frac{d\mathbf{\Omega}}{dt}$ into the Right-Hand-Side (RHS) of equation (B.2) we obtain that

$$\begin{aligned}\hbar S\frac{d\mathbf{\Omega}}{dt} = {} & A\boldsymbol{\mathcal{O}}_p{}^{(1)}(H + \eta) + AS\bar{\alpha}S\bar{\gamma}\ \mathbf{\Omega} \times \mathbf{\Omega} \times \hat{\boldsymbol{t}}(\hat{t} \cdot \hbar S\frac{d\Omega}{dt}) \\ & + AS\bar{\alpha}S\bar{\gamma}\ \mathbf{\Omega} \times \hat{\boldsymbol{t}}\ (t \cdot \Omega \times \hbar S\frac{d\Omega}{dt}),\end{aligned} \tag{B.4}$$

where we have defined the operator $\boldsymbol{\mathcal{O}}_p{}^{(1)}$ over as

$$\boldsymbol{\mathcal{O}}_p{}^{(1)}(\Lambda) = \Omega \times \Lambda - S\bar{\alpha}\Omega \times \Omega \times \Lambda - S\bar{\gamma}\Omega \times \hat{t}(\hat{t} \cdot \Omega \times \Lambda). \tag{B.5}$$

This definition, and the later ones, are meant to keep focus on the remaining terms, and specially with $(\frac{d\mathbf{\Omega}}{dt})$ in the RHS. The resembles between the operator $\boldsymbol{\mathcal{O}}_p^{(1)}$ and the operator for the monomer equation is no coincidence since they are obtained by the same operation. If we apply the dot-product to equation (B.2), we can obtain a very useful relation between the complicated terms in the last equation of motion. The relation is

$$S\bar{\alpha}\hat{t}\cdot\Omega\times\hbar S\frac{d\Omega}{dt}=\hat{t}\cdot\Omega\times[\bar{H}+\bar{\eta}]-\hat{t}\cdot\hbar S\frac{d\Omega}{dt}. \tag{B.6}$$

Replacing the above relation in equation (B.4) we obtain:

$$\hbar S\frac{d\mathbf{\Omega}}{dt}=A\boldsymbol{\mathcal{O}}_p^{(2)}(H+\eta)+AS\bar{\gamma}\left[S\bar{\alpha}\mathbf{\Omega}\times\mathbf{\Omega}\times\hat{\boldsymbol{t}}-\mathbf{\Omega}\times\hat{\boldsymbol{t}}\right]\ (\hat{t}\cdot\frac{d\mathbf{\Omega}}{dt}), \tag{B.7}$$

where, again, we define a new operator $\boldsymbol{\mathcal{O}}_p^{(2)}$ over a vector field as:

$$\boldsymbol{\mathcal{O}}_p^{(2)}(\Lambda)=\boldsymbol{\mathcal{O}}_p^{(1)}(\Lambda)+S\bar{\gamma}\ \mathbf{\Omega}\times\hat{\boldsymbol{t}}\ \left(\hat{t}\cdot\Omega\times\Lambda\right). \tag{B.8}$$

We see that in equation the last equation of motion have only one remaining term proportional to $(\frac{d\mathbf{\Omega}}{dt})$. So, to deal with this, we replace the expression for $\hbar S\frac{d\mathbf{\Omega}}{dt}$ into the RHS of equation (B.7) to get:

$$\hbar S\frac{d\mathbf{\Omega}}{dt}=A\boldsymbol{\mathcal{O}}_p^{(3)}(H+\eta)-(AS\bar{\gamma})^2S\bar{\alpha}\left[S\bar{\alpha}\mathbf{\Omega}\times\mathbf{\Omega}\times\hat{\boldsymbol{t}}-\mathbf{\Omega}\times\hat{\boldsymbol{t}}\right]\hat{t}\cdot\hbar S\frac{d\Omega}{dt}(1-(\Omega t)^2), \tag{B.9}$$

where $\boldsymbol{\mathcal{O}}_p^{(3)}$ is defined as:

$$\boldsymbol{\mathcal{O}}_p^{(3)}(\Lambda)=\boldsymbol{\mathcal{O}}_p^{(2)}(\Lambda)+AS\bar{\gamma}\left[S\bar{\alpha}\Omega\times\Omega\times\hat{t}-\Omega\times\hat{t}\right](\hat{t}\cdot\boldsymbol{\mathcal{O}}_p^{(2)}(\Lambda)). \tag{B.10}$$

Comparing the last two equation of motion, we can calculate a linear combination of them to get the canonical form. If we calculate: (B.9) + $AS\bar{\gamma}S\bar{\alpha}$ (B.7) $(1-(\Omega t)^2)$ we finally get the final canonical Langevin equation for $\mathbf{\Omega}$ in presence of spin-orbit coupling:

$$\hbar S\frac{d\Omega^\mu}{dt}=A\left(\delta^\mu{}_\nu-ACS\bar{\gamma}\mathcal{O}^{\mu c}t_ct_\nu\right)\mathcal{O}^{\nu b}(\bar{H}+\bar{\eta}), \tag{B.11}$$

with the final operator $\mathcal{O}^{\mu\nu}$ and the C-factor as:

$$\mathcal{O}^{\mu\nu}=\epsilon^{\mu c\nu}\Omega_c-S\bar{\alpha}(\Omega^\mu\Omega^\nu-\delta^{\mu\nu}), \tag{B.12}$$

$$C=\frac{1}{1+AS\bar{\gamma}S\bar{\alpha}(1-(\Omega t)^2)}. \tag{B.13}$$

As we stressed in the section 2.4.3 and deduced in Appendix A, the numerical value of $\beta$ is neglect-able, so the bar-transformation may fairly be approximated by a factor 1. Which in the end helps us to find and simplify the Fokker-Planck equation. With all this, the final version of the Langevin equation is:

$$\hbar S\frac{d\mathbf{\Omega}}{dt}=A\mathbf{\Omega}\times\left[\tilde{\boldsymbol{H}}+\tilde{\boldsymbol{\eta}}-S\alpha\ \mathbf{\Omega}\times(\tilde{\boldsymbol{H}}+\tilde{\boldsymbol{\eta}})\right], \tag{B.14}$$

where we define the "tilde-transformation" as:

$$\tilde{\mathbf{\Lambda}} = \mathbf{\Lambda} - ACS\gamma\hat{t} \cdot [\Omega \times \Lambda - S\alpha\Omega \times \Omega \times \Lambda]\, \hat{\boldsymbol{t}}. \tag{B.15}$$

We can see that the "tilde-transformation" re-define the effective field and the stochastic magnetic field by projecting the effects of the original fields with the spin-orbit direction. We have define $\tilde{H}$ and $\tilde{\eta}$ to resemble the Fokker-Planck equation of the monomer case, but they are far complicated due to the spin-orbit coupling. The non-stochastic effective field $\tilde{H}$ has no fixed direction as we could predict from the original effective field $H$, but now the actual field in the canonical Langevin equation is the sum of three vectorial contributions

$$\tilde{\boldsymbol{H}} = u\hat{\boldsymbol{z}} + v\hat{\boldsymbol{t}} + w(\hat{\boldsymbol{m}} \times \hat{\boldsymbol{t}}), \tag{B.16}$$

with

$$u = h + \hbar S^2 \Delta^2 J_{21}, \tag{B.17}$$

$$v = S\Delta G_{22}^{(t)} + 2\hbar S^2 \Delta^2 \Gamma_{22}(\Omega t) - ACS\gamma\hat{t} \cdot [\Omega \times H - S\alpha\Omega \times \Omega \times H]\,, \tag{B.18}$$

$$w = \hbar S^2 \Delta^2 D_{21}. \tag{B.19}$$

When we see the results of the monomer case and those reported in [12], it is clear that without SOC, the average value of the spin direction change between $\pm\hat{z}$. Therefore, depending on the numerical contribution of the effective interactions, the average value can have components in the x-direction due to the $v$ contribution and/or y-direction due to the $w$ contribution, which comes directly from the DM interaction.